TECHNICAL REPORT
66-58-CM

STUDIES IN THE PERFORATION OF THIN METALLIC PLATES BY PROJECTILE IMPACT: I. NORMAL IMPACT OF CIRCULAR CYLINDERS

by

L. E. Fugelso and F. H. Bloedow

MRD Division
General American Transportation Corporation
Niles, Illinois

Contract No. DA19-129-AMC-247(N)

June 1966

UNITED STATES ARMY
NATICK LABORATORIES
Natick, Massachusetts 01760

US ARMY MATERIEL COMMAND

Clothing and Organic Materials Divisi
C&OM-9

The findings in this report are not to be construed as an official Department of the Army position unless so designated by other authorized documents.

Citation of trade names in this report does not constitute an official indorsement or approval of the use of such items.

DDC AVAILABILITY NOTICE

Distribution of this document is unlimited.

DISPOSITION INSTRUCTIONS

Destroy; do not return.

Distribution of this
document is unlimited

AD ____________

TECHNICAL REPORT
66-58-CM

STUDIES IN THE PERFORATION OF THIN METALLIC PLATES BY PROJECTILE IMPACT:

I. NORMAL IMPACT OF CIRCULAR CYLINDERS

by

L. E. Fugelso and F. H. Bloedow
MRD DIVISION
General American Transportation Corporation
Niles, Illinois

Contract No. DA19-129-AMC-247(N)

June 1966

Project Reference:
1K024401A113

Series: C&OM-9

Clothing and Organic Materials Division
U. S. ARMY NATICK LABORATORIES
Natick, Massachusetts, 01760

FOREWORD

This is the final technical report under Contract DA19-129-AMC-247(N) for work performed for the U. S. Army Natick Laboratories, Natick, Massachusetts, by the MRD Division of General American Transportation Corporation, Niles, Illinois.

The report consists of two volumes. Volume I contains the analytical predictions and experimental verification of the predictions for the perforation of thin metallic plates by the normal impact of cylindrical projectiles. Volume II contains perforation predictions for thin metallic plates under the normal impact of various military projectiles.

The analytical portion of the report was conducted at the MRD Division by Mr. L. E. Fugelso, Principal Investigator, and the experimental portion by Mr. F. H. Bloedow at MRD's Ballistic Test Station, Colorado Springs, Colorado. Mr. A. L. Alesi of the U. S. Army Natick Laboratories was the technical monitor.

S. J. KENNEDY
Director
Clothing and Organic Materials Division

APPROVED:

DALE H. SIELING, Ph.D
Scientific Director

W. M. MANTZ
Colonel, QMC
Commanding

CONTENTS

CONTENTS (cont'd)

LIST OF FIGURES

LIST OF FIGURES (cont'd.)

LIST OF FIGURES (cont'd.)

LIST OF NOTATIONS

a	projectile radius
A	coefficient in viscoplastic approximation
c	coefficient in residual velocity expression
C_0, C_1	longitudinal wave velocities in projectile and plate
C_1, C_2	coefficients of fit to experimental data (Appendix A)
E	Young's modulus
f	geometric factor in critical perforation velocity expression
h	plate thickness
h_1, h_2	thicknesses of composite plate layers
H	total thickness of composite system
L	projectile length
m	mass of plug
M	mass of projectile
R	projectile radius
r, θ, z	cylindrical coordinates
t	time
t_f	time to fracture at constant stress
T	dimensionless shear stress
u_r, u_z	radial and vertical displacements
u, w	radial and vertical displacements
V	dimensionless vertical particle velocity
V_s	striking velocity
V_r	residual velocity

V_c	critical perforation velocity
V_1	measured residual velocity where (V_r/V_s) is one half of its limiting value. (Appendix A)
V_1, V_2	transition velocities (Appendix B)
X	coefficient in residual velocity expression, petalling and plugging modes
$\overline{X}$	coefficient in residual velocity expressions modified shear model
Y	coefficient in resitual velocity expressions
Z	mechanical impedance
α	angle between normal of surface of projectile and plane of plate
β	coefficient in viscoplastic approximation
γ	dimensionless shear strain
ϵ_{ij}	strain tensor
ζ^*	vertical distance measured from area surface of plate
λ, μ	Lame's constants
ν	Poisson's ratio
$\rho_0\ \rho_1$	densities of projectile and plate
ρ_1, ρ_2	densities of composite plate layers
ρ	density
σ_{ij}	stress tensor
$\left.\begin{array}{l}\sigma_{rr}, \sigma_{\theta\theta}, \\ \sigma_{zz}, \tau_{rz}, \\ \sigma_r, \sigma_\theta, \\ \sigma_z, \tau_{rz}\end{array}\right\}$	radial, tangential, normal (vertical) and shear stresses in axisymmetric deformation
σ_y	generalized yield stress

σ_{ty}	tensile yield stress
σ_{tu}	tensile ultimate stress
σ_{cu}	compressive ultimate stress
σ_1, σ_2	ultimate stresses of composite plate layers
σ_I	average stress at projectile-plate interface
$\sigma_z^{\,o}$	average stress at projectile-plate interface by linear elastic approximation
τ	dimensionless time, or dimensionless shear stress

ABSTRACT

The ballistic parameters were determined analytically and experimentally for the perforation of aluminum alloy and titanium alloy plates by normal impact of steel cylinders. Analytical predictions of the perforation parameters were prepared on the basis of theoretical models of the perforation process. Experimental determination of the critical perforation and residual velocities discriminated among the various models and further experimentation verified the analytical description of the perforation process.

One model of perforation was found which adequately describes the ballistic parameters for the normal impact of steel cylinders into aluminum alloy and titanium alloy plates for impact velocities up to 5000 ft/sec and plate thicknesses up to 0.25 inches.

SECTION 1

INTRODUCTION

1.1 Objectives

The results of an analytical and experimental investigation of the perforation of thin metallic plates by the normal impact of steel cylinders are presented in this report. This study follows a previous research program which investigated the basic physical mechanisms of deformation and failure of metallic plates under ballistic impact.

Two previous reports described the results of analytical and theoretical investigations into the nature of the perforation process. The subject matter was highly mathematical and concerned itself mostly with descriptions or attempts at descriptions of the physical phenomena that occur during impact. Analytical and numerical solutions for the propagation of stresses into single and composite plate systems were given by the linear theory of elasticity; for a simplified geometry of the single plate, a solution to the propagation of stresses in an elastic-plastic plate was obtained. Supplementary investigations of the properties of materials needed for evaluation of fracture and plastic flow were also performed.

The previous analytical work delineated several mechanisms through which the plate may fail under ballistic impact. Each mechanism of plate failure defines a model of perforation. Each model of perforation defines a characteristic critical perforation velocity and characteristic residual velocities. These ballistic parameters are functions of plate geometry, projectile geometry, projectile material properties and plate material properties.

The objective of this study was to determine which of the models of perforation is descriptive of the perforation of thin metallic plates.

1.2 Method of Approach

To accomplish the objective of this study, the various modes of failure were delineated. The critical perforation velocity and residual velocities were predicted for the perforation of single metal plates under normal impact by right circular cylinders. In addition, an experimental determination of these quantities was made.

The investigation of the perforation parameters was composed of two phases:

Phase I: Critical velocity predictions were prepared for all the models of perforation for a selected cylindrical projectile and two different plate materials. Predictions were made for several possible models of perforation. The only parameter allowed to vary was the plate thickness. Tests were then conducted to experimentally determine the critical perforation velocities under these conditions. Comparison of the analytic predictions and the experimental results showed that two models of perforation used in combination fitted the experimental data. Another model of perforation also fitted the experimental data. Each of the models has distinguishing characteristics which suggested the subsequent choice of the projectile and plate parameters for the second phase of the investigation.

Phase II: Further experimental determinations of the critical perforation velocities for one of the plate materials were made, using cylindrical projectiles of different sizes. The projectiles used in these tests were chosen using the experimental data and the theoretical models of perforation. The projectiles were selected to provide a distinguishing test among the perforation models that might adequately explain and describe the process.

1.3 Summary and Conclusions

The analytical and experimental portions of the research program were carried out as indicated in Section 1.2. The previous analytical work was reviewed and several possible modes of failure of the plate under ballistic attack were delineated. Analytical expressions were derived for the critical perforation velocity and the residual velocities for each of the several modes of failure of the plate system. The ballistic parameters, in particular the critical perforation velocity, were computed for the normal impact of right circular cylinders of hard steel into two different metallic alloys. The critical perforation velocity and the residual velocity of the projectile as a function of the striking velocity of the projectile were experimentally determined for the impact of steel cylinders into two metallic alloy plates.

Experimental data were compared with theoretical predictions in both phases of the work. The "modified shear plug" mode of failure of the plate was deemed to be the most descriptive for prediction of the critical perforation velocity for the range of impact velocities, plate thicknesses, plate materials and projectiles tested. This model gave accurate predictions for the critical perforation velocities. The residual velocity versus striking velocity curves as predicted by the model are in good agreement with the experimental observations. Further, the model is readily adaptable to the computation of the perforation characteristics of projectiles of different nose shapes.

Under slightly different conditions of impact of the projectiles, and at higher impact velocities, the mode of the failure of the plate may change. This point will be discussed in the companion volume to this report in conjunction with the prediction of the critical perforation velocities of military projectiles.

1.4 Organization of the Remainder of the Report

In Chapter 2, a brief non-mathematical summary of the physics of the perforation and deformation of a thin metallic plate under ballistic impact is given, together with a list of the critical velocity formulae for the several modes of failure.

Chapter 3 presents the comparison between theory and experiment for the perforation of the plate by normal impact of right circular cylinders.

Two appendices are attached to the report. The first appendix describes the experiments. The second appendix presents a detailed description of the physics of impact and perforation, the mathematical models used for the description, the detailed findings of the analytical research conducted on this problem, and the complete derivation of the model for perforation which best fits the experimental data.

A companion volume contains predictions of the critical and residual velocities expected for normal impact of various steel projectiles into several plate materials. The projectiles are fragment simulators and sharp steel bullets of various dimensions. Steel, titanium alloy and aluminum alloy plates are the plates considered. Description of the application of the theory to the determination of an optimum armor system is also given. Comparison of the predictions with experimental data on the perforation of the metal plates by the projectiles is given.

SECTION 2

THE PHYSICAL PHENOMENA OF THE PERFORATION PROCESS

This section summarizes the basic sequence of events in the plate during impact and perforation, delineates the models of fracture to which the plate is subjected, and enumerates the perforation predictions for each mode of failure. Appendix B contains a detailed and, for the most part, non-mathematical description of the physics of perforation.

Consider a right circular cylindrical projectile of radius a, and length L approaching a plate of uniform thickness, h. The projectile is oriented so that its axis is perpendicular to the plate. The projectile approaches the plate with a velocity V_s, which is perpendicular to the surface of the plate. There is no lateral velocity component. When the projectile strikes the plate, the entire flat end of the cylinder will strike the flat surface of the plate. The density of the plate is ρ_1 and the density of the projectile is ρ_o. (See Figure 1.)

The physical processes that occur immediately after the projectile impacts the plate are:

1. A large stress is generated by the impact at the interface between the projectile and the plate. This stress is, to first approximation, proportional to both the acoustic impedance of the plate-projectile combination and the impact velocity. The impact stress is a monotonic function of the impact velocity.

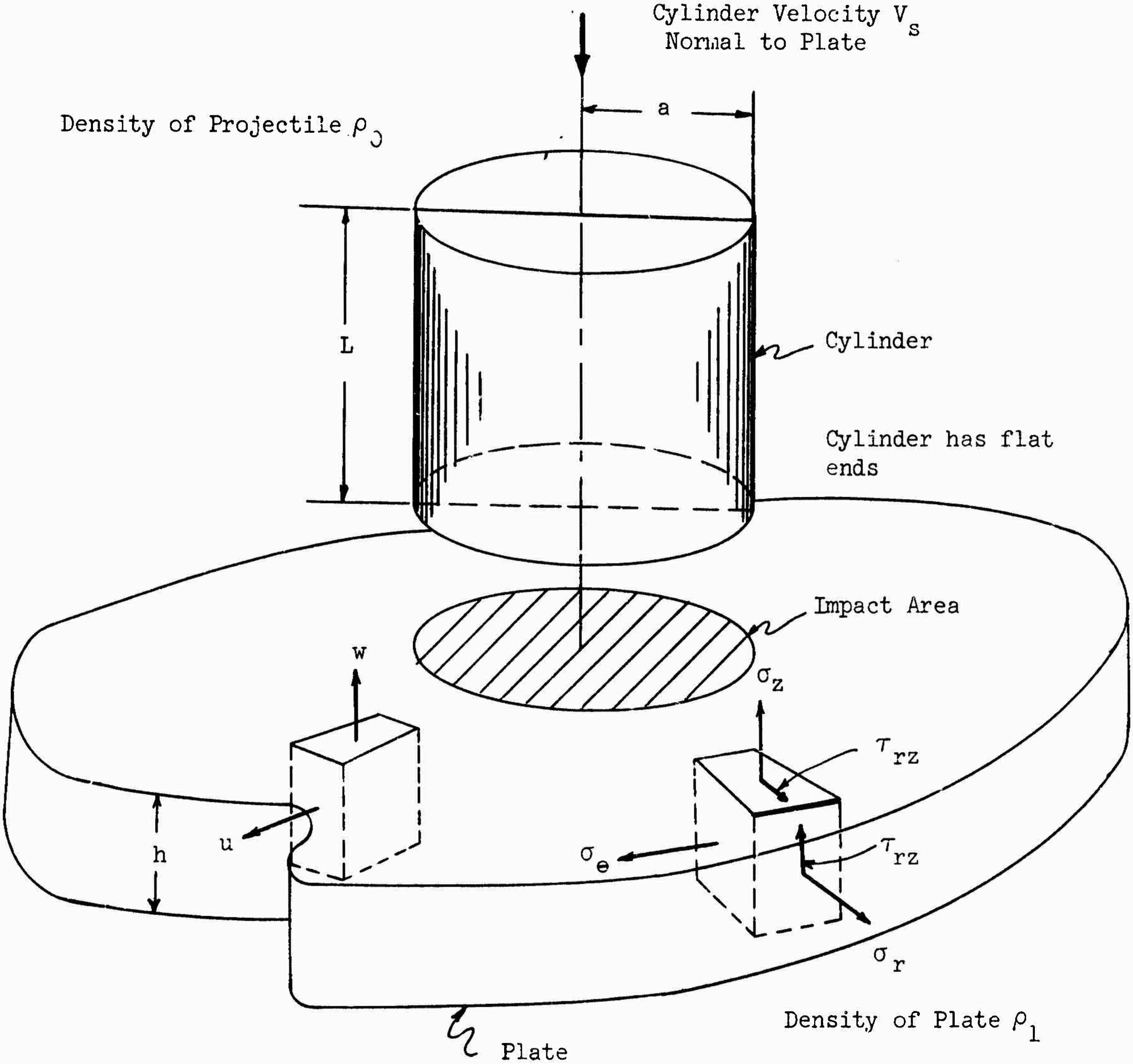

Figure 1 GEOMETRY OF IMPACT AND DEFINITION OF TERMS

2. Two stress waves are propagated into the plate: a fast dilatational wave and a slower shear wave. The stress in the first wave is compressive. The stress in this first wave rises very rapidly and then decays very rapidly. Immediately behind this spike a large stress is left, but not as large as the stress in the spike. The second stress wave is the shear wave. For the normal impact of a cylinder into a half-space, the transient stresses in this wave are small. After the passage of the shear front in a half-space, the quasi-static or steady state solution is established very rapidly.

3. These stress waves reflect from the back surface of the plate, which is a free surface. The first of these reflected stress waves is tensile. Meanwhile, two stress waves are propagating into the projectile and, after traversing the projectile, will reflect from the end and return to the impact surface. These stress waves will reflect from the original interface, the reflected stress wave again traversing the plate. These reflections will continue for a long time.

4. After the stress wave has completed the first full traverse of the plate, the normal stress becomes small. The portion of the plate under the projectile is in motion with a normal velocity slightly less than the impact velocity. High radial and tangential stresses are developed in the plate. High shear stresses are generated in the plate near the lip of the projectile.

In response to the stresses that are generated in the plate system, the plate may possibly fail by one of several mechanisms. They are:

1. Fracture in the Direct Wave - The plate may fracture in response to the high compressive stresses that are generated in the stress spike near the first stress wave front that propagates into the plate.

2. Radial Fracture in the First Stress Wave - After the stress spike near the wave front of the longitudinal wave has passed, the radial stress in the plate becomes tensile while the normal stress remains compressive.

3. Spall - The plate may fracture in response to high tensile vertical stress generated by the reflection of the stress wave from the back surface.

4. Petalling - After the passage of the first stress waves, the plate may fracture in response to high radial and circumferential tensile stresses that are developed in the plate near the lip of the projectile.

5. Plugging - After the passage of the first stress wave, the plate may fail in response to the large shear stress that is developed near the edge of the projectile.

The determination of the ballistic performance of a plate or laminated plate system under impact by a projectile has two basic problems.

1. Does the plate or laminated plate system fail or break?

2. Does the projectile stop or, at least, how much does it slow down?

To answer the first question, the transient stress pattern in the plate that arises from the sudden generation of stress at the contact surface must be known, together with the criterion for failure for the material in response to these time-dependent stress fields.

To answer the second question, we need to know the magnitude of the forces resisting the motion of the projectile and how long they are maintained. The magnitude of the resisting force is given by the impact stress generated over the contact area of the plate and projectile. This force will be maintained until the plate breaks or until modified by the multiple reflections of stress waves that occur in a plate system.

The critical velocity for perforation is given by answering the second question, while the critical velocity for spalling without perforation is given by the answer to the first question. In the following paragraphs, the perforation limits and the residual velocity of the projectile will be given as a function of natural parameters for the various modes of failure. These critical perforation velocities and residual velocities were calculated on the basis of stress patterns developed in the plate. For the first three modes of failure the stress wave propagation in the plate was assumed linear elastic. Further, stresses were computed on the assumption that the projectile did not deform. Shatter of the projectile is ignored here.

The material parameters and their effect on the various modes of failure are listed below:

1. Fracture in the Direct Wave - The material parameters involved in the direct wave fracture at the back side of the plate are the Brinell hardness of the plate (or, equivalently, the yield strength), the density of the plate, and the compressive ultimate stress. Increases in any of these reduce the penetration due to fracture in the direct wave. The critical velocity for perforation is

$$V_c = \left(\frac{1 - 2\nu}{1 - \nu}\right) \frac{\sigma_{ty}}{Z} f^{1/2} \qquad (1)$$

where σ_{ty} is the tensile stress

Z is the acoustic impedance, given by

$$Z = \frac{\rho_1 C_1 \rho_0 C_0}{\rho_1 C_1 + \rho_0 C_0} V_s \qquad (2)$$

ρ_0, ρ_1 are the densities of projectile and plate, respectively.

C_0, C_1 are the longitudinal sonic velocities of projectile and plate, respectively.

f is a geometric factor given by $1 + h^2/a^2$

h is the plate thickness

a is the projectile radius

V_s is the striking velocity

where ν is Poisson's ratio of the material

2. Radial Fracture - The critical velocity for failure in the reflected stress wave may occur when the radial stress exceeds the yield stress. For a metal plate under normal impact from a rigid circular cylinder, this critical velocity is given approximately by

$$V_c = \frac{\sigma_{ty}}{Z} \left[\frac{2(1 - \nu) f}{(1 - \nu) + 2\nu f}\right]^{1/2} \qquad (3)$$

3. <u>Spall</u> - The material and geometrical parameters that govern the spall are the thickness to bullet radius ratio and the tensile strength of the plate in the direction of the projectile approach. The critical perforation velocity is proportional to the tensile yield strength and a geometric function. The critical velocity for failure by spall is determined by the vertical or normal stress and is bounded and closely approximated by the expression

$$V_c = \frac{\sigma_{ty}}{Z}\left[\frac{f}{1 - f^{1/2}}\right] \tag{4}$$

If the time to fracture, t_f, at a given stress level is taken into account in this mode of failure, the impact stress required to cause failure is raised. The critical perforation velocity is

$$V_c = \left(\frac{1 - 2\nu}{1 - \nu}\right) \frac{\sigma_{ty}}{Z} f^{1/2} e^{\frac{10 t_f C_1}{a}} \tag{5}$$

with t_f = time to fracture

C_1 = longitudinal sonic velocity

Computations using $t_f = 10^{-8}$ sec were used at first, which agrees with the experimental data for time to fracture in terms of pure aluminum. The effect of time delay to fracture does not significantly alter the predictions of the critical perforation velocity.

The stresses in the spike decay extremely rapidly by dissipation in plastic flow. Explicit expressions for the decay of a stress wave by plastic flow have been computed for the propagation of a spherical wave (Fugelso 1962) and a cylindrically expanding wave (Fugelso, Arentz, and Davidson 1962). For impact stresses far above the yield stress for the distance the stress wave must propagate in the present problem, the stresses should decay by a factor of 1.5 to 2 by the time the stress wave reaches the back of the plate. Thus the critical perforation velocity estimate should be raised by a factor of 1.5 to 2.

4. & 5. Plugging and Petalling - If the plate does not fail by fracture as the first-stress wave passes, then the failure of the plate by plugging and petalling must be considered. Plugging is failure of the plate by shear under the rim of the bullet, whereby a plug of plate material is ejected. Petalling occurs when the plate fails in response to the tensile membrane stresses that are generated. The critical velocities for perforation are similar for the petalling and plugging failure modes. The static components of the resisting force to the projectile motion are given by elementary plate theory. In the case of the shear fracture (plugging model) the resisting force of the plate was taken as the maximum shear stress developed in plastic flow. This is integrated across the plate.

$$\sigma = \sigma_{ty} \left(\frac{h}{a}\right) \tag{6}$$

The resisting force to the projectile motion is given by the maximum stress resultant in the plate.

$$\sigma = 4\sigma_{ty} \left(\frac{h}{a}\right) \tag{7}$$

with σ_{ty} = tensile yield stress of the plate material

The critical perforation velocity here is given:

$$V_c = X^{1/2}(e^Y - 1)^{1/2} \tag{8}$$

$$Y = \frac{2\rho_1 h}{\rho_0 L}$$

$$X = \frac{\sigma_{ty}}{\rho_1}\left(\frac{h}{a}\right) \quad \text{for plugging}$$

$$X = \frac{4\sigma_{ty}}{\rho_1}\left(\frac{h}{a}\right) \quad \text{for petalling}$$

For both mechanisms, the critical perforation velocity is a monotonic function of the tensile yield stress of the plate and the plate thickness to projectile length ratio.

The mechanisms are normally restricted from thin to moderately thick elastic plates ($h/a < 1$) and become the dominant mechanisms of failure for thin plate and low impact velocities.

One further revision of the shear model was made and calculations performed. The static component of the resisting force of the plate was taken as σ_{tu} (the tensile ultimate strength) times the impacted area. The resisting force was chosen to be independent of plate thickness (unlike the previous model, which had the static resisting forces proportional to the plate thickness). The resulting formula for the critical velocity for the perforation of a thin plate under normal impact of a right circular cylinder is

$$V_c = \bar{X}^{1/2}(e^Y - 1)^{1/2}$$

$$\bar{X} = \frac{\sigma_{tu}}{\rho_1} \tag{9}$$

$$Y = \frac{2\rho_1 h}{\rho_0 L}$$

where σ_{tu} is the tensile ultimate stress

ρ_0, ρ_1 are the densities of the projectile and plate

h is the thickness of the plate

L is the length of the projectile

A complete derivation of the "modified shear plug" model is given in full detail in Appendix B.

Figures 2 and 3 show the functional behavior of each of the models of perforation as a function of increasing (h/a) ratios. From the inspection of Figure 2, spall can immediately be eliminated as descriptive of the critical perforation velocity. For thin plates and sufficiently long projectiles, the critical velocity for spall failure has a minimum near $\frac{h}{a} = 1.5$ and increases without bound for both thicker and thinner plates. The radial fracture and fracture in the direct wave model are almost identical in their predictions of the critical perforation velocity. Figure 3 shows typical behavior of the critical perforation velocity for the petalling, plugging and modified shear model as functions of the plate thickness to projectile radius ratio. The graph shows the predicted critical perforation velocity for 7075-T6 aluminum plate being impacted by a .22 caliber 4340 steel cylinder.

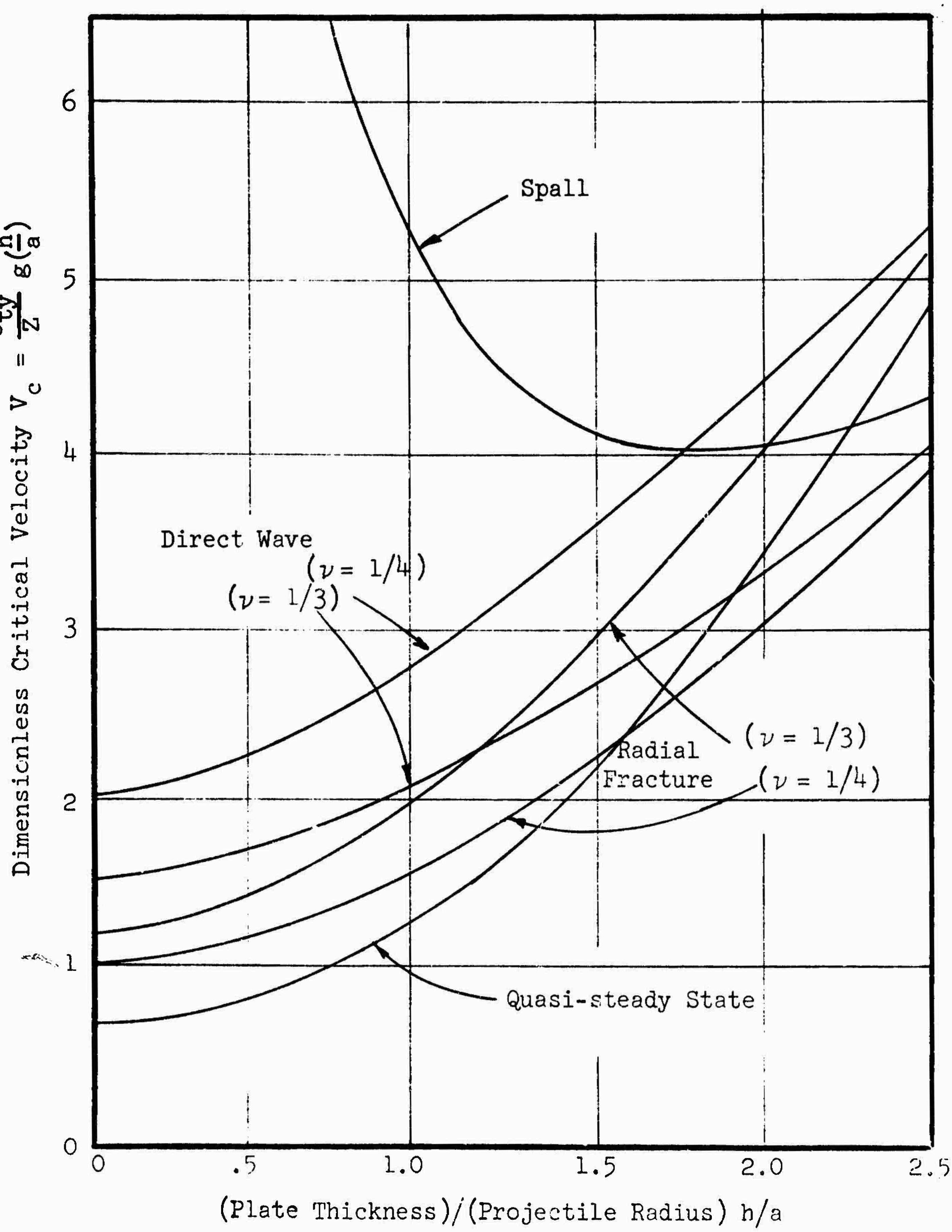

Figure 2 DEPENDENCE OF CRITICAL PERFORATION VELOCITY ON PLATE THICKNESS

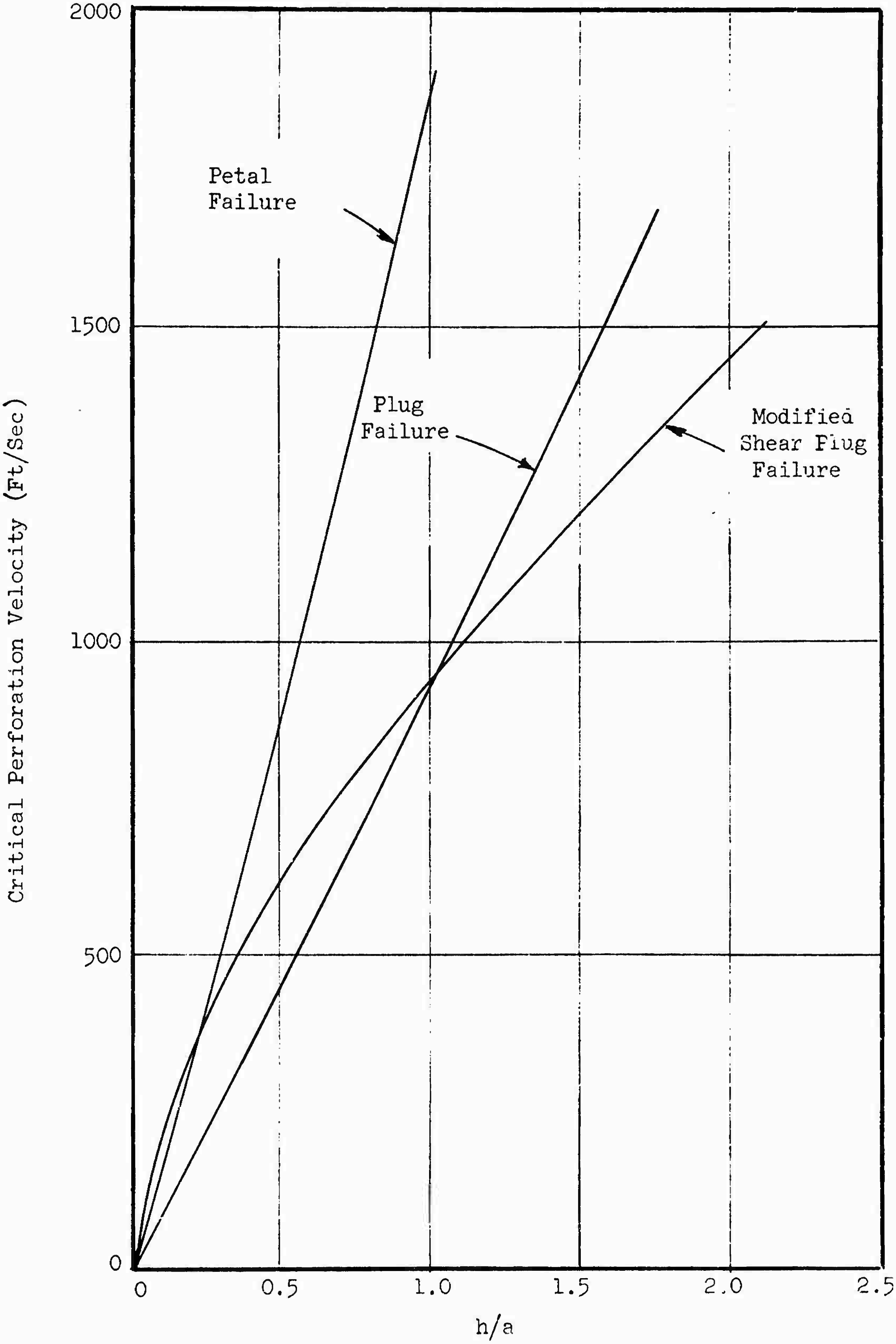

Figure 3 TYPICAL CRITICAL VELOCITY PREDICTIONS
PLATE: Al7075-T6
PROJECTILE 4340 STEEL CYLINDER a = 0.11" L = 0.25"

SECTION 3

CALCULATIONS AND EXPERIMENTAL RESULTS

3.1 Experimental

Predictions of the critical perforation velocities for the various models of perforation were made for two plate materials under normal impact by right circular cylinders. The plate materials were the titanium alloy Ti 5 Al 2.5 Sn and the aluminum alloy 7075-T6. The impacting cylinders were 4340 steel (normalized).

Experiments were performed to obtain residual velocity vs. striking velocity curves and critical perforation velocities. These results were used to establish and to distinguish the various perforation models. Three types of projectiles were shot at various thicknesses of two types of target plates. The projectiles and the plates used in the experimental phases of this study are described in Tables I and II.

TABLE I

PROJECTILE DATA

Type	Diameter	Length	Weight*
1	0.218 inch	0.250 inch	18.2 grains
2	0.218 inch	0.375 inch	27.7 grains
3	0.299 inch	0.341 inch	47.3 grains

Material - 4340 steel-normalized

Yield stress - 180,000 psi

Hardness - Brinell 388; Rockwell C-42

*approximate

TABLE II

METAL TARGET PLATE DATA			
Material	Thicknesses (inches)	Mean Value Yield Stress (psi)	Hardness
Aluminum 7075-T6	0.010, 0.050, 0.090, 0.250	74,000	Vickers 180 Rockwell A 55.5
Titanium 2.5 Sn 5 Al	0.032, 0.048, 0.076, 0.100	117,500	Vickers 320 Rockwell A 67.75

The experimental portions of this study had two phases.

<u>Phase I</u> - V_r (residual velocity) vs V_s (striking velocity) curves were measured for four thicknesses for each of two target materials, 7075-T6 aluminum alloy and Ti 2.5 Sn 5Al alloy, using a single type of projectile. Type 1 projectile was used for this experimental phase. These tests provided the data for verification and modification of the existing perforation models.

<u>Phase II</u> - Determination of V_r vs V_s curves for the thicknesses of one target material using two different types of projectiles. The Phase II tests were conducted using projectile types 2 and 3 and 0.050 and 0.090 7075-T6 aluminum target plates. These tests provided data for checking the modified perforation models and for distinguishing between the perforation models.

The physical properties of the target and projectile materials were determined. Material properties determined were the stress-strain curves, Young's modulus and hardness.

Details of the experimental program and the experimental data are given in Appendix A.

3.2 Critical Perforation Velocity Measurements

A summary of the critical velocity for perforation, V_c, generated on this program is given in Table III.

TABLE III

TARGET MATERIAL, THICKNESS, V_c

		Critical Perforation Velocity, V_c* (fps)		
		Projectile		
Material	Thickness (inches)	Type 1	Type 2	Type 3
Aluminum 7075-T6	.250	1450		
	.090	750	650	650
	.050	650	550	500
	.010	450 $\pm$ 100		
Titanium 5 Al 2.5 Sn	.097	1200		
	.076	1050		
	.048	900		
	.032	800 $\pm$ 100		

*Values of V_c are $\pm$ 50 fps unless otherwise indicated.

3.3 Comparison of Theory and Experiment

The critical perforation velocities were computed for three models of perforation for the two target materials and the projectile 1. The material parameters used in the computation are listed in Table IV.

TABLE IV

MATERIAL PARAMETERS USED FOR THEORETICAL CALCULATIONS			
Projectile:			
Material	4340 Steel	4340 Steel	4340 Steel
Length	.25"	.37"	.37"
Radius	.11"	.11"	.15"
Density	.283 lbs/in^3	.283 lbs/in^3	.283 lbs/in^3
σ_{ty}	180,000 psi	180,000 psi	180,000 psi

Target Plates:		
Material	Al 7075-T6	Ti 5Al-2.5 Sn
Density	0.100 lbs/in^3	.161 lbs/in^3
E	10.3 x 10^6 psi	16 x 10^6 psi
G	3.4 x 10^6 psi	6 x 10^6 psi
σ_{ty} tensile yield stress	67,100 psi	120,000 psi
σ_{tu} tensile ultimate	77,000 psi	125,000 psi
h thickness range	0.0"-.25"	

The predictions for the critical perforation velocities for normal impact of right circular cylinders of 4340 steel into Ti 5Al 2.5 Sn and 7075-T6 Al plates are shown in Figures 4, 5, 6, and 7. Three theoretical models of perforation are shown on the graphs. They are:

1. Fracture in direct wave
2. Petalling failure
3. Modified shear plug failure

The predicted critical perforation velocities were compared with the measured critical velocities for both plate materials for a given projectile (Phase I). The property of the plate system that was varied was the plate thickness (Figures 4 and 5).

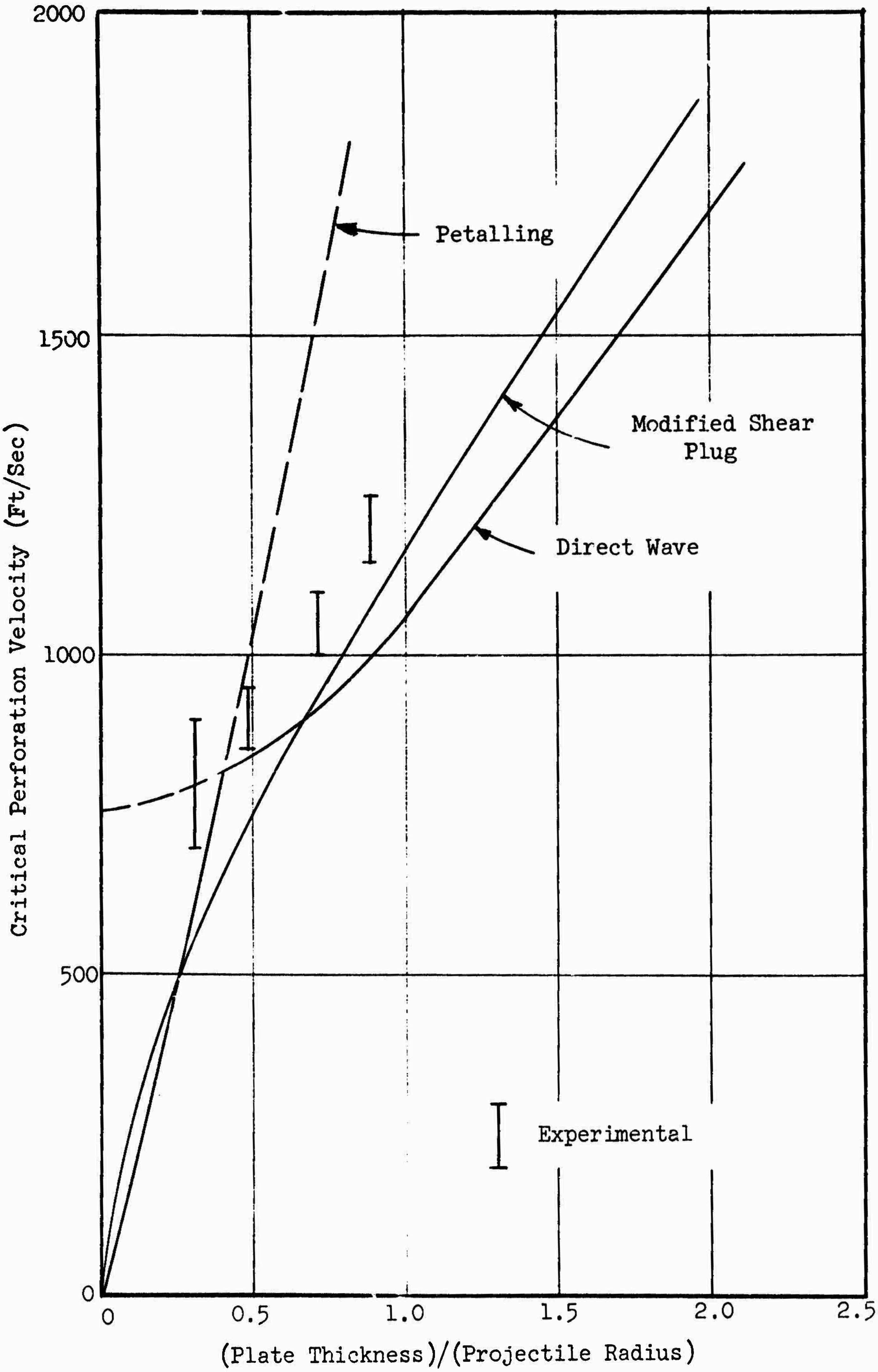

Figure 4 CRITICAL PERFORATION VELOCITY VERSUS PLATF THICKNESS
PLATE: Ti 5Al 2.5 Sn
PROJECTILE: 4340 STEEL CYLINDER a = 0.109 IN. L = 0.25 IN.

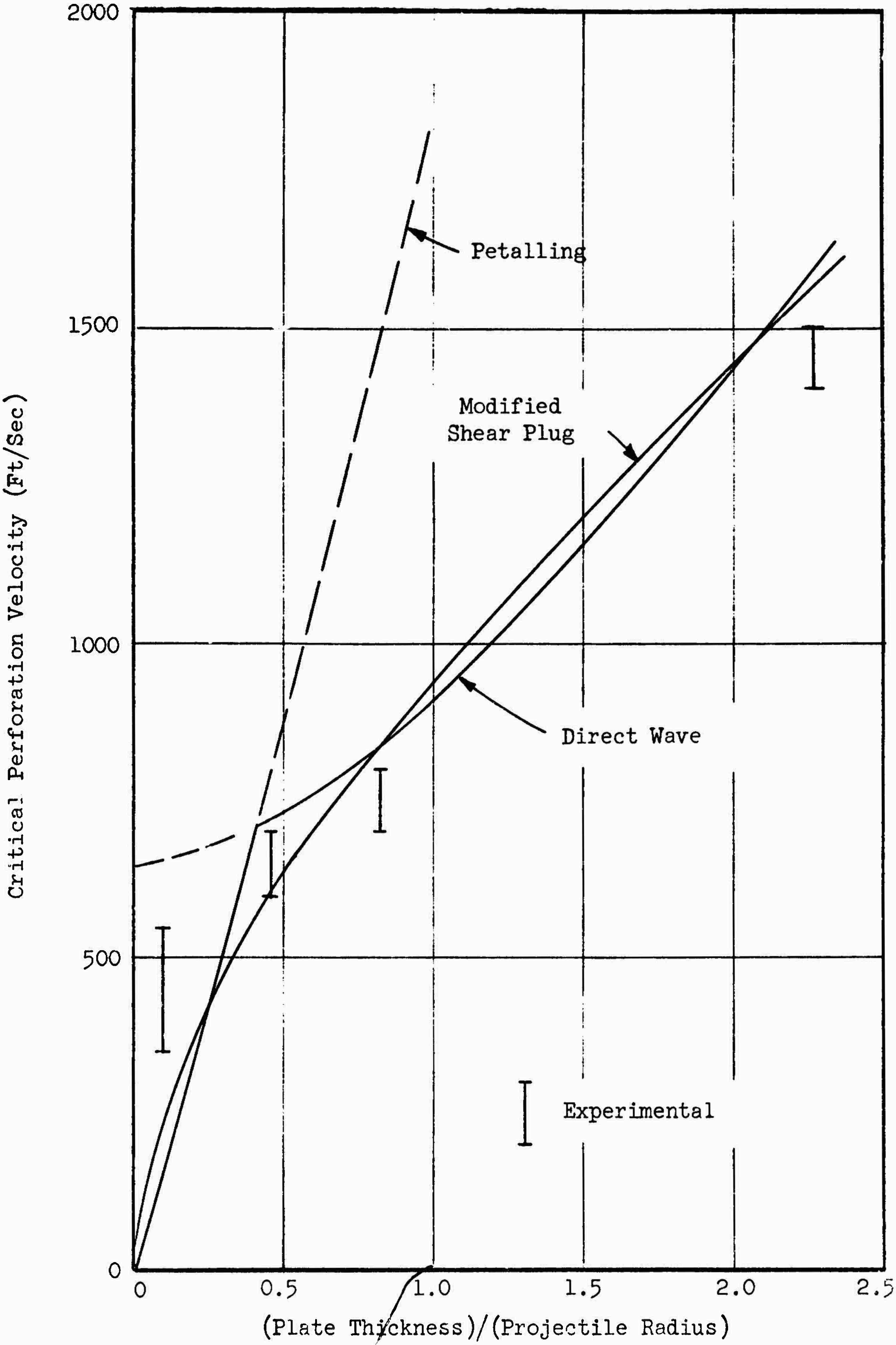

Figure 5 CRITICAL PERFORATION VELOCITY VERSUS PLATE THICKNESS
PLATE: 7075-T6 Al
PROJECTILE: 4340 STEEL CYLINDER a = 0.109 IN. L = 0.25 IN.

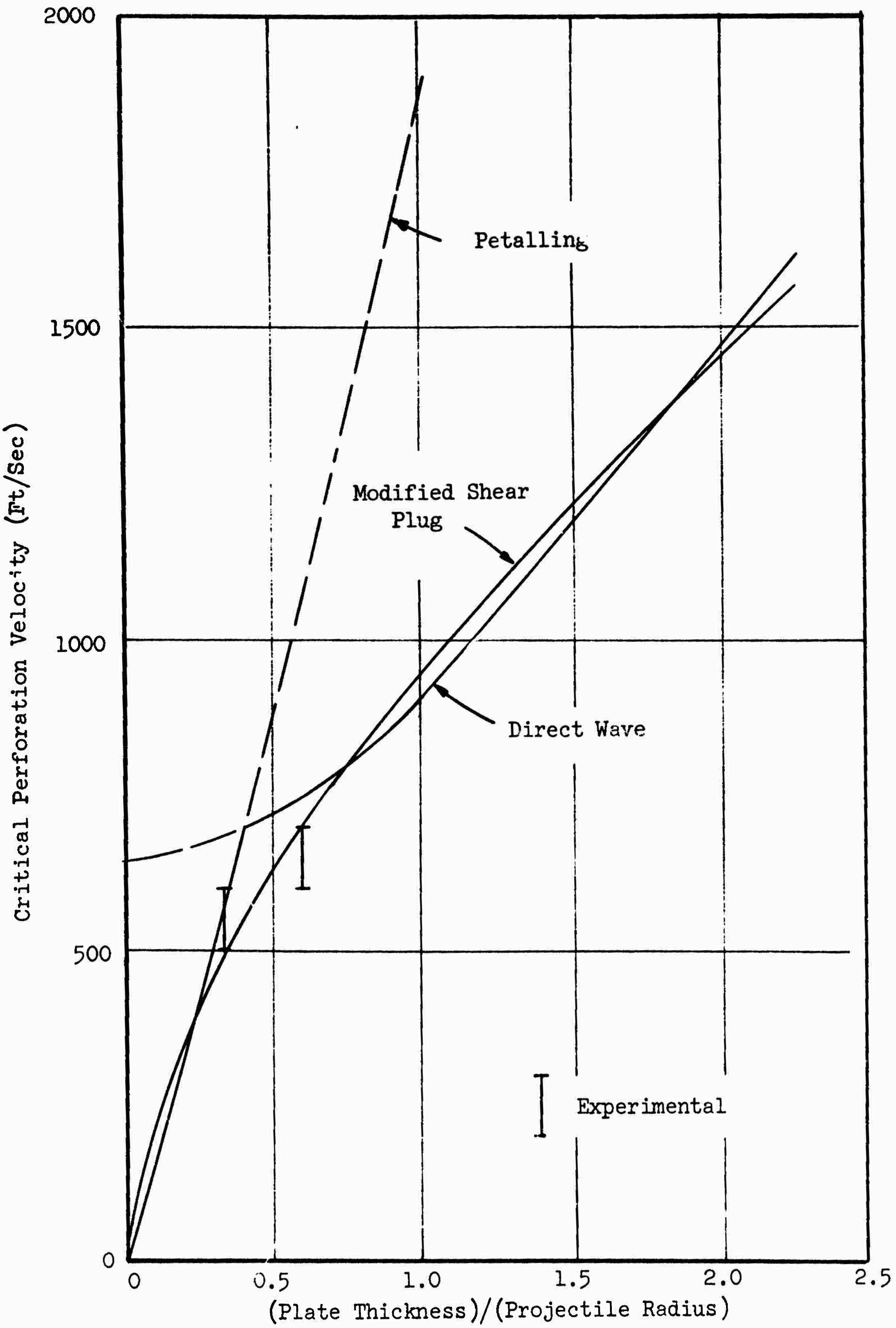

Figure 6 CRITICAL PERFORATION VELOCITY VERSUS PLATE THICKNESS
PLATE: 7075-T6 Al
PROJECTILE: 4340 STEEL CYLINDER a = 0.15 IN. L = 0.33 IN.

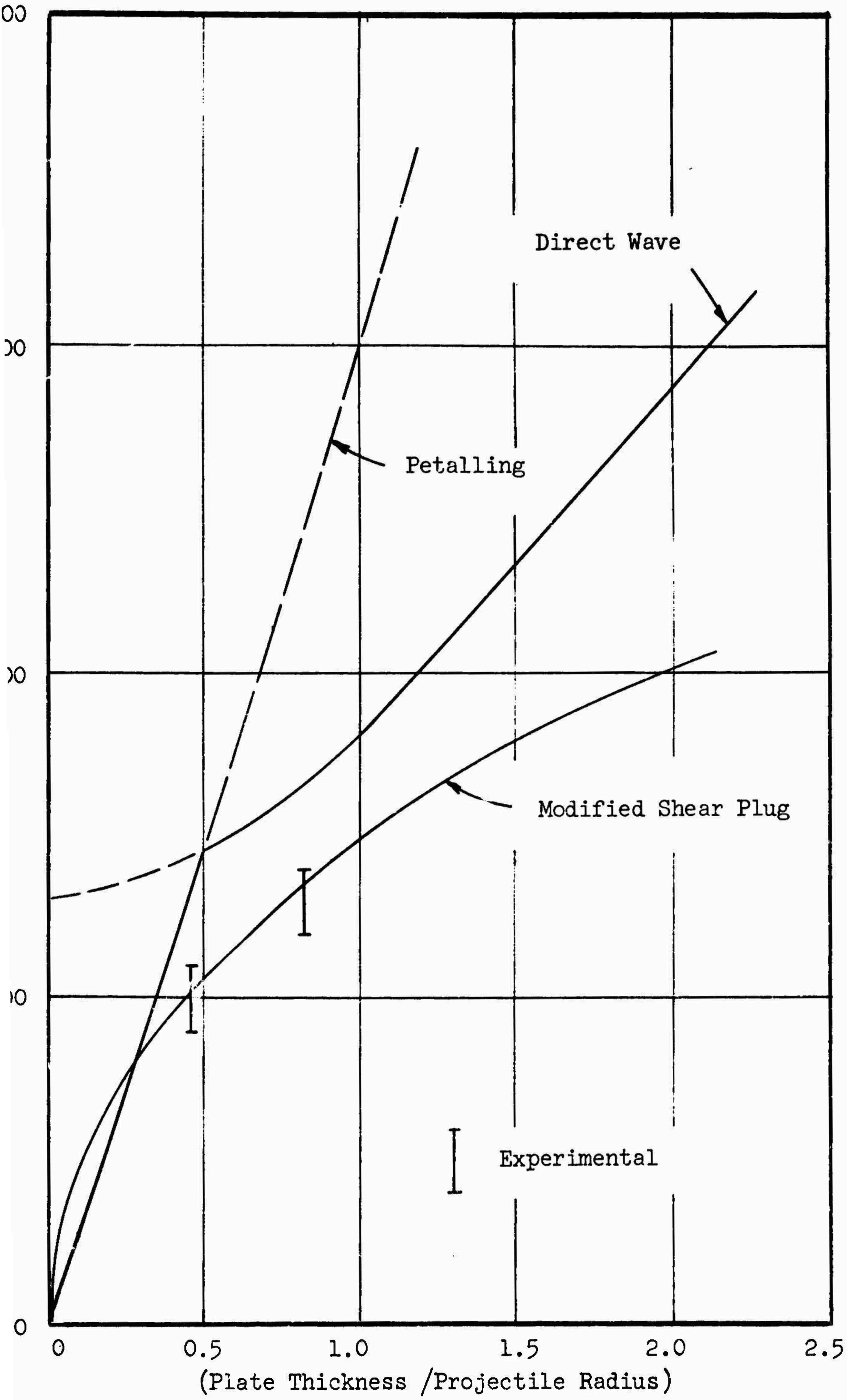

gure 7 CRITICAL PERFORATION VELOCITY VERSUS PLATE THICKNESS
PLATE: 7075-T6 Al
PROJECTILE: 4340 STEEL CYLINDER a = 0.109 IN. L = 0.375 IN.

One of the theoretical models provided a good qualitative and quantitative fit to the experimentally determined critical perforation velocities over the range of plate thickness and velocities tested. This model was the "modified shear plug" mode of failure.

Two of the theoretical curves used in combination gave a reasonable qualitative and quantitative description of the critical limit velocity for perforation. These modes were the "petalling" mode for very thin plates and the fracture in the direct wave mode for thicker plates, the critical velocity being determined by taking the lower of critical velocities predicted.

The Phase II experiments were determined from properties of the modes of failure. The "petalling" and "modified shear plug" modes of failure predict an influence of projectile length (mass per unit striking area) of the projectile on the critical perforation velocity. These curves have opposite convexities in the region of interest. The critical perforation velocity for the combined model description will follow either the fracture in the direct wave curve or the petalling curve. If the experimental data is described by the direct wave curve, the value of the critical perforation velocity will be a function of $\frac{h}{a}$ and independent of $\frac{h}{L}$, being proportional to $\left(1 + \left(\frac{h}{a}\right)^2\right)^{1/2}$. If the experimental data is described by the petalling mode, the critical perforation velocity is proportional to $\left(\frac{h}{a}\right)^{1/2}\left(\frac{h}{L}\right)^{1/2} = \left(\frac{h}{a}\right)/\left(\frac{L}{a}\right)^{1/2}$. If the modified shear plug model is descriptive of the critical failure of the plate, the behavior of the critical perforation velocity is proportional to $\left(\frac{h}{L}\right)^{1/2} = \left(\frac{h}{a}\right)^{1/2}/\left(\frac{h}{L}\right)^{1/2}$.

Near the intersection of the direct wave failure curve and the petalling curve, the differences among these three theoretical curves is quite large. Therefore, the experiments on Phase II were planned. Additional critical perforation velocities were determined for one of the plate materials, 7075-T6 Al. In one set of experiments, the size of the projectile was increased while retaining geometric similarity to the smaller projectiles (Projectile 3). The ratio (h/a) was increased simultaneously with L/a. The ratio h/L was held constant. In the other set of experiments, the length of the projectile was increased but the striking area was kept the same as the previous projectile (Projectile 2). The ratio h/a was held constant, while L/a and consequently, h/L were changed. The theoretical critical velocities were determined for these two cases. The critical perforation velocities were measured for these cases. Figures 6 and 7 show the experimentally determined values and the analytical prediction.

The Phase II experiments indicate that the "modified shear plug" mode of failure gives the best description of the perforation limit velocity for the plate materials tested.

One point remained to be determined. Was the effective stress acting against the projectile approximated by the yield stress or the ultimate stress?

The tensile yield stress and the tensile ultimate stress of the titanium and the aluminum alloys tested are about the same. For certain steels this is not the case and the experimental determination of perforation velocities for steel-steel impact will clarify whether σ_{tu} or σ_{ty} is descriptive of the impact process. Figure 8 shows the summary of the NRDC experimental data

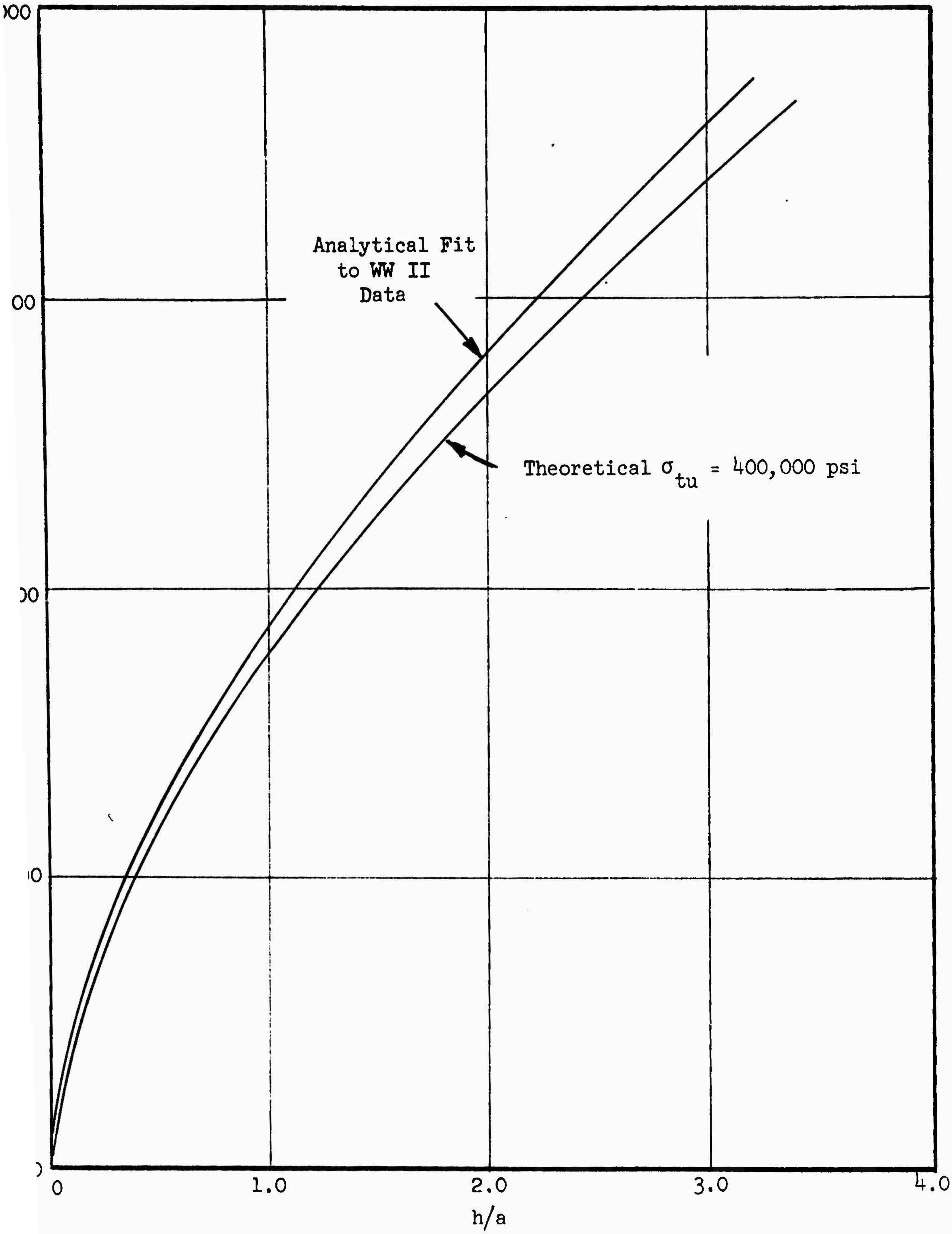

Figure 8 COMPARISON OF THEORETICAL AND EXPERIMENTAL CRITICAL PERFORATION VELOCITIES FOR ARMOR STEEL (STEEL PROJECTILE a = 0.122")

(Curtiss 1946) on low velocity steel-steel impact together with the "modified shear plug" model. (The critical velocity for perforation was modified slightly for nose shape. See Vol. II for details.) The projectiles were .244 cal 4340 steel bullets and the plate was hardened armor steel with varying Brinell hardness (250-450).

The tensile ultimate stresses for armor steel and naval ship plate steel (Bridgman 1952) were used to compute the critical velocity curves. The modified shear plug model was used. Good agreement using tensile ultimate stress on armor steel was obtained for plate thickness-projectile radius ratios from 0 to 12.

SECTION 4

CONCLUSIONS AND RECOMMENDATIONS

The main goal and objective of this research project was the determination of the descriptive model of failure of thin metallic plates under ballistic impact by metallic projectiles. The experimental discrimination and verification of the model of failure was accomplished.

A review of previous analytical research on the determination of the stresses in the plate due to impact led to the delineation of several models of failure of the plates. For each model of failure, analytic expressions for the critical perforation velocity and for the residual velocity versus striking velocity were formulated as a function of plate thickness, projectile geometry, and plate and projectile properties. Calculations of ballistic parameters, in particular the critical perforation velocity, were made for the ballistic impact of two thin metallic plates composed of an aluminum alloy and a titanium alloy, respectively, by right circular cylinders of steel.

The critical perforation velocity and the residual velocity versus striking velocity curves were experimentally determined for the normal impact of right circular cylinders of steel into these two alloy plates. The experimentally determined critical perforation velocities and residual velocities agreed very well with one of the theoretical models for failure of the plate over the range of plate thicknesses and impact velocities tested. The plate thickness varied up to 0.25" and the normal impact velocity range covered velocities to 4000 ft/sec.

The particular model of plate failure that best describes the ballistic performance of a thin metallic plate under the ballistic attack of cylindrical projectiles is the "modified shear plug" model of failure. In this model of plate failure, the impacting projectile pushes the material in the plate out of the way. The resisting force of the plate against the projectile motion is composed of the inertial resistance of the plate material and the compressive ultimate stress of the plate in unconfined compression. The critical perforation velocity and the residual velocities are expressible in closed form for the cylindrical projectile. The computations are easily extended to the cases of normal impact of any axisymmetric projectile. Representative calculations for projectiles in this class are given in the second volume of this report.

The critical velocity for perforation for a cylindrical projectile is a function of the compressive ultimate stress of the plate material, the density of the plate material, the density of the projectile and the plate thickness to-projectile length ratio. The critical velocity for perforation is proportional to the ultimate stress of the plate and inversely proportional to the plate density. The critical velocity is a monotonically increasing function (almost exponential) of the ratio of the mass-per-unit area of the plate to mass-per-unit area of the projectile.

After the critical perforation velocity has been surpassed, the residual velocity to striking velocity ratio rapidly increases with increasing value of the striking velocity. This ratio soon reaches a limiting value less than unity.

One of the ultimate goals of this research program was to give information which will increase the ballistic performance of light armor systems. The second volume of this report applies two of these models of perforation to evaluate ballistic performance of light metallic plates by cylinders and military projectiles. Recommendations on the improvement of armor systems is given in that volume.

APPENDIX A

EXPERIMENTAL DETERMINATION OF THE

RESIDUAL VELOCITIES FOR NORMAL IMPACT OF

RIGHT CIRCULAR CYLINDERS INTO THIN METALLIC PLATES

A.1 Introduction

Experimental determination of the ballistic performance of thin metallic alloy plates subject to normal impact by right circular steel cylinders was made. The details of these experiments are given in this appendix.

The experiments determined the residual velocities and the critical limit perforation velocities for the normal impact of 4340 steel cylinders into selected titanium and aluminum alloys. This experimental program coincided with the readily computable cases generated by the theoretical and analytical phases of the perforation problem. The experiments were designed to check the velocity of the various models of perforation and to discriminate among the various models.

A.2 Experimental Setup

A.2.1 Apparatus

The experimental setup consisted of a gun fixture, a test fixture which held the target plate, a ballistic pendulum and several velocity screen mounts. It is shown schematically in Figure A-1.

The gun fixture and the test fixture are separated by about 6 feet. Along the projectile flight path, a series of velocity screens (paper sheets with a continuous, printed silver circuit) and a ballistic pendulum are placed. Four screens are placed between the gun muzzle and target plate. Two screens are placed between the target and the ballistic pendulum, which is immediately behind the target fixture. Three average velocities are obtained in front of the target plate and 1 velocity is obtained behind for the screen measurements.

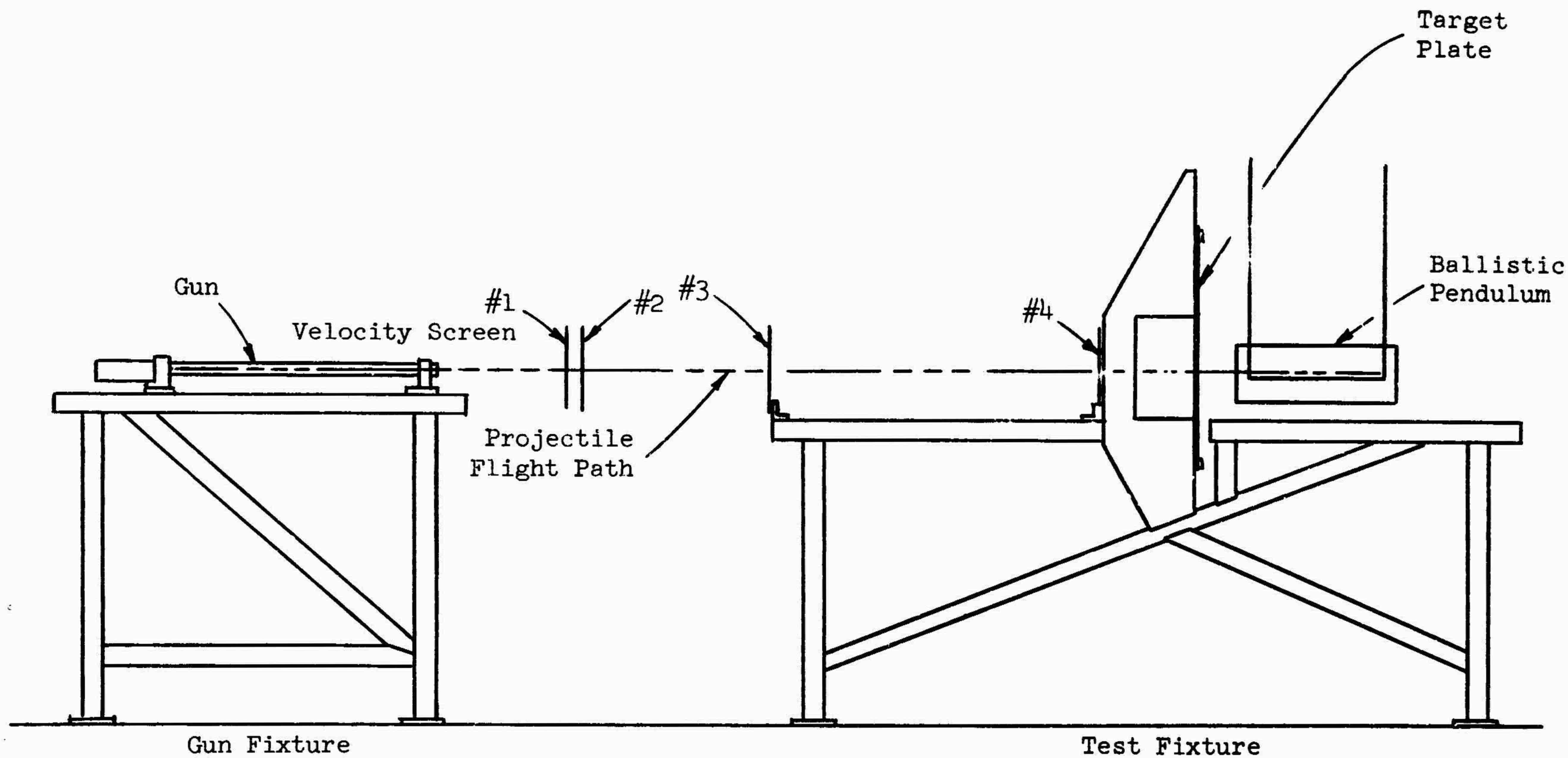

Figure A-1 DIAGRAM OF EXPERIMENTAL SETUP

The ballistic pendulum is about three meters in suspended length and its mass may be varied from about two kilograms to nine kilograms.

Target plates varying in width from about one foot to three feet are easily accommodated in the plate holder. Two types of projectile launchers were used: a caliber .220 Swift type for projectiles from 0.2180 to 0.2185 inches in diameter, and a caliber .350 Magnum type for projectiles from 0.2990 to 0.2995 inches in diameter. Both of the launchers have smooth bore barrels.

A.2.2 Experimental Procedure

Measurements of the velocity of the projectile before and after it perforated the target plate were made for a sequence of initial velocities.

The sequence of the experimental shots was the same for all target plates. The sequence consisted of eight pairs of shots in three sets. The first set of three pairs of shots was fired at a velocity somewhat above the knee of the analytically predicted V_r versus V_s curve (See Figure A-2). The second set consisted of one pair at the high end of the curve and one pair near the knee of the curve. The third set of three pairs were near the V_c value of the curve. The velocities used in sets 2 and 3 were dependent upon the previously obtained results. Thus, for each plate tested, a V_r versus V_s curve was obtained for comparison with the analytically determined curves.

Visual inspection and metallurgical examination of the plate in the neighborhood of the perforation were made as necessary to assist in the determination of the mode of failure.

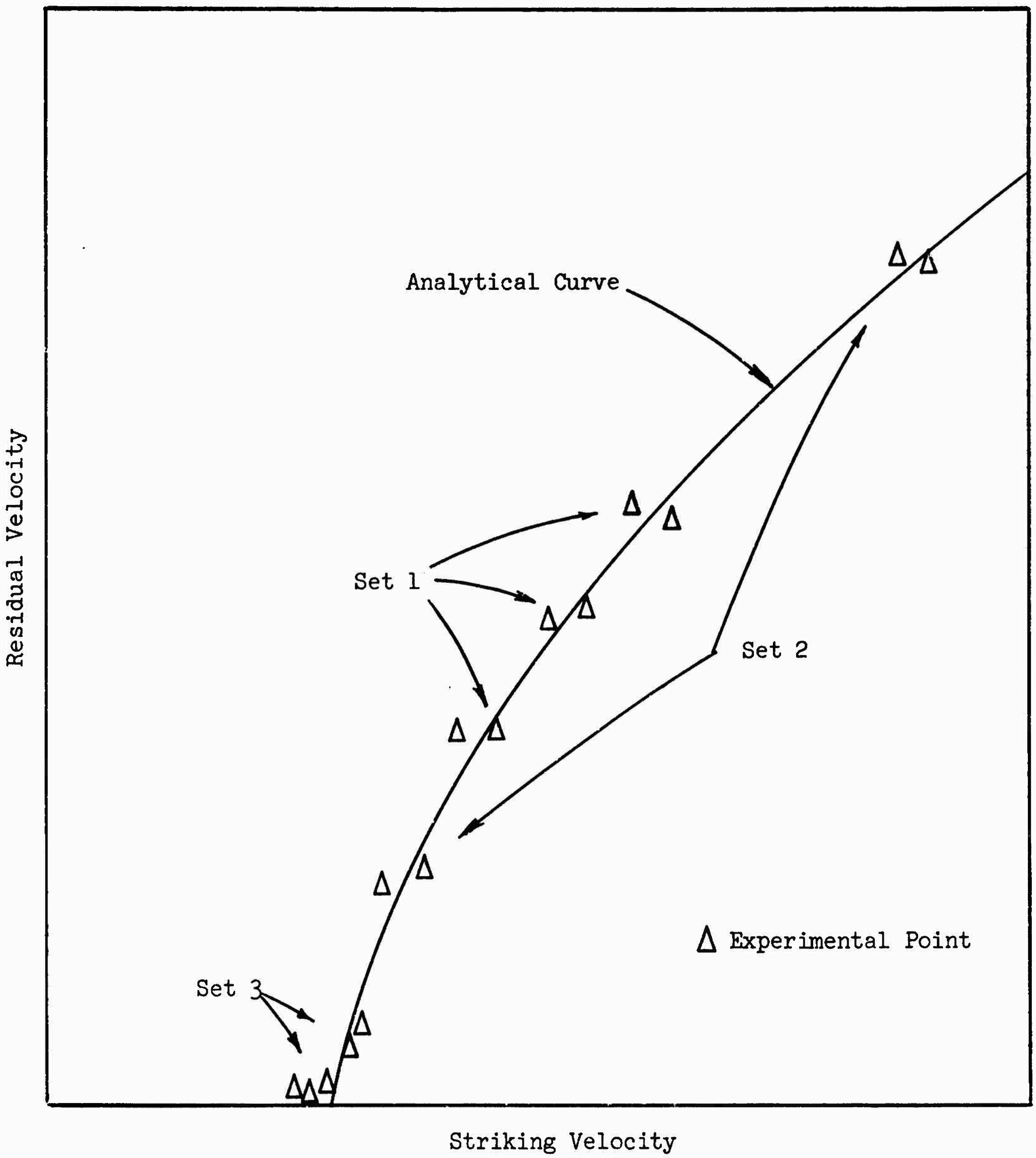

Figure A-2 GROUPING OF TEST SHOTS FOR DETERMINING RESIDUAL VELOCITY VERSUS STRIKING VELOCITY CURVE

Several mechanical properties of the target plate were also determined as a part of the experimental portion of this study.

A.2.3 Special Problems and Solutions

During the initial stages of the experimental portion of this study, several problems were encountered.

One problem encountered envolved the measurement of the residual velocity with a decade counter. During the early phase of this study, a determination of the residual velocity by means of a pair of velocity screens spaced five centimeters apart, close behind the target plate, was attempted. These screens were connected to a sensitive decade counter.

On the initial tests, the residual velocity measurements obtained from the counter differed significantly from the ballistic pendulum measurements, particularly at higher velocities (see decade counter measurements on Figure A-3). This discrepancy was thought due to small particles coming off the plate prior to the plug and/or the projectile coming through the plate. These small particles were traveling at velocities near the striking velocity, but had energy only sufficient to interrupt the first velocity screen, starting the decade counter. The counter was stopped when a more massive particle, such as the projectile or plug, interrupted the second screen. Two attempts were made to correct this situation. First, a spall shield was used in front of the first velocity screen after the target plate. This was a wooden plate with a hole in it which would permit the passage of only those particles leaving the plate almost normally. This did not solve the problem. Figure A-5 shows the residual velocity measurements with the spall shield in place. Second, the velocity screens were moved away from the plate. The "punchout" material was forced to pass through several sheets of paper before encountering the velocity screens. This also failed to solve the problem. Figure A-4 shows the velocity measurements with the paper sheets in place. Interposing several thicknesses of paper was used while firing at the 0.090" aluminum plate. The intent was to stop all particles other than the projectile and plug. The effect of the paper was to create a greater divergence between the measured ballistic-pendulum and decade-counter velocities. This result indicated that the particles had not been stopped, even when an excessive number of paper sheets were used (16 sheets). While the use of such a quantity of paper might not affect the ballistic pendulum reading appreciably at higher residual velocities, it most certainly would affect the readings at the lower residual velocities.

It appeared unwarranted to pursue this problem further, and this velocity measurement system was discontinued. Another factor leading to the discontinuation was that about 10 percent of the counter readings were obviously spurious. The cause of the obviously spurious results was not found, but it was possibly due to the high sensitivity of the counter and the proximity of the other electronic equipment.

Another problem expected and encountered, was the determination of the mass of the material affecting the ballistic pendulum. In the initial series of tests, the mass affecting the pendulum could not be determined with as high a degree of accuracy as had been anticipated. Therefore, the ballistic pendulum was modified so that a large percentage of the mass affecting the pendulum could be recovered and its weight determined.

Another minor problem encountered was that of the projectile tumbling in flight before striking the target plate. There was a high tendency for the short cylindrical projectile to tumble at muzzle velocities above 3600 fps, and a slight tendency for tumbling to occur in the 500 fps to 1000 fps muzzle velocity range. The tumbling of the projectile was apparently confined to these areas and was relatively intermittent even within these areas. No special attempt was made to correct the situation.

On the initial set of shots, some of the projectiles did not strike the target plate normally. A few projectiles were canted as much as 15 degrees when striking the target plate. The misalignment of this order, or less, does not change the qualitative features of the deformation and perforation processes. Its quantitative effect in this velocity regime is assumed to be small.

A.2.4 <u>Accuracy of Results</u>

The experimental results are sufficiently accurate for the purpose of this study. A maximum error of $\pm$ 10 percent in the residual velocities could exist at low residual velocity (< 500 fps), but this error decreases as the residual velocity increases (at V_r of about 2000 fps, the error is $\pm$ 2 percent). The maximum absolute error in the residual velocity expected in our experiments is on the order of $\pm$ 30 feet per second.

The accuracy of the test results is primarily fixed by the accuracy of the determination of the mass of the pendulum and the measurement of the pendulum swing distance.

The distance through which the pendulum moves is easily determined within 0.05 centimeters. For the majority of the tests which resulted in residual velocities of less than 500 fps, the swing distance of the pendulum was more than 1 centimeter. The maximum error of the pendulum swing measurement was $\pm$ 5 percent. The range of the residual velocity was known and a relatively large movement of the pendulum (hence a smaller error) was obtained by proper variation of the pendulum's mass.

The determination of the mass affecting the pendulum is more difficult since it is not practical to recover every bit of the mass from the pendulum. Fortunately, this is not required. If all mass other than the projectile were disregarded, the error in the residual velocity would be less then $\pm$ 10 percent in all the plates tested with the exception of the 0.25-inch aluminum and 0.1-inch titanium plates. For these two plates, the error incurred by disregarding the mass other than the projectile could run as high as $\pm$ 25 percent. The recovery of any relatively large mass other than the projectile, such as a plug, considerably reduced these error figures.

The errors in the determination of the residual velocity were less than $\pm$ 5 percent for V_r less than 1000 fps, and less than $\pm$ 3 percent for V_r greater than 1000 fps.

A.2.5 Reduction of the Data and the Determination of the Critical Perforation Velocity

The experimental data furnished are a sequence of striking velocities (V_s) and the corresponding residual velocity after perforation (V_r). If the projectile did not perforate the plate, the residual velocity was zero. One of the main problems of the experimental procedure is the determination of the critical perforation velocity, V_c. This velocity is the striking velocity below which there is no perforation and above which there is perforation.

The critical perforation velocity cannot be precisely measured. A number of factors with random variations, such as canting or nonuniformity of plate strength, limit the sharpness of the transition from nonperforating impact to perforating impact. A preliminary estimate of the critical perforation velocity was obtained by taking the highest experimental velocity where no perforation occurred. This is a lower bound to the critical perforation velocity. The difficulty in obtaining precisely the striking velocity near the critical velocity requires an extrapolation from the residual velocities at higher striking velocities.

The analytical portion of the study indicates that the residual velocity-striking velocity curve is of the form for a given plate and projectile.

$$V_r^2 = C_1 V_s^2 - C_2 \qquad V_s > \sqrt{\frac{C_2}{C_1}}$$

$$= 0 \qquad V_s < \sqrt{\frac{C_2}{C_1}}$$

where C_1 and C_2 are constants.

A least square fit of the residual velocity and the striking velocity obtained the constants C_1 and C_2. The critical perforation velocity, V_c, is the striking velocity at which the residual velocity just goes to zero. Thus,

$$V_c = \sqrt{\frac{C_2}{C_1}}$$

The computation of the critical perforation velocity by the direct determination of the constants was very inaccurate. The following procedure was applied to determine V_c. The values of V_r/V_s were plotted versus V_s. The limiting value of V_r/V_s as V_s becomes large was easily determined. Denote this limiting value by $(V_c/V_s)_\infty$. The striking velocity at which the ratio V_r/V_s attains one-half of the limiting ratio was also determined. Denote this velocity by V_1. Using the analytical form of the residual velocity curve,

$$V_c = 0.89\ V_1$$

A.3 Experimental Results

A.3.1 Phasing of Test and General Data

The experiments obtained the residual velocity vs. striking velocity curves for use in checking and modifying various penetration models. Three types of projectiles were shot at various thicknesses of the types of metal target plates.

Properties of the three types of projectiles and the metal plates used in the experimental phases of this study are given in Tables I and II.

TABLE I

PROJECTILE DATA			
Type	Diameter	Length	Weight*
1	0.218 inch	0.250 inch	18.3 grains
2	0.218 inch	0.375 inch	27.7 grains
3	0.299 inch	0.341 inch	47.3 grains
Material - 4340 steel-normalized Yield Stress - 140,000 psi Hardness - Brinell 388 Rockwell C-42			

*approximate

TABLE II

METAL TARGET PLATE DATA			
Material	Thickness (inches)	Yield Stress (psi)	Hardness
Aluminum	0.010, 0.050, 0.090, 0.250	74,000	Vickers 180 Rockwell A 55.5
Titanium	0.032, 0.048, 0.076, 0.097	117,500	Vickers 320 Rockwell A 67.75

The experimental portions of this study were conducted in two phases:

Phase I - Residual velocity (V_r) versus striking velocity (V_s) curves were determined for four thicknesses for each of two target materials using a single type of projectile. These tests provided data for verification and modification of the existing penetration models.

Phase II - V_r vs V_s curves were determined for two thicknesses of one target material using two different types of projectiles. These tests provided data for checking the modified penetration models.

An additional phase of the experimental study was the determination of the physical properties of the target and projectile materials. Material pr··erties obtained were stress-strain curves, Young's modulus, and the tensile yield stress.

A.3.2 Critical Velocity and Residual Velocity Measurements

A summary of the critical perforation velocities, V_c, generated on this program is given in Table III.

Phase I Tests - V_r vs V_s curves were determined for four thicknesses of 7075-T6 aluminum target material and for four thicknesses of titanium 2.5 Sn 5 Al aluminum alloy target material. Type 1 projectiles were used for this experimental phase.

TABLE III

TARGET MATERIAL, THICKNESS, V_c

		Critical Perforation Velocity, V_c* (fps)		
		Projectile		
Material	Thickness (inches)	1	2	3
Aluminum 7075-T6	.250	1450		
	.090	750	650	650
	.050	650	550	500
	.010	500 ± 100		
Titanium 5 Al 2.5 Sn	.097	1200		
	076	1050		
	.048	900		
	.032	800 ± 100		

*Values of V_c are ± 50 fps unless otherwise indicated.

Figures 3 through 10 present the data obtained in Phase I and show both the experimental points and an approximate V_r vs V_s curve. Figures 11 and 12 show the V_r vs V_s curves of the two tested target materials as they appear as a family.

<u>Phase II Tests</u> - Phase II tests were conducted using projectile types 2 and 3 and 0.050 and 0.090 7075-T6 aluminum target plates.

Figures 13, 14, 15, and 16 present the data obtained, showing both the experimental points and an approximate V_r vs V_s curve. The family of V_r vs V_s curves of the three types of projectiles for each of the two plate thicknesses tested are shown in Figure 17 and 18.

A summary of the material properties tests is given in Table IV and a typical set of data is shown plotted in Figure 19.

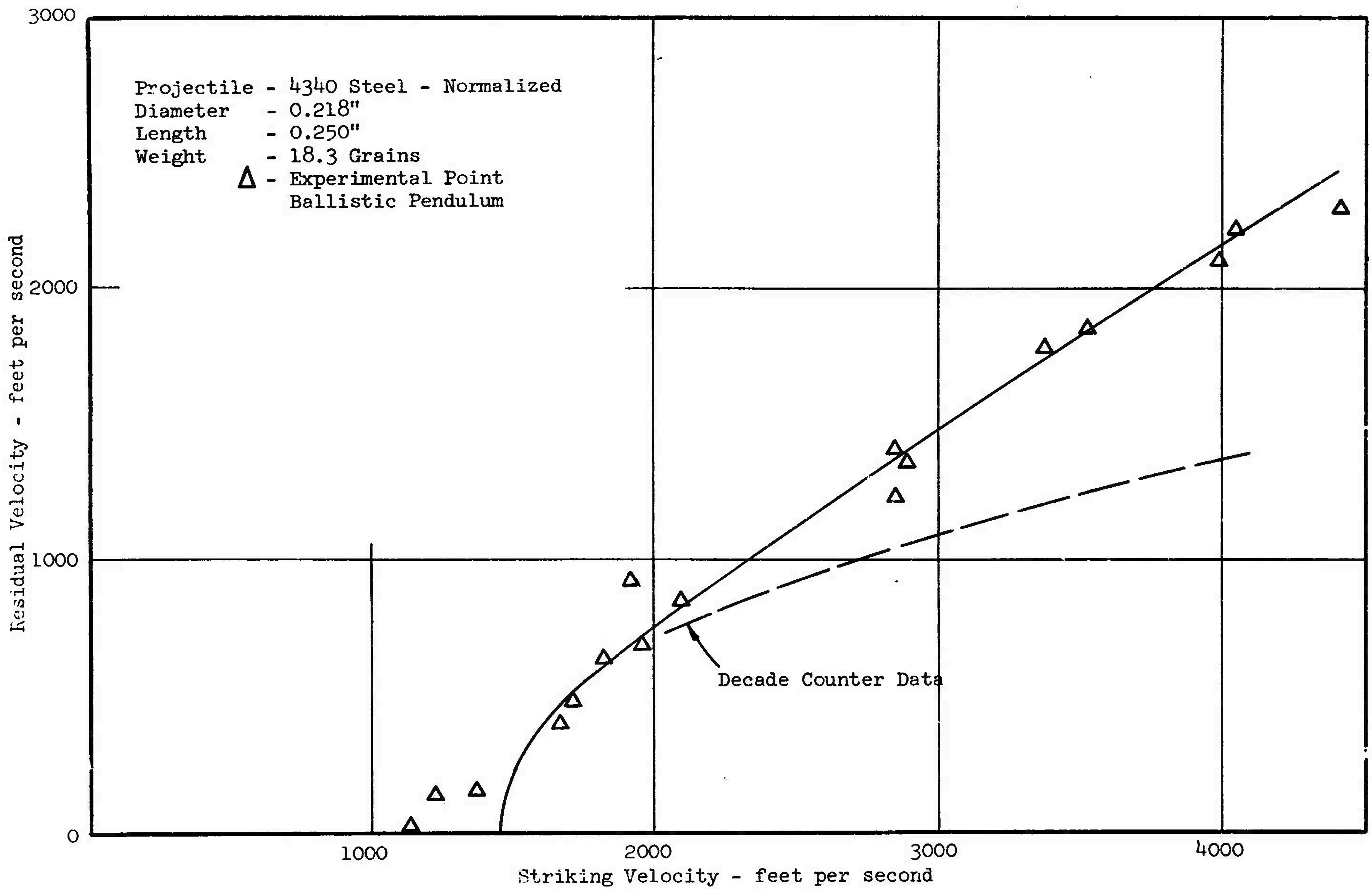

Figure A-3 RESIDUAL VELOCITY VS. STRIKING VELOCITY FOR 0.250" 7075-T6 ALUMINUM TARGET MATERIAL

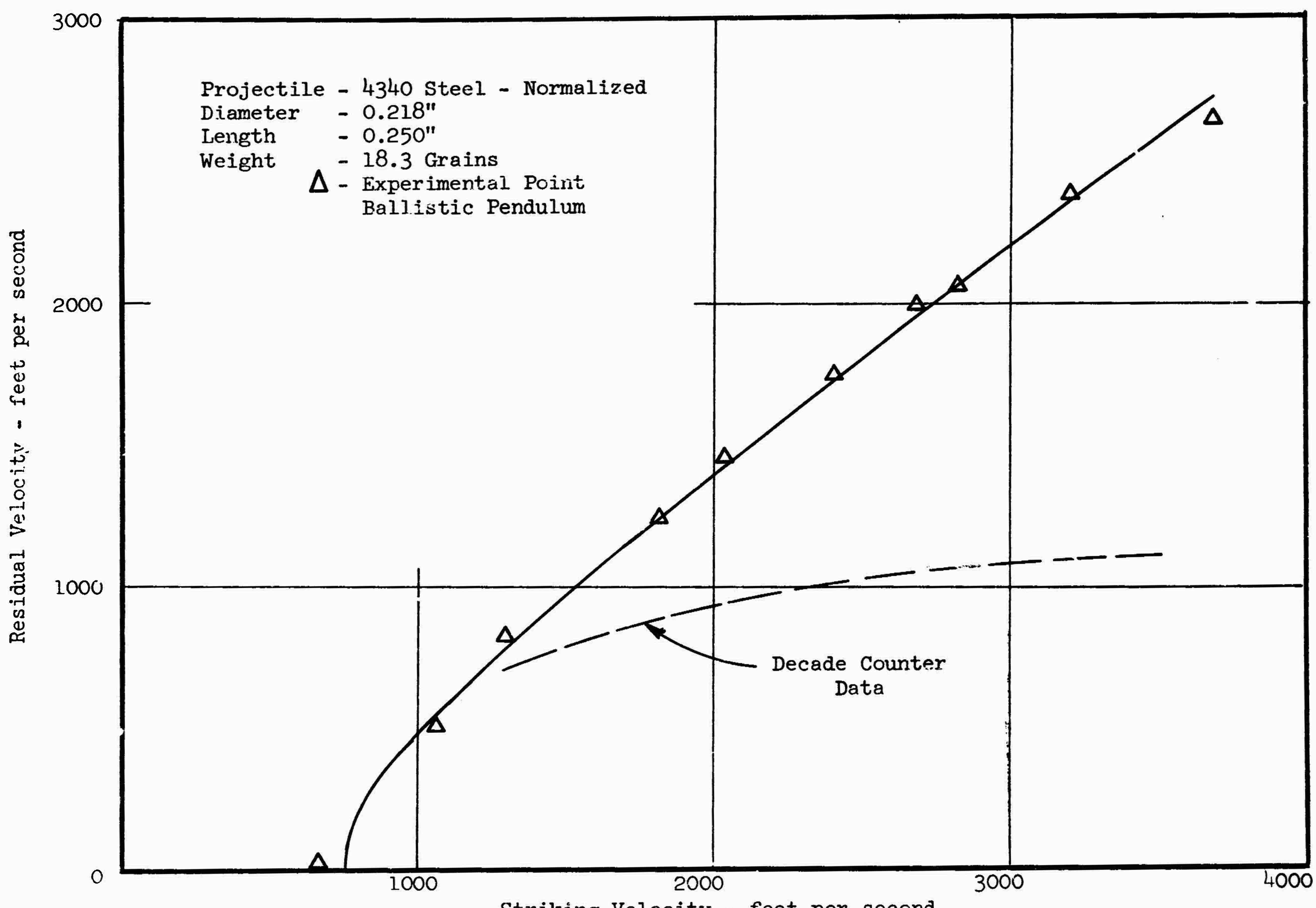

Figure A-4 RESIDUAL VELOCITY VS. STRIKING VELOCITY FOR 0.090" 7075-T6 ALUMINUM TARGET MATERIAL

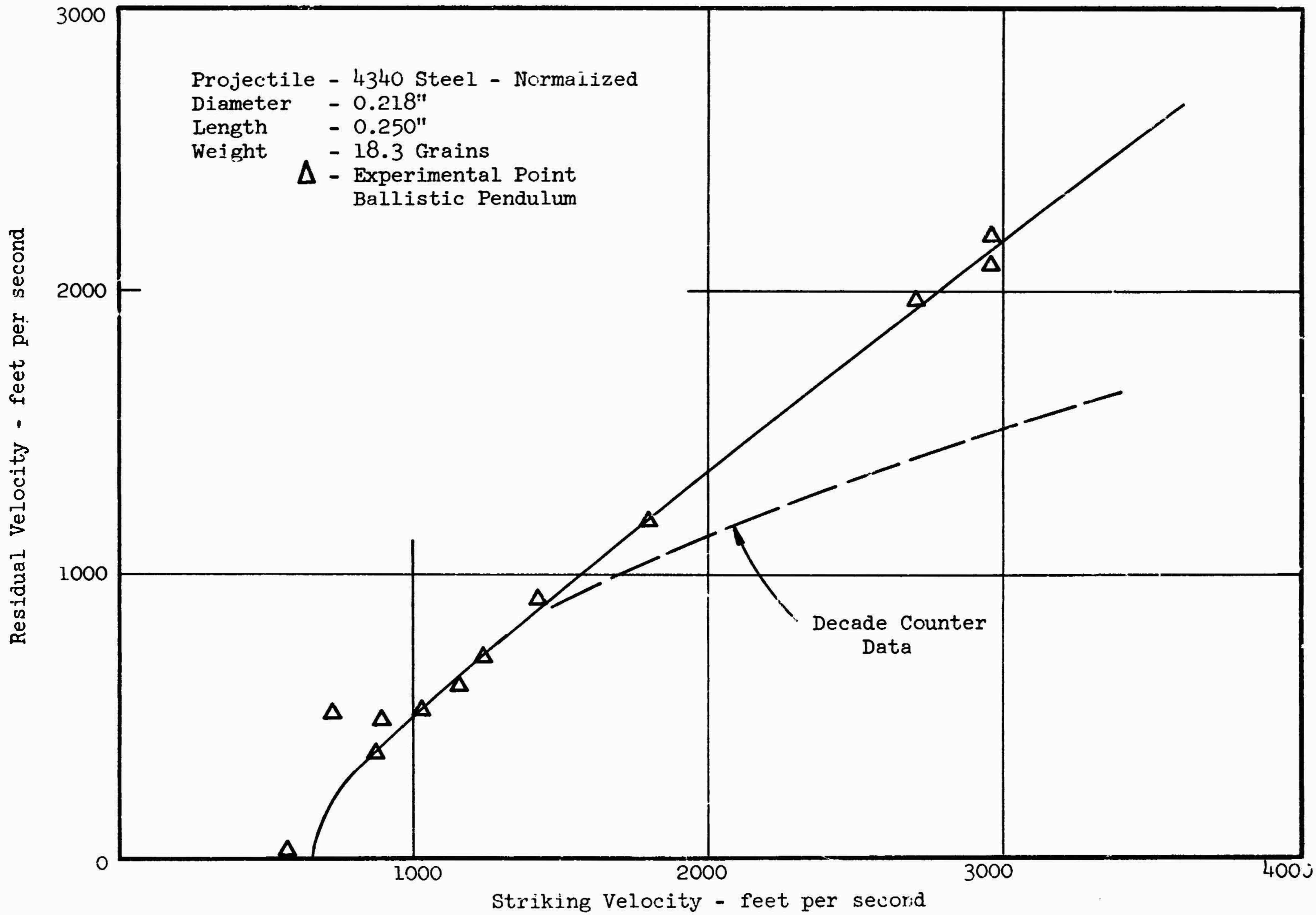

Figure A-5 RESIDUAL VELOCITY VS. STRIKING VELOCITY FOR 0.050" 7075-T6 ALUMINUM TARGET MATERIAL

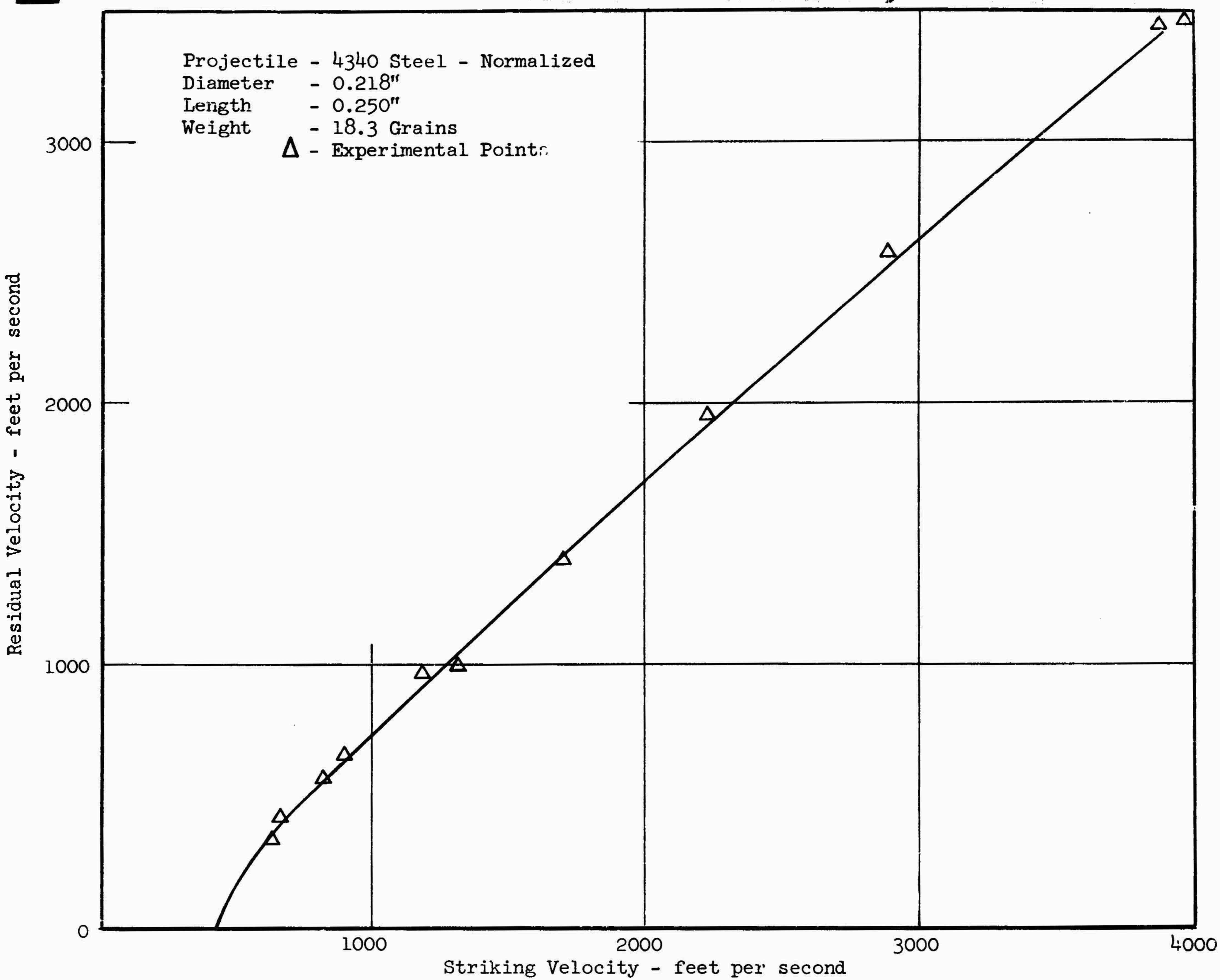

Figure A-6 RESIDUAL VELOCITY VS. STRIKING VELOCITY FOR 0.010" 7075-T6 ALUMINUM TARGET MATERIAL

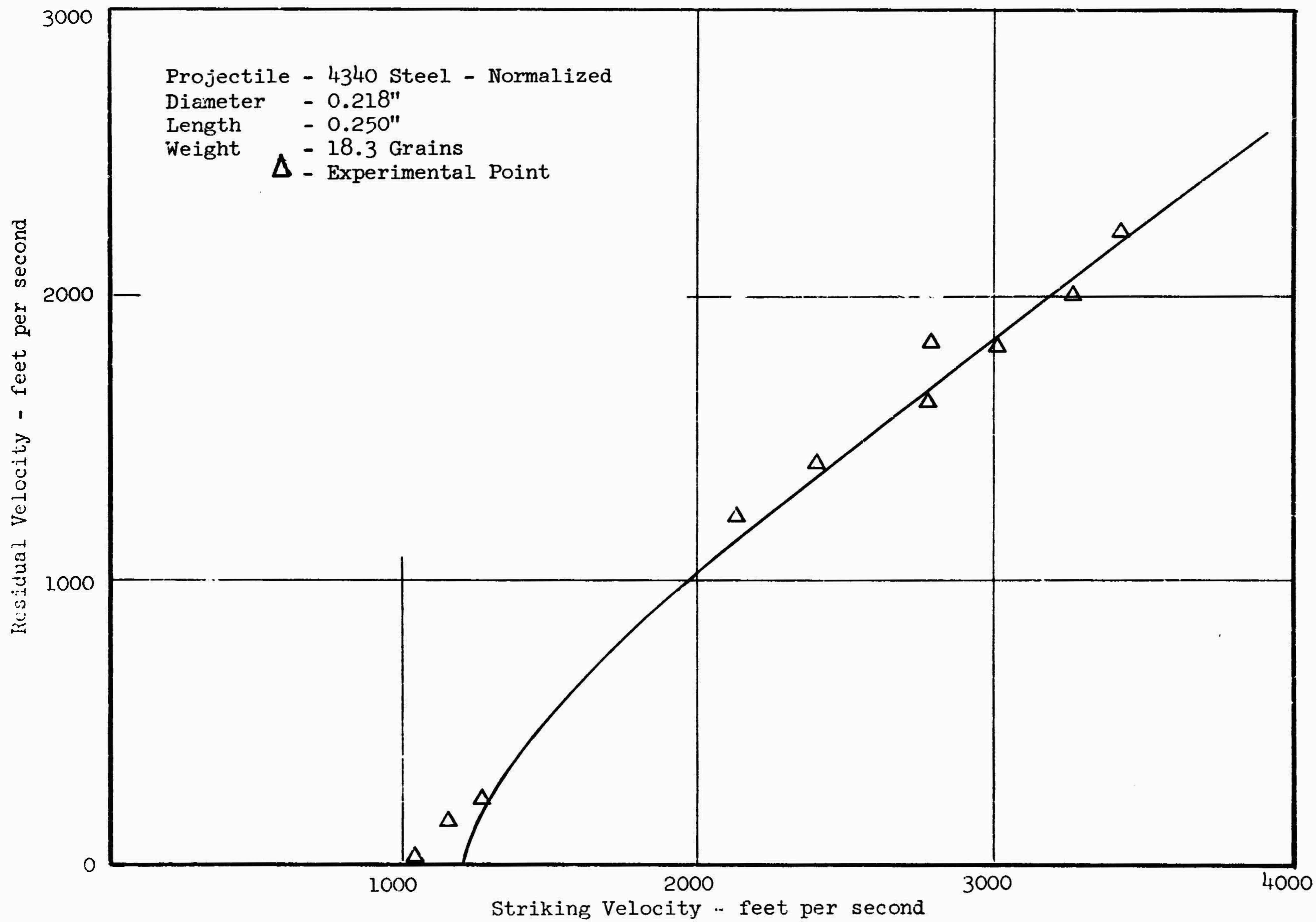

Figure A-7 RESIDUAL VELOCITY VS. STRIKING VELOCITY FOR 0.100" TITANIUM ALLOY TARGET MATERIAL

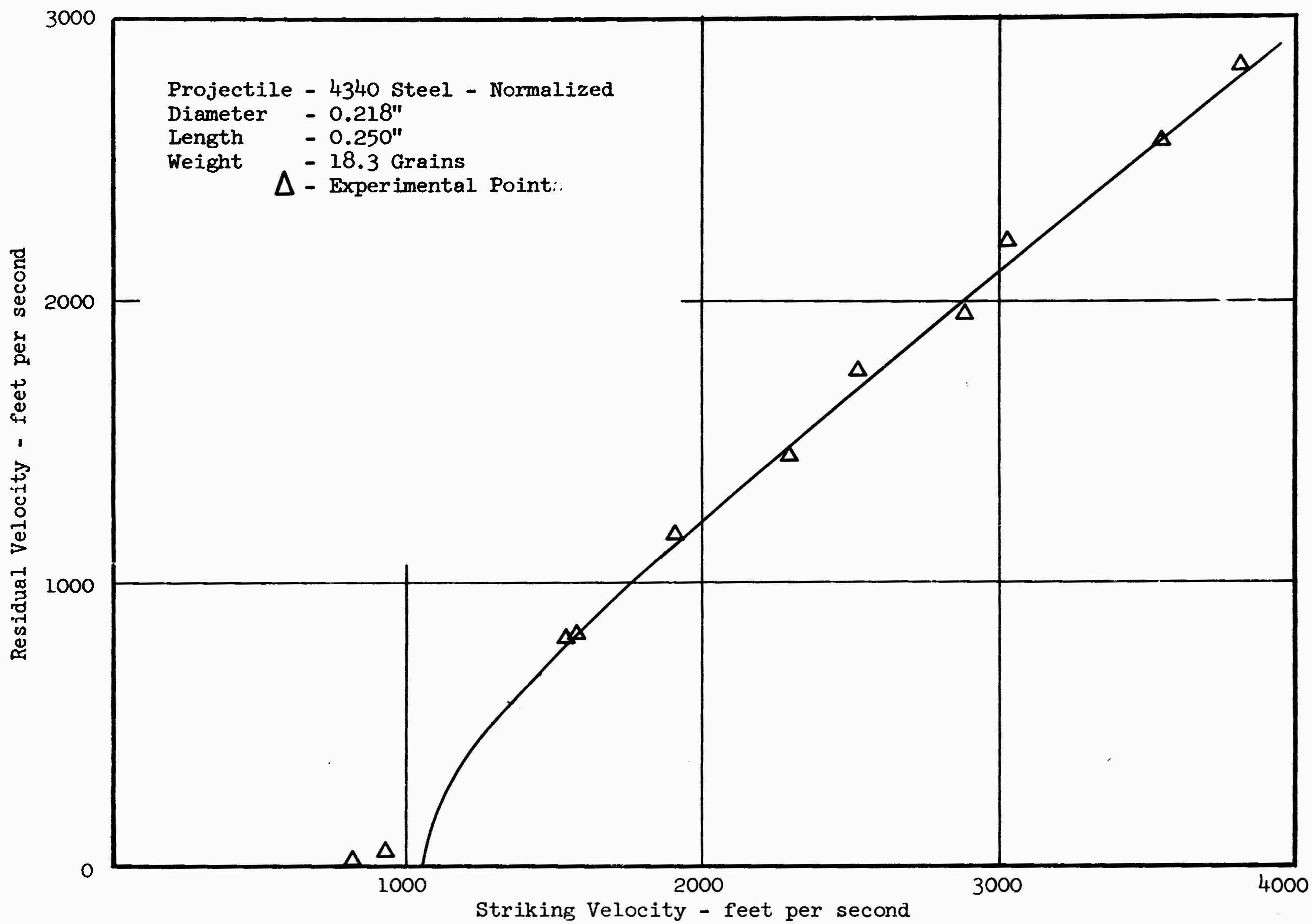

Figure A-8 RESIDUAL VELOCITY VS. STRIKING VELOCITY FOR 0.076" TITANIUM ALLOY TARGET MATERIAL

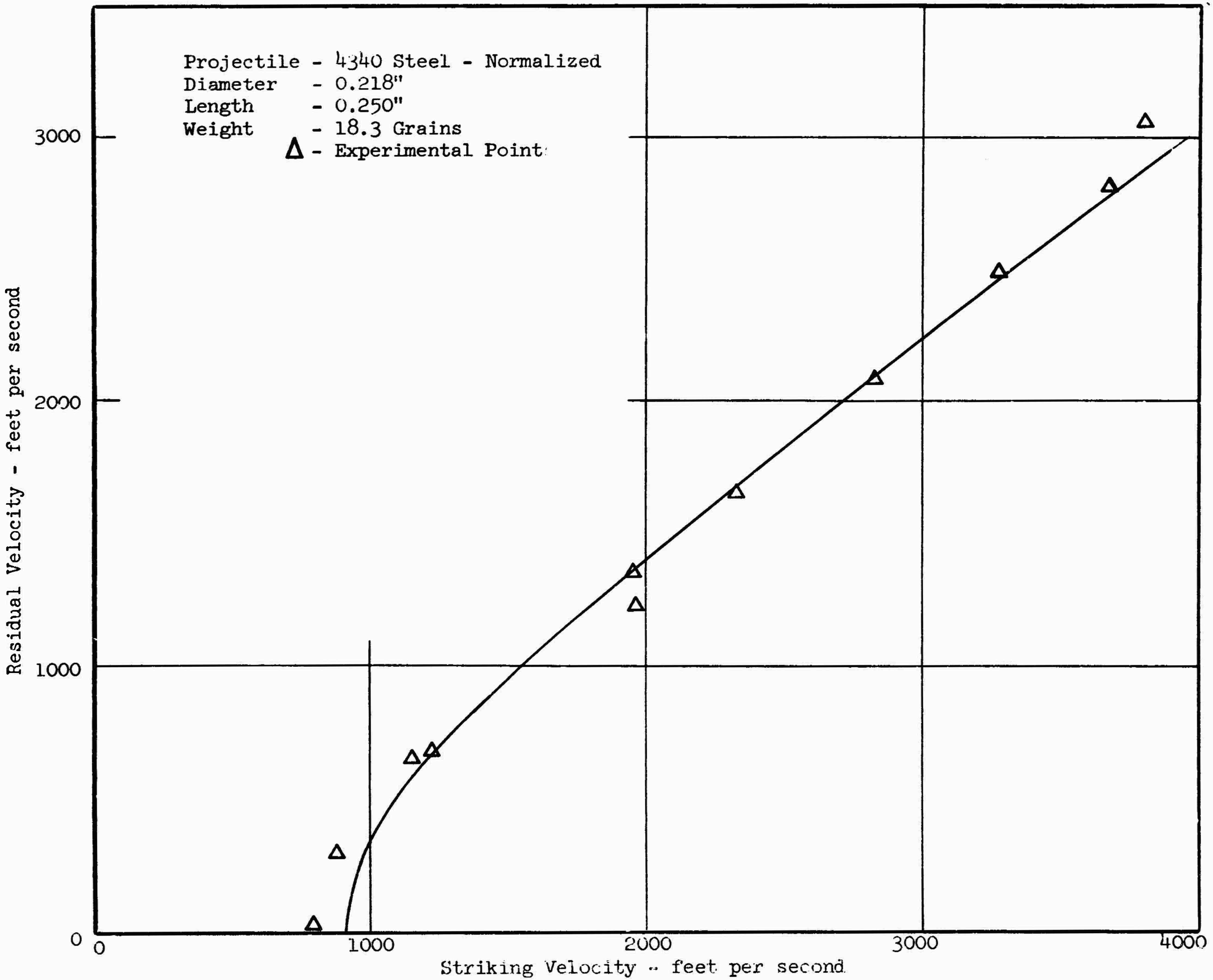

Figure A 9 RESIDUAL VELOCITY VS. STRIKING VELOCITY FOR 0.048" TITANIUM ALLOY TARGET MATERIAL

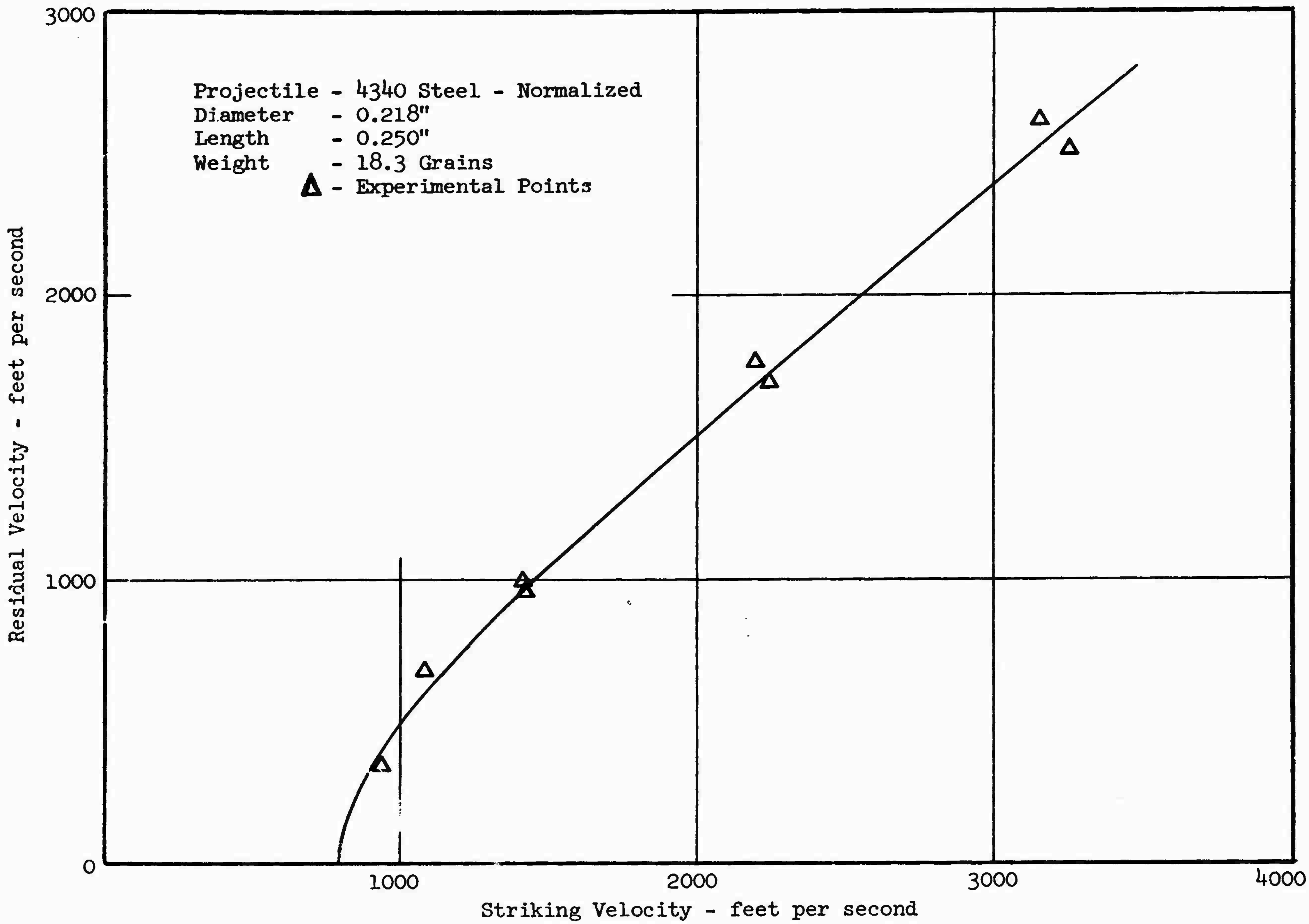

Figure A-10 RESIDUAL VELOCITY VS. STRIKING VELOCITY FOR 0.032" TITANIUM ALLOY TARGET MATERIAL

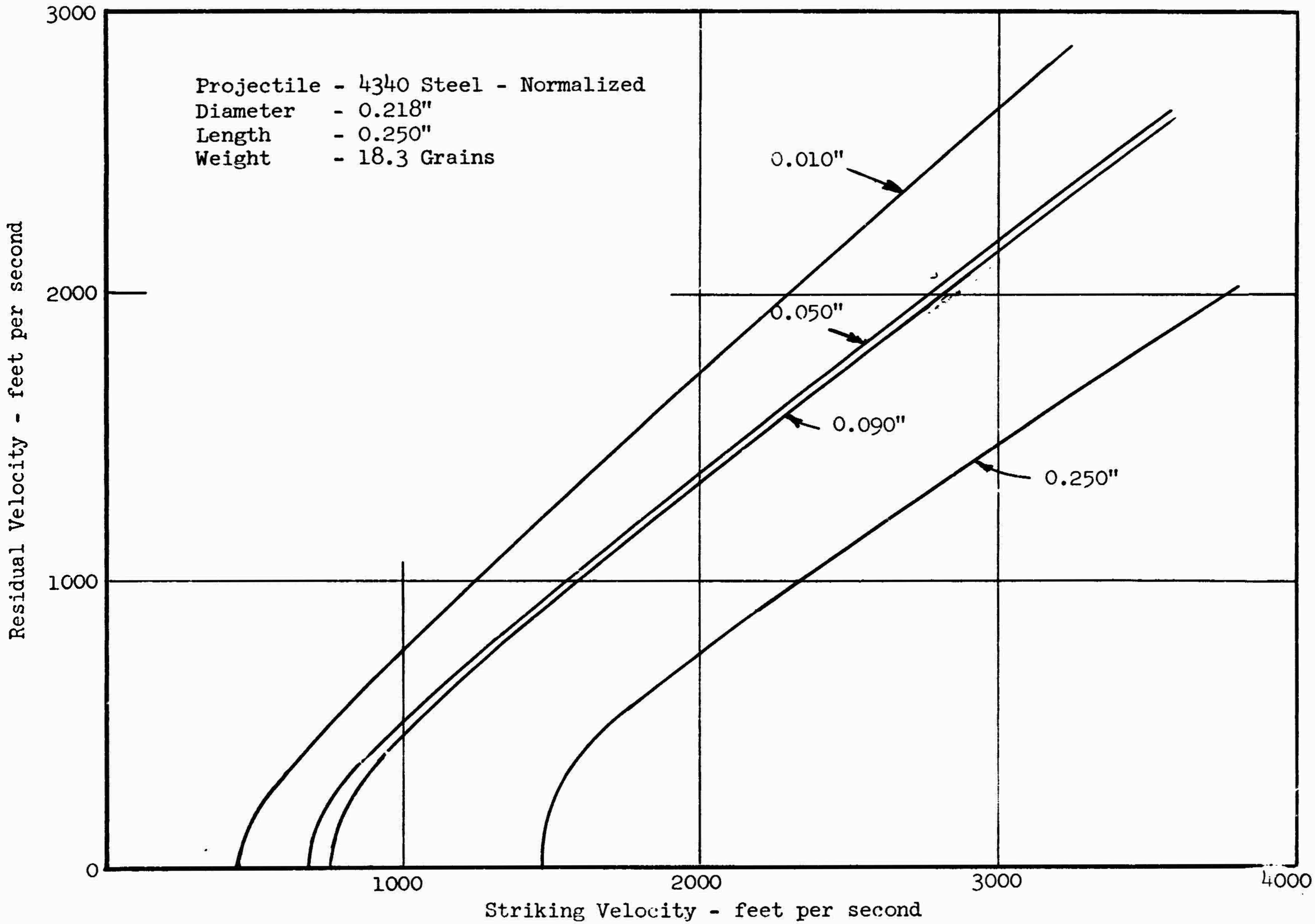

Figure A-11 RESIDUAL VELOCITY VS. STRIKING VELOCITY AS A FUNCTION OF TARGET THICKNESS FOR 7075-T6 ALUMINUM TARGET MATERIAL

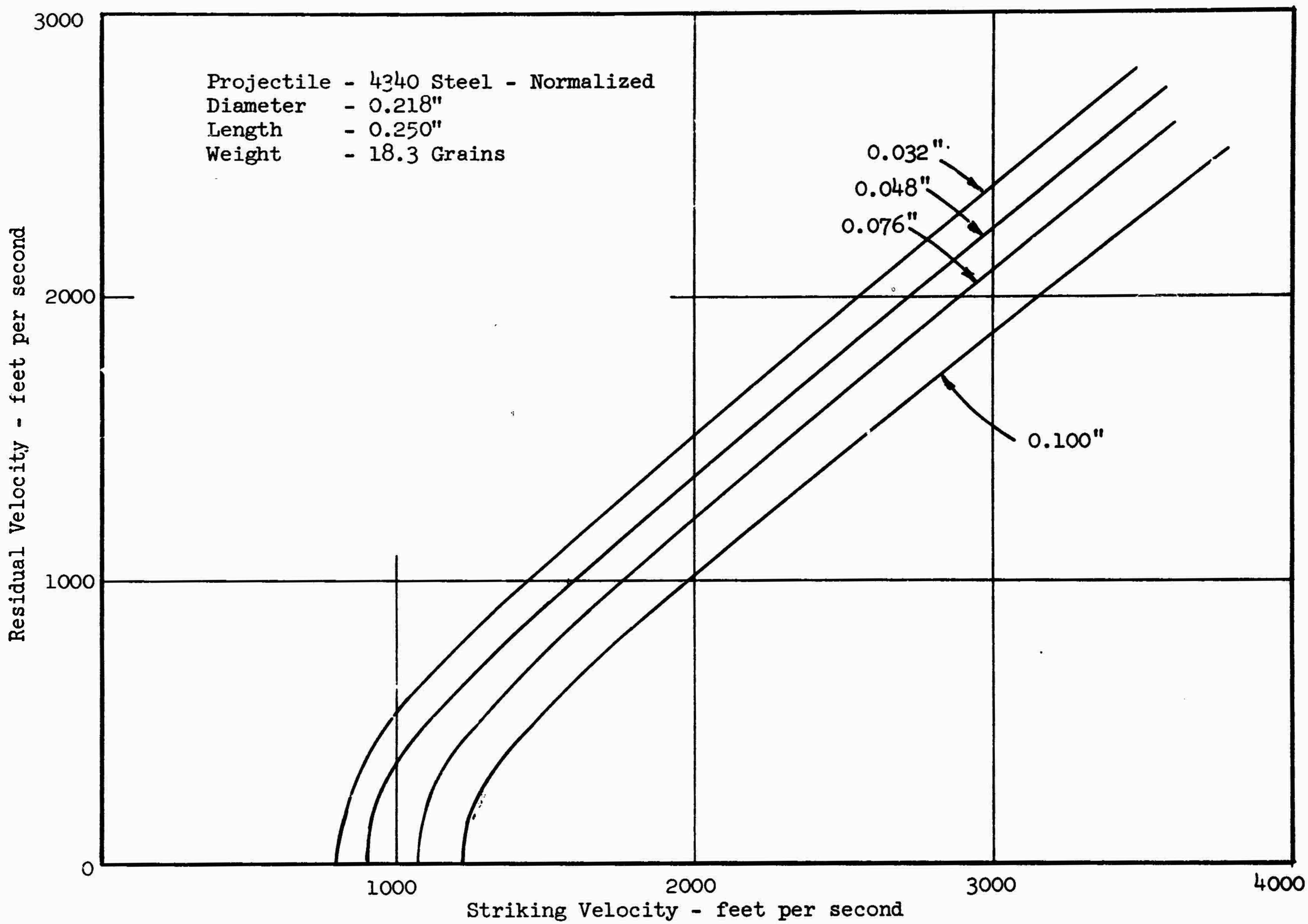

Figure A-12 RESIDUAL VELOCITY VS. STRIKING VELOCITY AS A FUNCTION OF TARGET THICKNESS FOR TITANIUM ALLOY TARGET MATERIAL

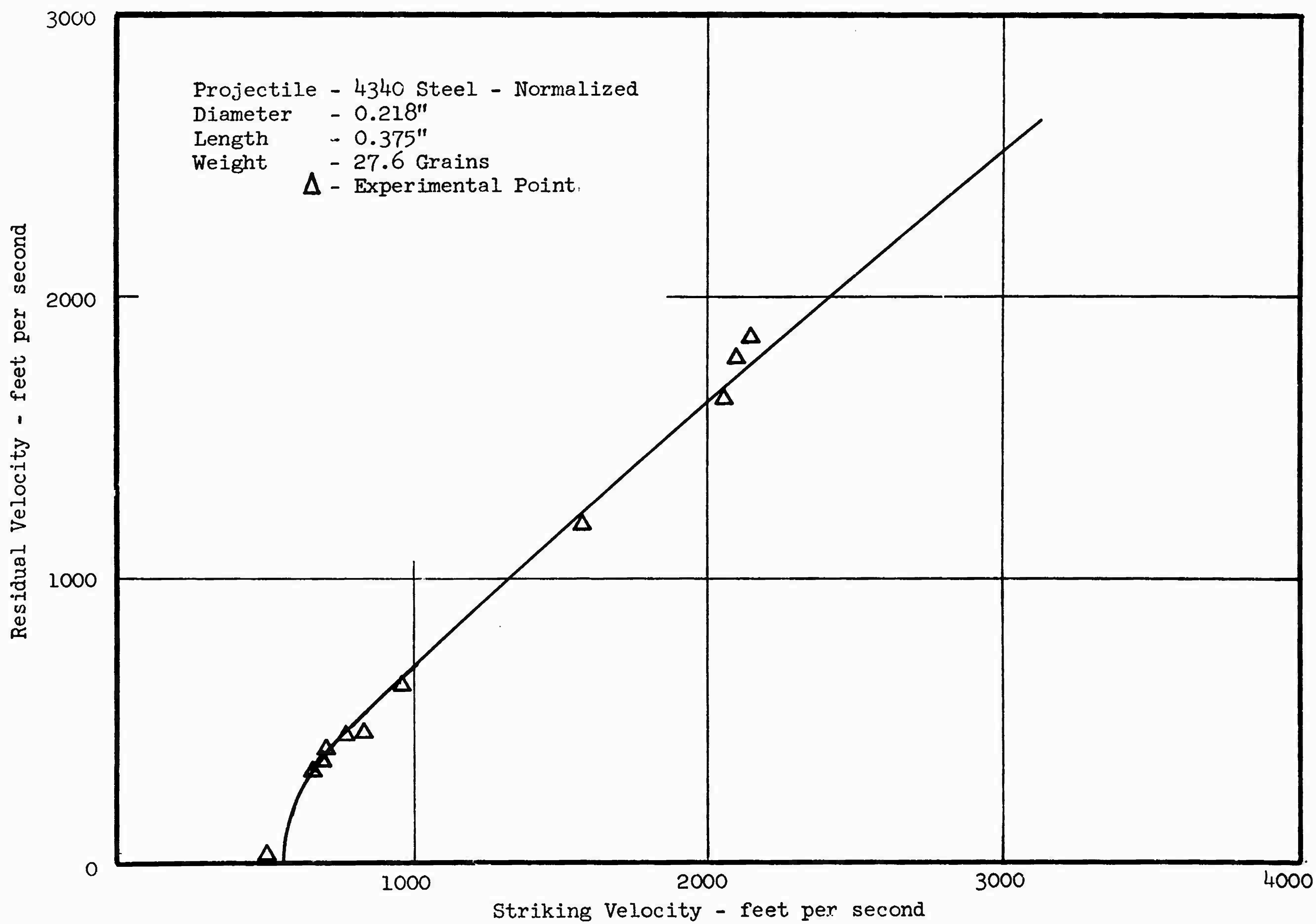

Figure A-13 RESIDUAL VELOCITY VS. STRIKING VELOCITY FOR 0.050" 7075-T6 ALUMINUM TARGET MATERIAL

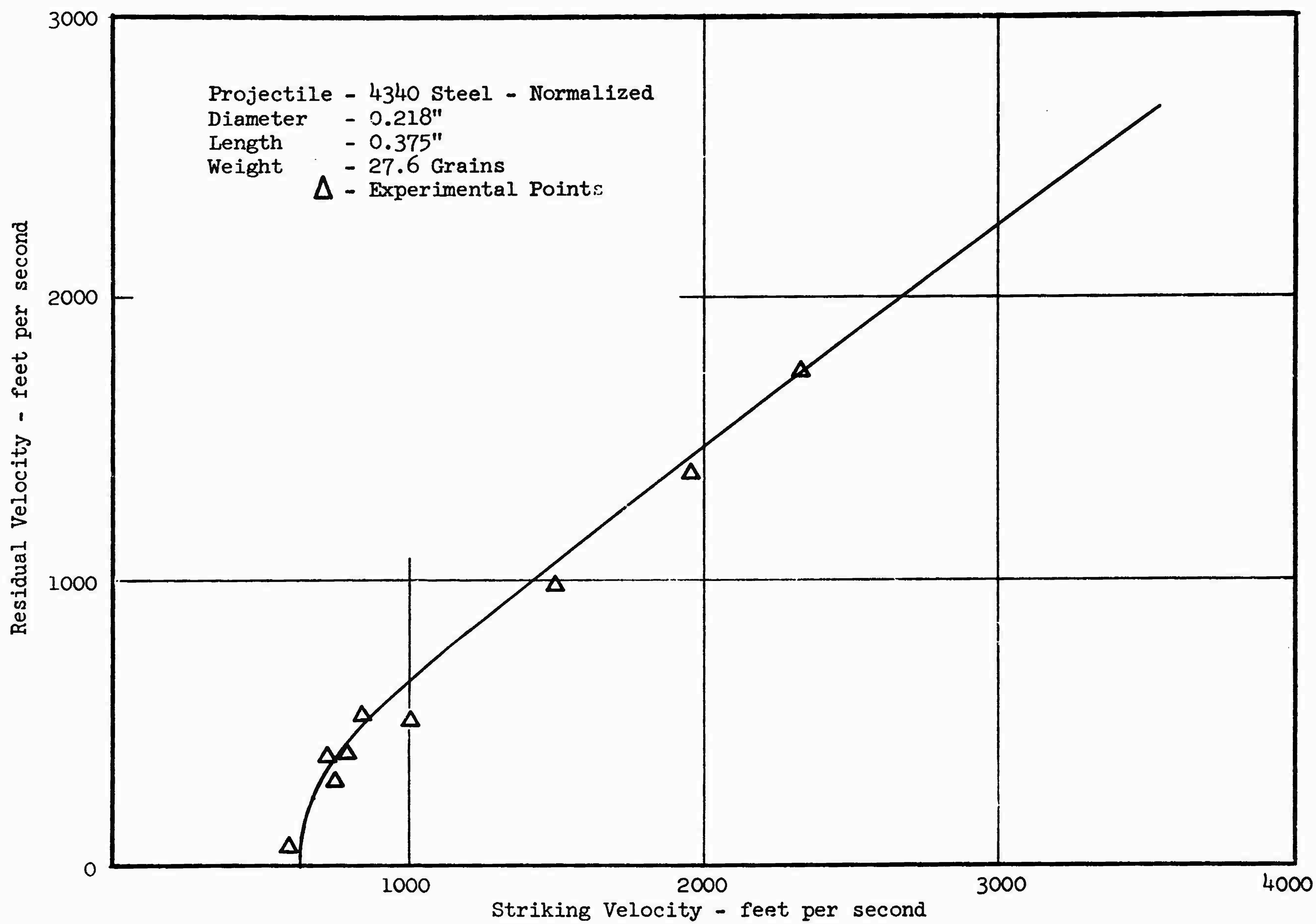

Figure A-14 RESIDUAL VELOCITY VS. STRIKING VELOCITY FOR 0.090" 7075-T6 ALUMINUM TARGET MATERIAL

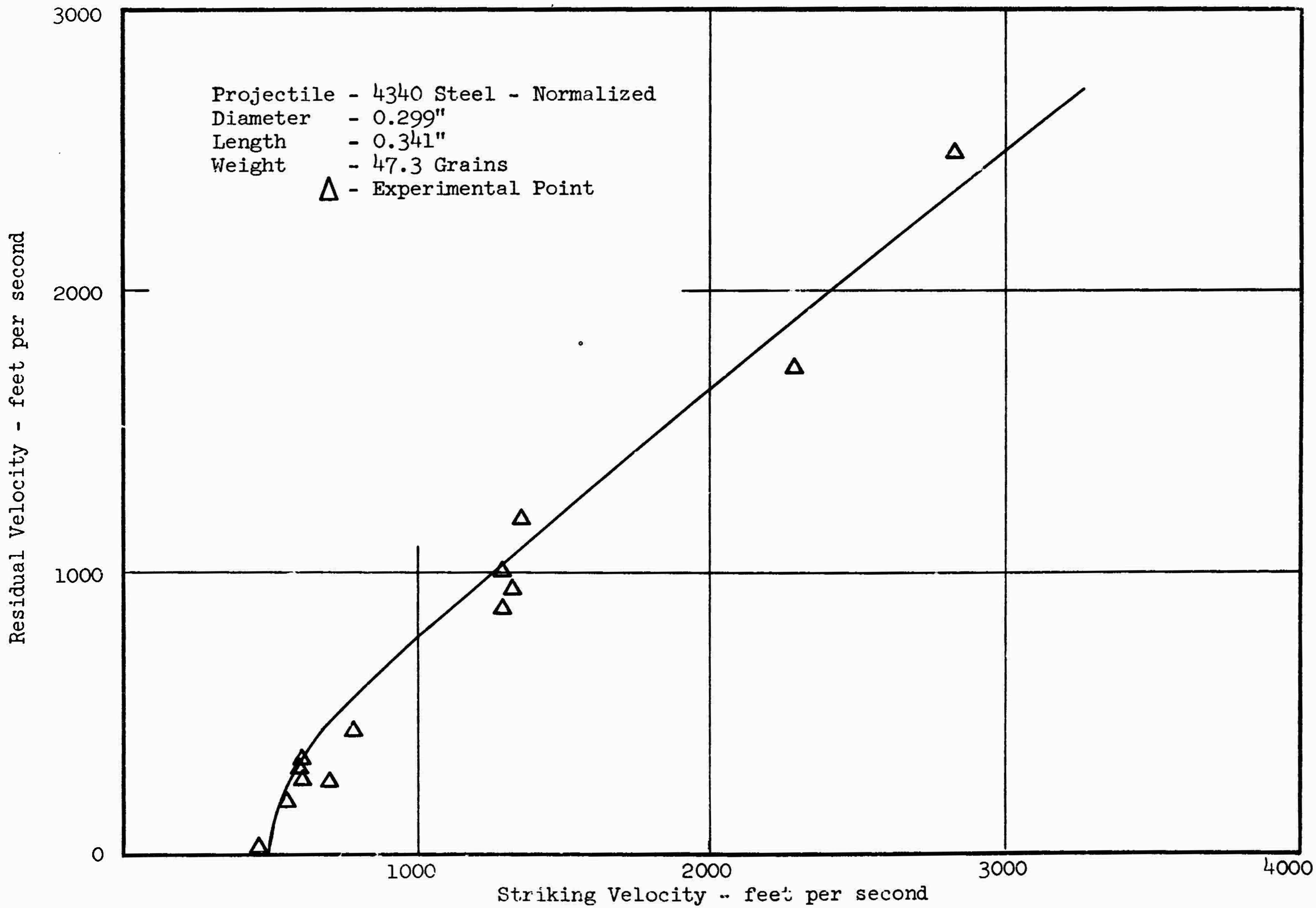

Figure A-15 RESIDUAL VELOCITY VS. STRIKING VELOCITY FOR 0.050" 7075-T6 ALUMINUM TARGET MATERIAL

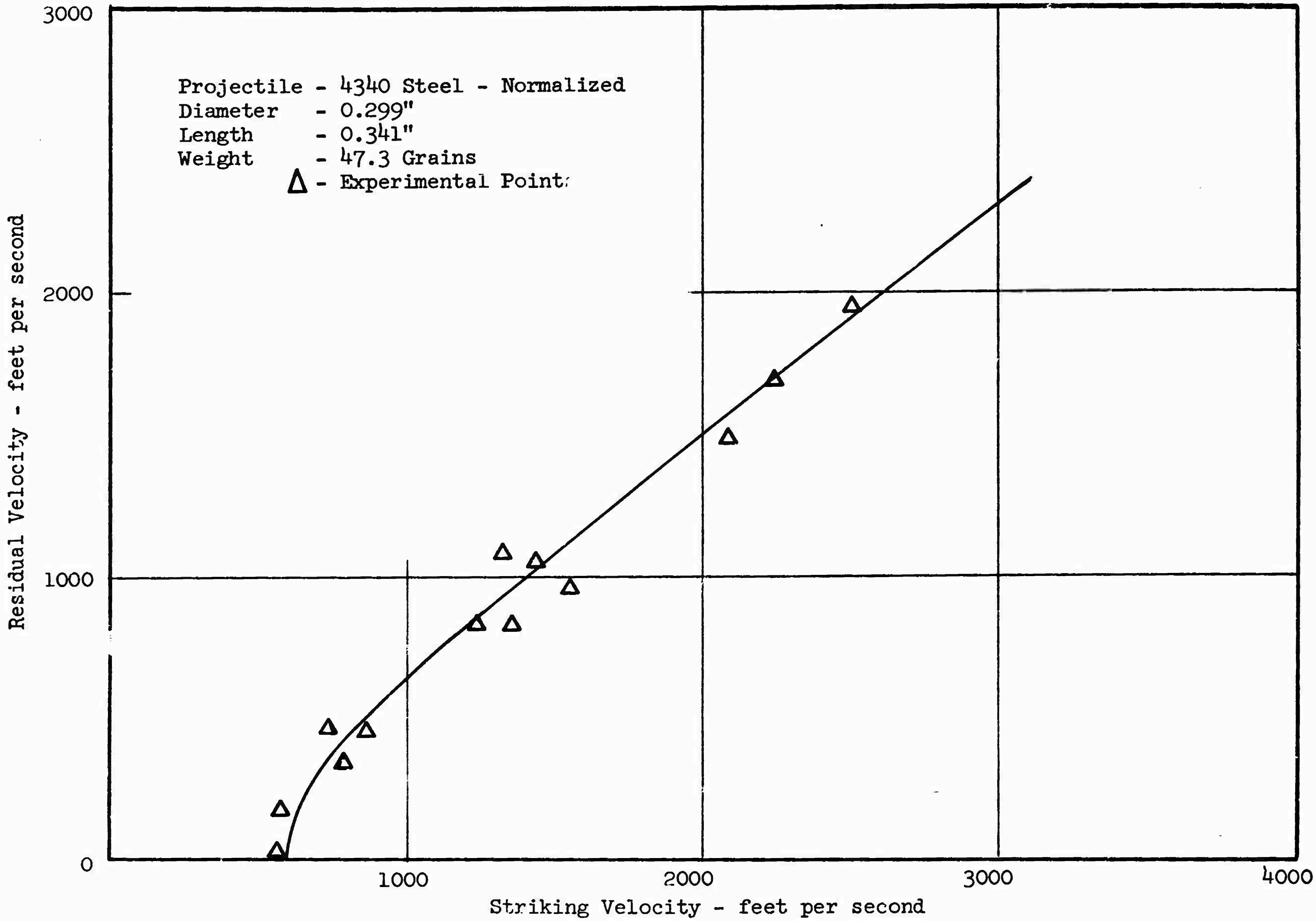

Figure A-16 RESIDUAL VELOCITY VS. STRIKING VELOCITY FOR 0.090" 7075-T6 ALUMINUM TARGET MATERIAL

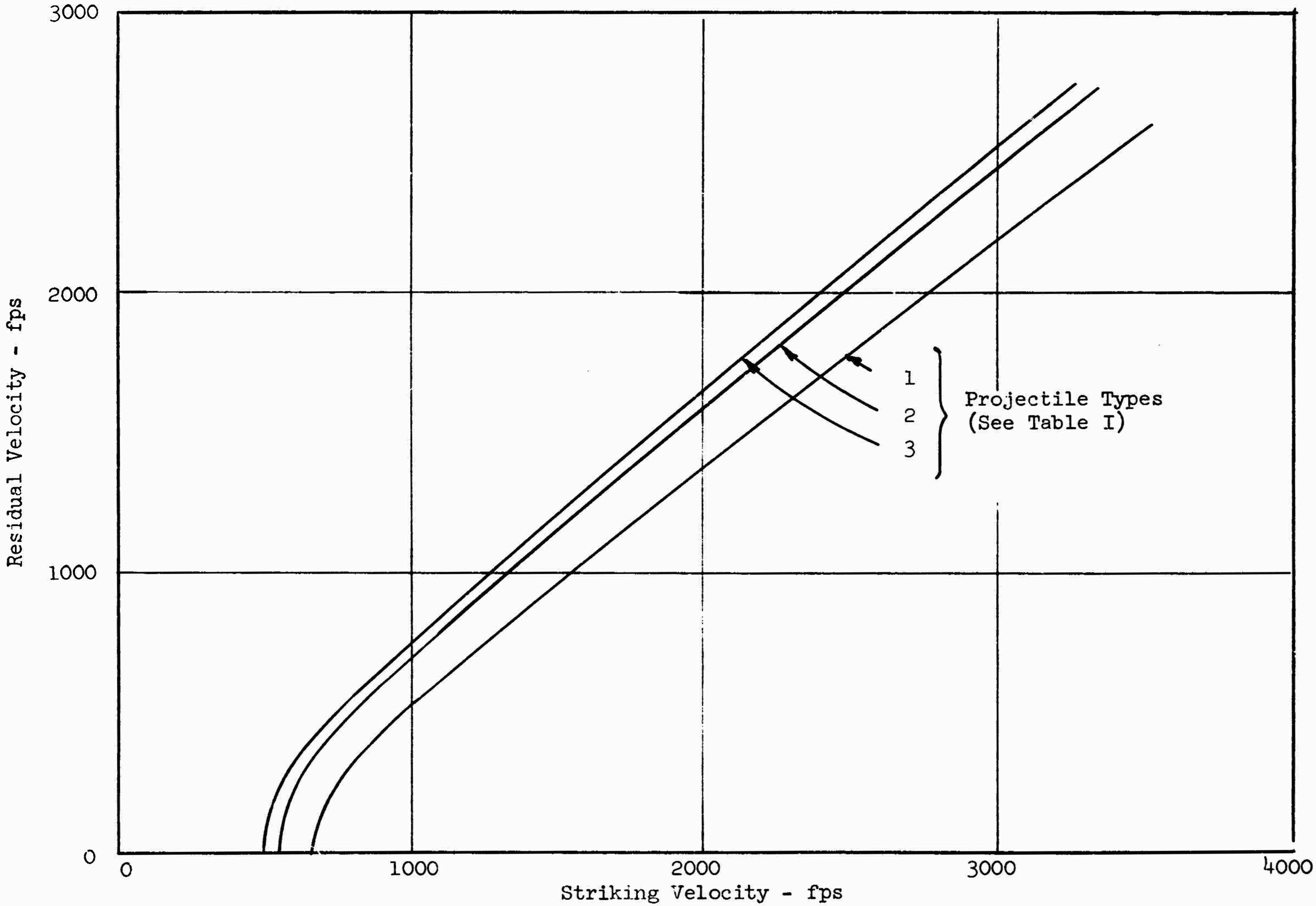

Figure A-17 RESIDUAL VELOCITY VS. STRIKING VELOCITY AS A FUNCTION OF PROJECTILE GEOMETRY FOR 0.050 INCH THICK 7075-T6 ALUMINUM

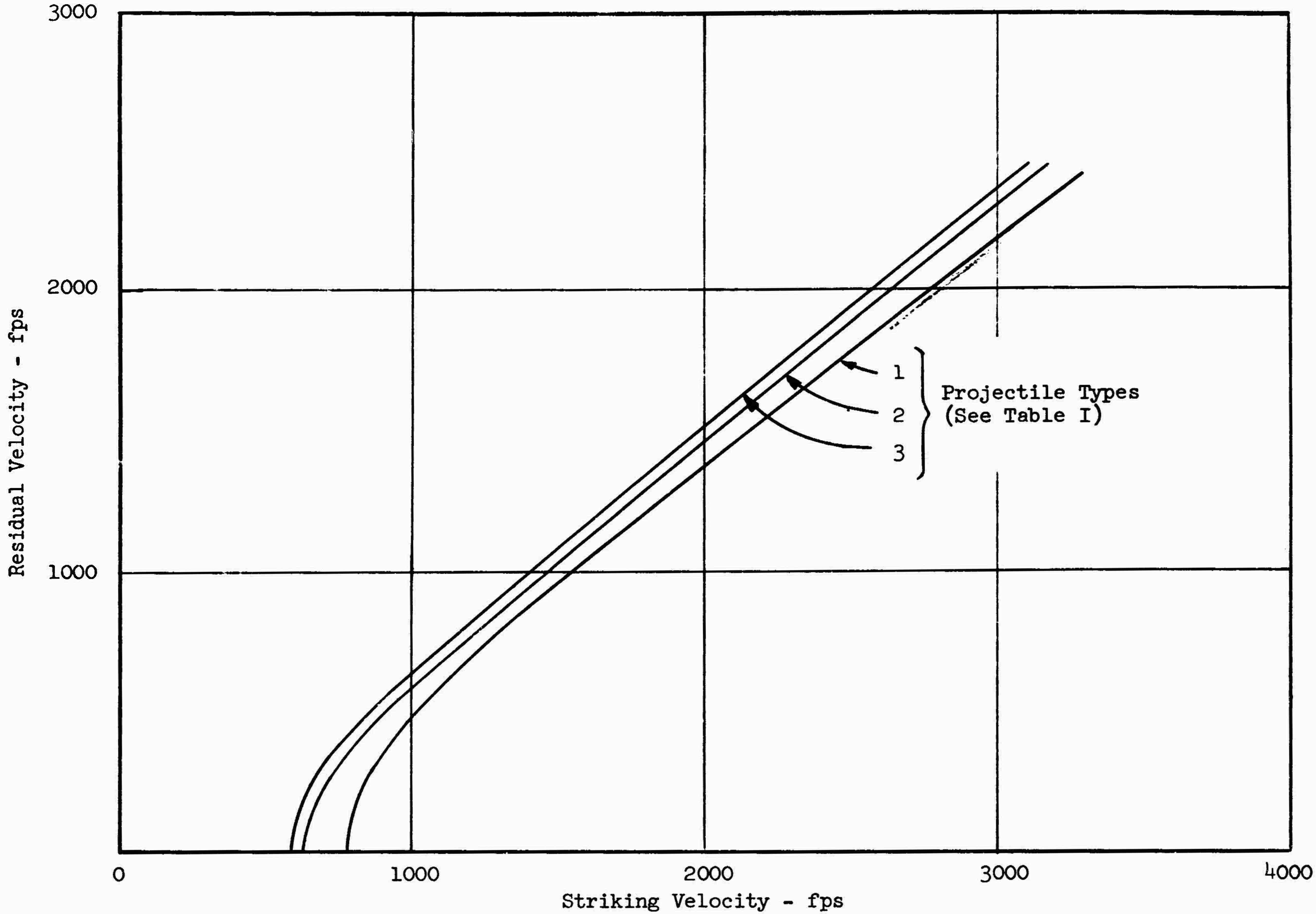

Figure A-18 RESIDUAL VELOCITY VS. STRIKING VELOCITY AS A FUNCTION OF PROJECTILE GEOMETRY FOR 0.090 INCH THICK 7075-T6 ALUMINUM

TABLE IV

MATERIAL PROPERTIES					
Material: 7075-T6 Aluminum					
Thickness (inches)	Young's Modulus (psi)	Yield Stress (psi)	Hardness: Vickers	Hardness: Rockwell A-Scale	Ultimate Stress* (psi)
0.250	10.2×10^6	75,500	190	56.0	83,500
0.090	10.1×10^6	74,500	195	57.0	84,500
0.050	10.0×10^6	74,000	188	55.5	83,000
0.010	9.8×10^6	72,000	177	(53.5)**	78,000
Mean Values	10.0×10^6	74,000	188	55.5	82,000
Material: Titanium Alloy Ti 5 Al 2.5 Sn					
0.100	16.5×10^6	116,500	(317)	66.5	120,000
0.070	16.0×10^6	115,500	(325)	67.0	122,000
0.049	16.8×10^6	122,000	(309)	66.0	130,000
0.033	16.1×10^6	118,000	(334)	67.5	132,500
Mean Values	16.4×10^6	117,500	(320)	66.75	126,500

* Estimate based upon final tensile test load.
** Numbers in () represent equivalents, not experimental data.

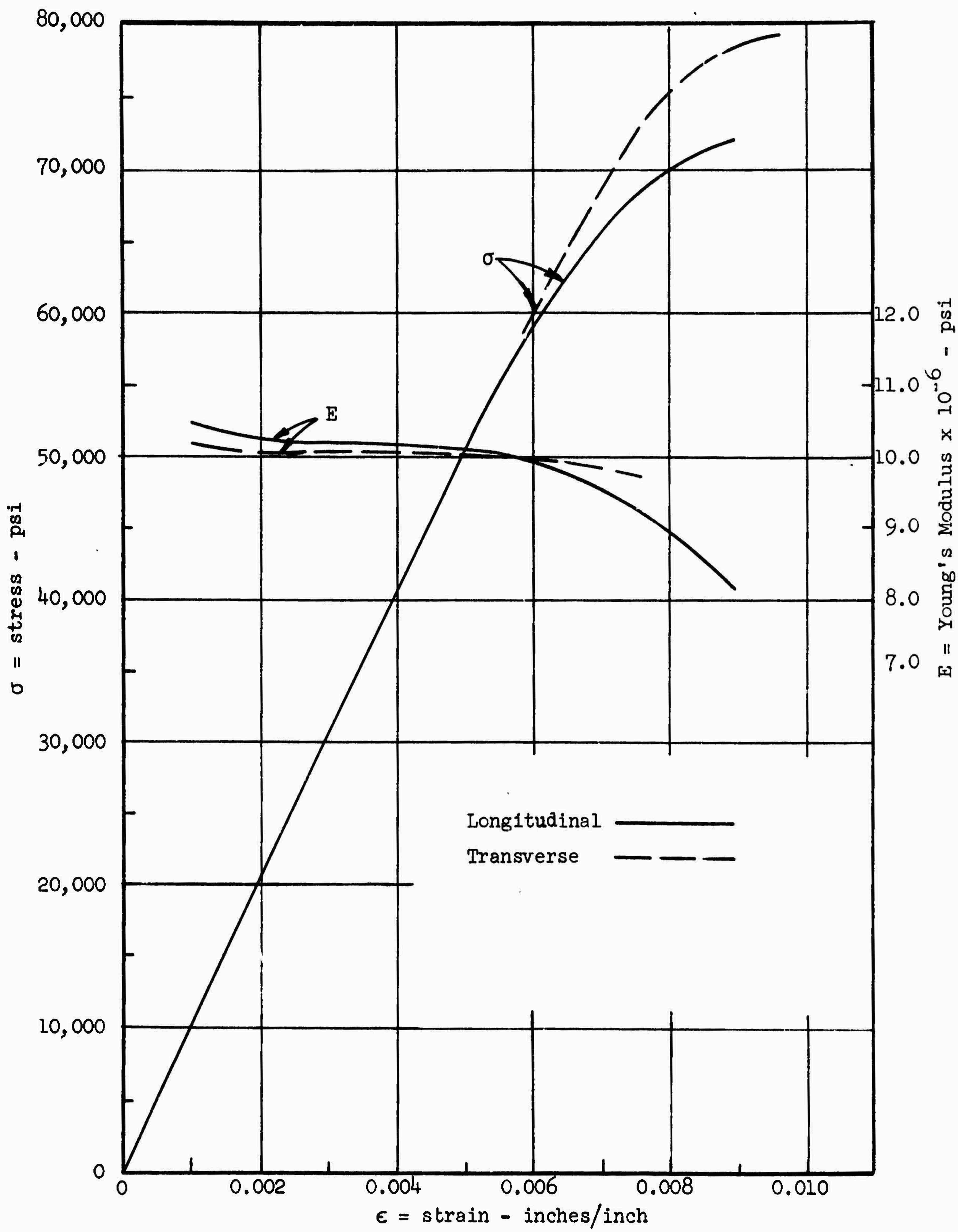

Figure A-19 TENSILE STRESS-STRAIN CURVES AND YOUNG'S MODULUS FOR 0.090" 7075-T6 ALUMINUM TARGET PLATE SAMPLES

APPENDIX B

PHYSICS OF THE PERFORATION OF THIN METALLIC PLATES BY PROJECTILE IMPACT

B.1 Major Problem Areas

This appendix presents a summary of the analytical and the theoretical studies on penetration and perforation of thin metallic plates by normal impact of projectiles. For the most part, this appendix is a review of the theoretical models, assumptions, and results of the previous reports (Fugelso, Arentz, and Poczátek 1961, and Fugelso, Arentz, and Davidson 1962). Some corrections have been made where necessary and some points have been more fully described. For the mathematical detail the reader is referred to the previous studies.

Consider a right circular cylindrical projectile of radius, a, length, L, and mass, M, approaching a plate of uniform thickness, h. The projectile is oriented so that its axis is perpendicular to the plate. The projectile approaches the plate with a velocity, V_s, which is perpendicular to the surface of the plate. There is no lateral velocity component. When the projectile strikes the plate, the entire flat end of the cylinder will strike the flat surface of the plate. The density of the plate is ρ_1 and the density of the projectile is ρ_0 (See Figure 1). The question that must be answered is, "Will the projectile perforate the plate?"

Hopkins and Kolsky (1960) presented a decomposition of impact phenomena based on the predominant mechanism of deformation. Regions wherein the deformation was predominantly elastic deformation, plastic deformation or hydrodynamic flow were estimated on the basis of the stress generated at the surface. The impact stresses are expressed in terms of the impact velocity for one-dimensional impact.

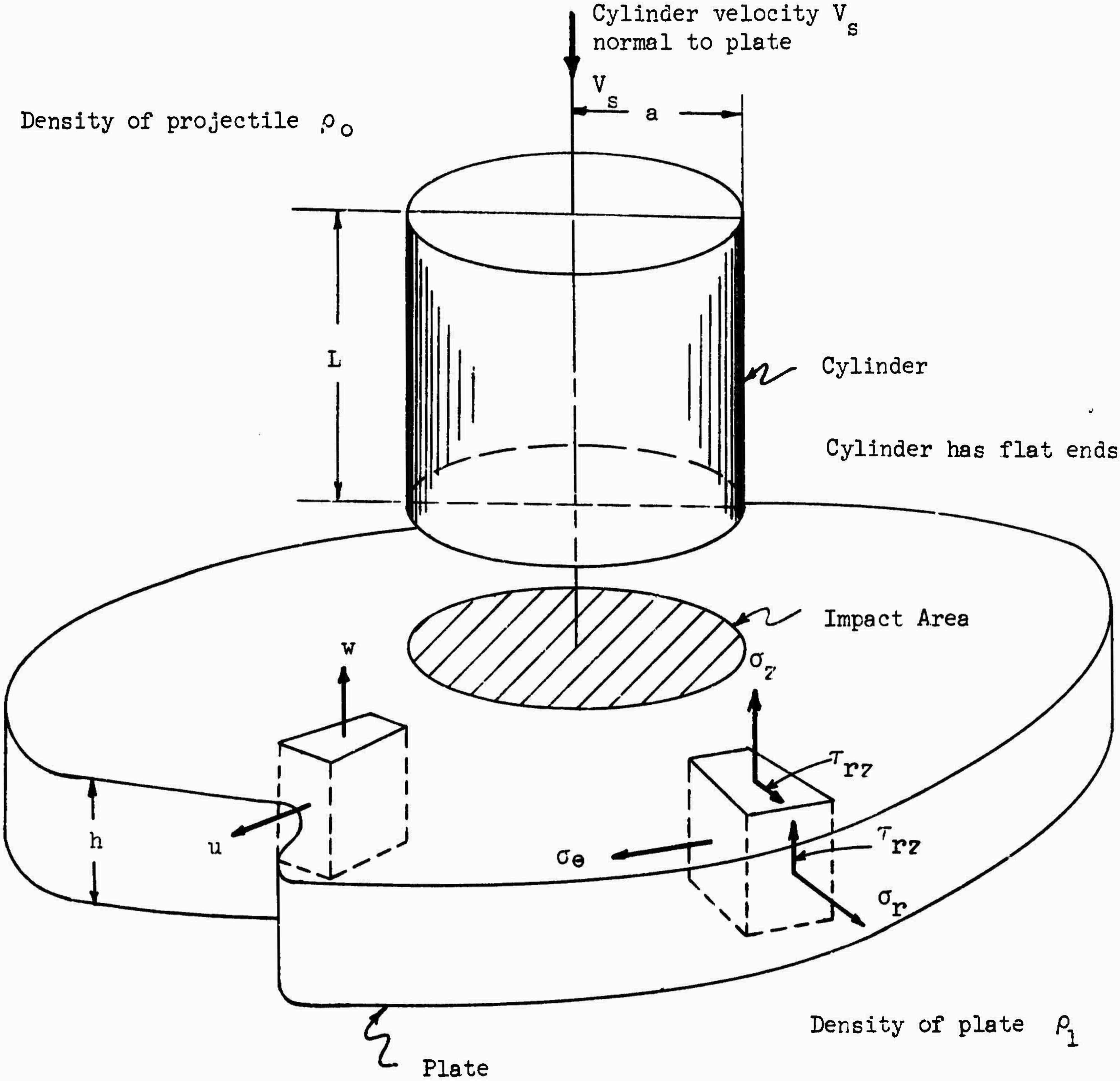

Figure B-1 GEOMETRY OF IMPACT AND DEFINITION OF TERMS

The upper bound on the impact velocity for the elastic region, which in turn is the lower bound on the impact velocity for the plastic region, is the impact velocity which generates the static yield stress in the plate.

$$v_1 = \frac{\sigma_y}{\rho c} \quad \text{Elastic-Plastic Transition Velocity}$$

The upper bound on the impact velocity for the region in which plastic deformation is dominant is the velocity at which the hydrodynamic decelerating force on the projectile is greater than the yield strength of the plate.

$$v_2 = \left(\frac{\sigma_y}{\rho}\right)^{1/2} \quad \text{Plastic-Hydrodynamic Transition Velocity}$$

Typical values for the transition velocities for one-dimensional (uniaxial) impact are given in Table B-1. The effects of each mode of deformation persist throughout the entire range of impact velocities. Thus a more detailed study of penetration was warranted than was carried out in the previous study.

TABLE B-1

TRANSITION VELOCITIES FOR IMPACT (FT/SEC)*					
Transition Velocities	Steel	Duralum	Al	Cu	Pb
v_1	150	200	43	25	7
v_2	1180	1410	625	425	130

*Projectile and plate materials are the same.

To determine the plate's failure under ballistic impact, several problems had to be solved. The dynamic problem of the stress wave propagation in the plate had to be solved. After the stresses had been determined, the areas of the plate where failure was likely to occur could be delineated. Specifically, the following stress wave propagation problems were solved:

1. The transient stress wave propagation in a plate system under the normal impact of a cylindrical projectile was solved analytically and numerically for:

   a. Single layer of an isotropic metal

   b. Double layer of an isotropic metal

2. An approximate solution for the propagation of large transverse deflection of the plate was established numerically, including the effects of plastic flow.

It was found that several properties of material deformation under rapid transient loading had to be defined. Therefore, a phase of the prior effort was devoted to material properties at high strain rates. Specifically, the following problem areas were investigated:

1. A theory for macroscopic plastic flow under transient loading conditions was developed using the properties of inter-and intra-crystalline imperfections (Fugelso 1962). These results were correlated with the experimental data available on the high strain.

2. A theory for fracture of metals under transient loading was developed, utilizing elasticity and the flow theory developed above, and compared with existing data on fracture of metals at high stress levels.

The solutions to the stress wave propagation problems delineated several regions of the plate where the stresses might cause fracture. Each possible mode of fracture of the plate in response to the stresses defined a model of failure of the plate. Each model of failure (1) required certain levels of impact stresses to activate the mode of fracture and (2) generated a retarding force on the projectile.

After the stress wave propagation was solved and the models of failure delineated, the deceleration of the projectile was computed, using the appropriate interface stresses to oppose and resist the projectile's motion. From these solutions, predictions for the critical perforation velocities and the residual velocity versus striking velocity were derived.

The next section reviews the problem of the determination of the stress wave propagation, indicates the specific problems solved, lists the assumptions involved, and presents the solutions and the results of the calculations.

Section B-3 defines the modes of failure of the plate and summarizes the derivations of the ballistic performance parameters.

B.2 Stress Wave Propagation in the Plate

B.2.1 Introduction

The propagation of stresses into the plate due to the impact stresses generated at the contact interface were solved by two approximate methods. Each approximation was designed to demonstrate certain qualitative and quantitative features of the transient stress distribution in the plate.

The first problem solved was the propagation of a stress wave propagating into a plate which was a linear elastic medium. The second problem was the propagation of transverse deflections of a thin plate composed of material whose description included plastic deformation.

B.2.2 Linear Elastic Wave Propagation

The first group of problems solved was the propagation of a linear elastic stress wave. These problems were solved to determine the qualitative description of the various stress components throughout the plate as a function of position and time, and to obtain a quantitative estimate of these stresses.

The equations of motion for axisymmetric deformation are:

$$\frac{\partial \sigma_r}{\partial r} + \frac{\partial \tau_{rz}}{\partial z} + \frac{\sigma_r - \sigma_\theta}{r} = \rho \frac{\partial^2 u_r}{\partial t^2}$$

$$\frac{\partial \tau_{rz}}{\partial r} + \frac{\partial \sigma_z}{\partial z} + \frac{\tau_{rz}}{r} = \rho \frac{\partial^2 u_z}{\partial t^2}$$

where $\sigma_r, \sigma_\theta, \sigma_z, \tau_{rz}$ are the stresses in the plate

u_r, u_z are the radial and vertical displacement

ρ is the density of the plate

r, z are the radial and vertical coordinates

t is the time

The linear elastic stress-strain relationships used in the computation are

$$\sigma_r = (\lambda + 2\mu)\frac{\partial u_r}{\partial r} + \lambda(\frac{u_r}{r} + \frac{\partial u_z}{\partial z})$$

$$\sigma_z = (\lambda + 2\mu)\frac{\partial u_z}{\partial z} + \lambda(\frac{u_r}{r} + \frac{\partial u_r}{\partial r})$$

$$\sigma_\theta = (\lambda + 2\mu)\frac{u_r}{r} + \lambda(\frac{\partial u_r}{\partial r} + \frac{\partial u_z}{\partial z})$$

$$\tau_{rz} = \mu(\frac{\partial u_r}{\partial z} + \frac{\partial u_z}{\partial r})$$

where λ, μ are Lame's constants

The boundary condition at the bullet-plate interface was chosen to be a uniform vertical stress acting over the contact area. While this is not the exact distribution of stress expected there, it is close enough to determine the physics involved in the process of deformation and to approximate the perforation parameters. The other exterior surfaces are free from all tractions.

Formal solutions for the equations of motion were obtained by application of Fourier-Hankel integral transforms. These equations were solved by partially analytical and partially numerical techniques for the following three problems:

1. <u>Elastic Stress Waves in a Half Space:</u> The stress wave propagation in an elastic half space under the action of a vertical stress applied uniformly over a circular region was solved. Numerical solutions for the stresses, displacements and velocities throughout the region were computed.

Figures B-2 and B-3 show the progression of the vertical stress into the half space at various times. Figure B-4 shows a profile of the vertical stress on the axis of symmetry. Figure B-5 shows the vertical and radial stresses on the axis of symmetry.

Quantitative and qualitative features of interest are:

a. The stress jump at the wave front under the bullet is almost uniform with r. The magnitude of the jump at the wave front decays as

$$\sigma_z = \sigma_z^o \left(1 + \left(\frac{z}{a}\right)^2\right)^{-1/2}$$

where σ_z^o is the uniform stress acting on the surface

b. This stress spike near the wave front decays very rapidly behind the shock front.

c. The given static solution is established (to within 5%) after the passage of the shear wave front. The magnitude of the static part here is

$$\sigma_z^s = \sigma_z^o \left(1 + \left(\frac{z}{a}\right)^2\right)^{-1}$$

2. Elastic Stress Waves in Plates: The vertical and radial stresses on the axis of symmetry for an elastic plate in response to suddenly applied, uniformly distributed vertical pressure were calculated. Typical values for the vertical and radial stress for a moderately thick plate ($\frac{h}{a} = 0.8$) for two different plate materials are shown in Figures B-6 and B-7.

A large compressive vertical stress is generated in the spike as the wave travels across the plate. The vertical stress remains compressive in the first wave after the spike has decayed. The vertical stress is reflected with a reversed sign at the free surface. The combined vertical stress becomes

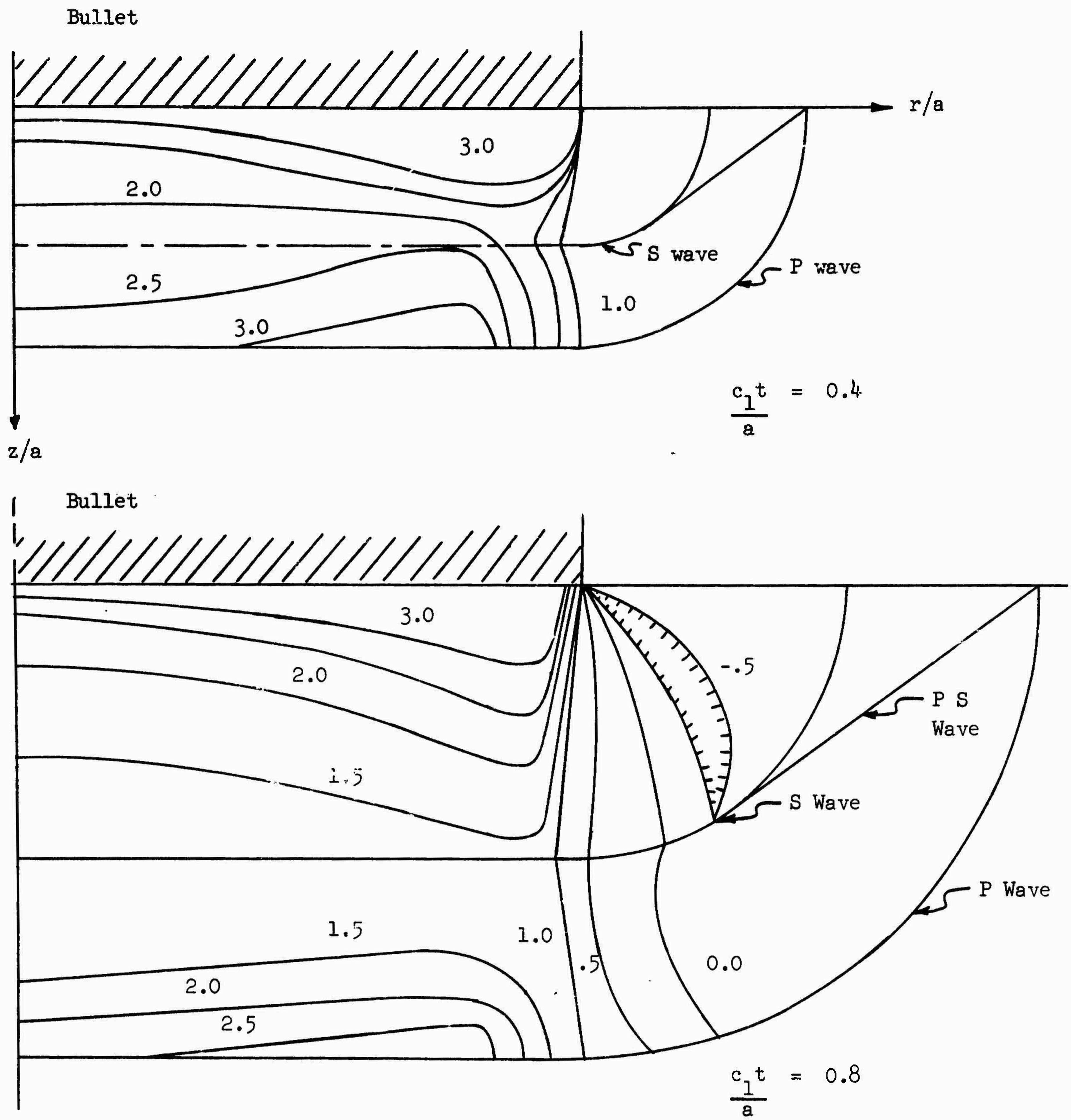

Figure B-2 CONTOURS OF VERTICAL STRESS ($\pi \sigma_z$) UNDER THE BULLET AT VARIOUS TIMES AFTER IMPACT (POSITIVE SIGN IS COMPRESSIVE)

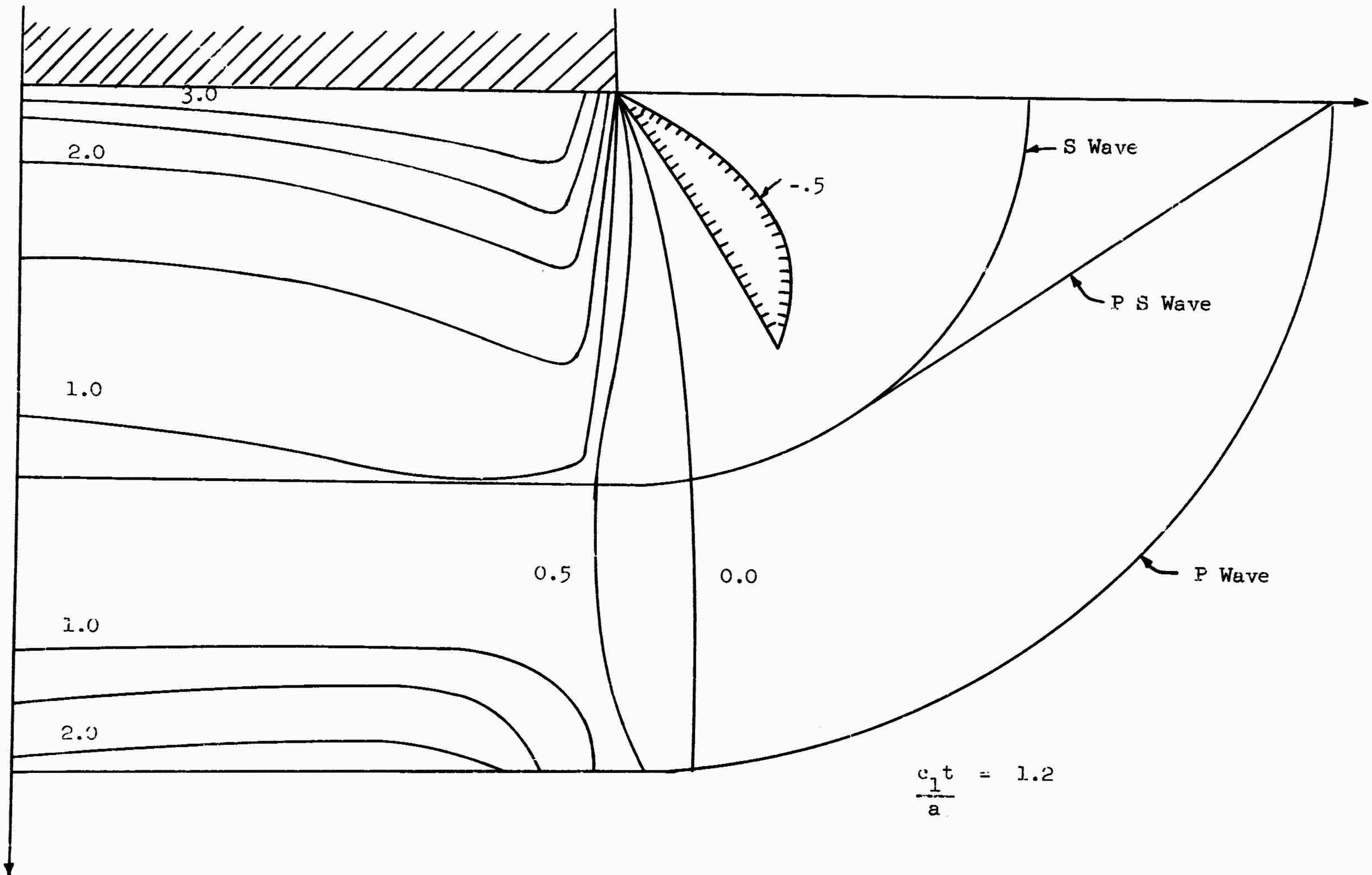

Figure B-3 VERTICAL STRESS IN THE PLATE

CONTOURS OF $\frac{\sigma_z}{\pi P_o}$

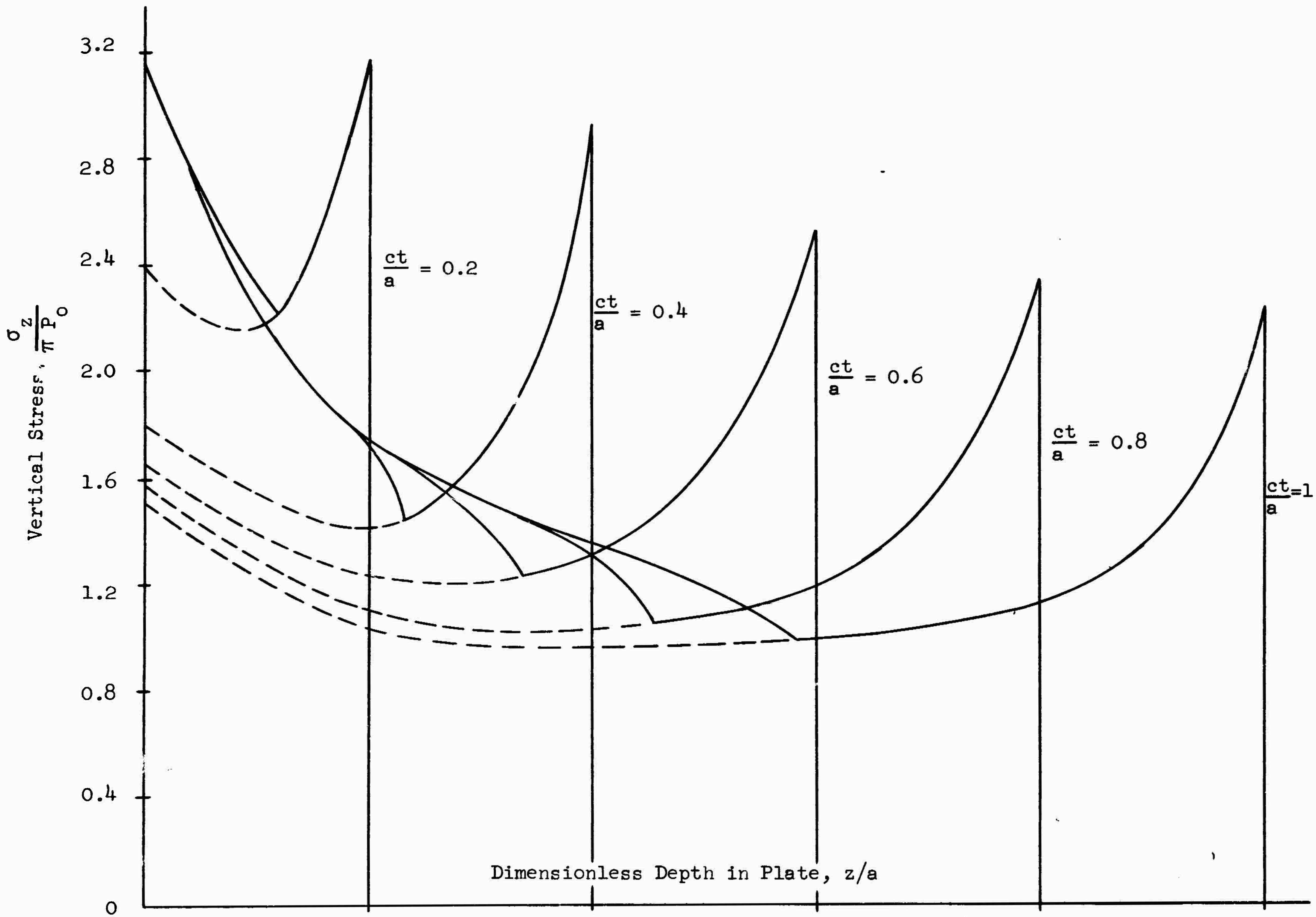

Figure B-4 VERTICAL STRESS VERSUS DEPTH (r = 0)

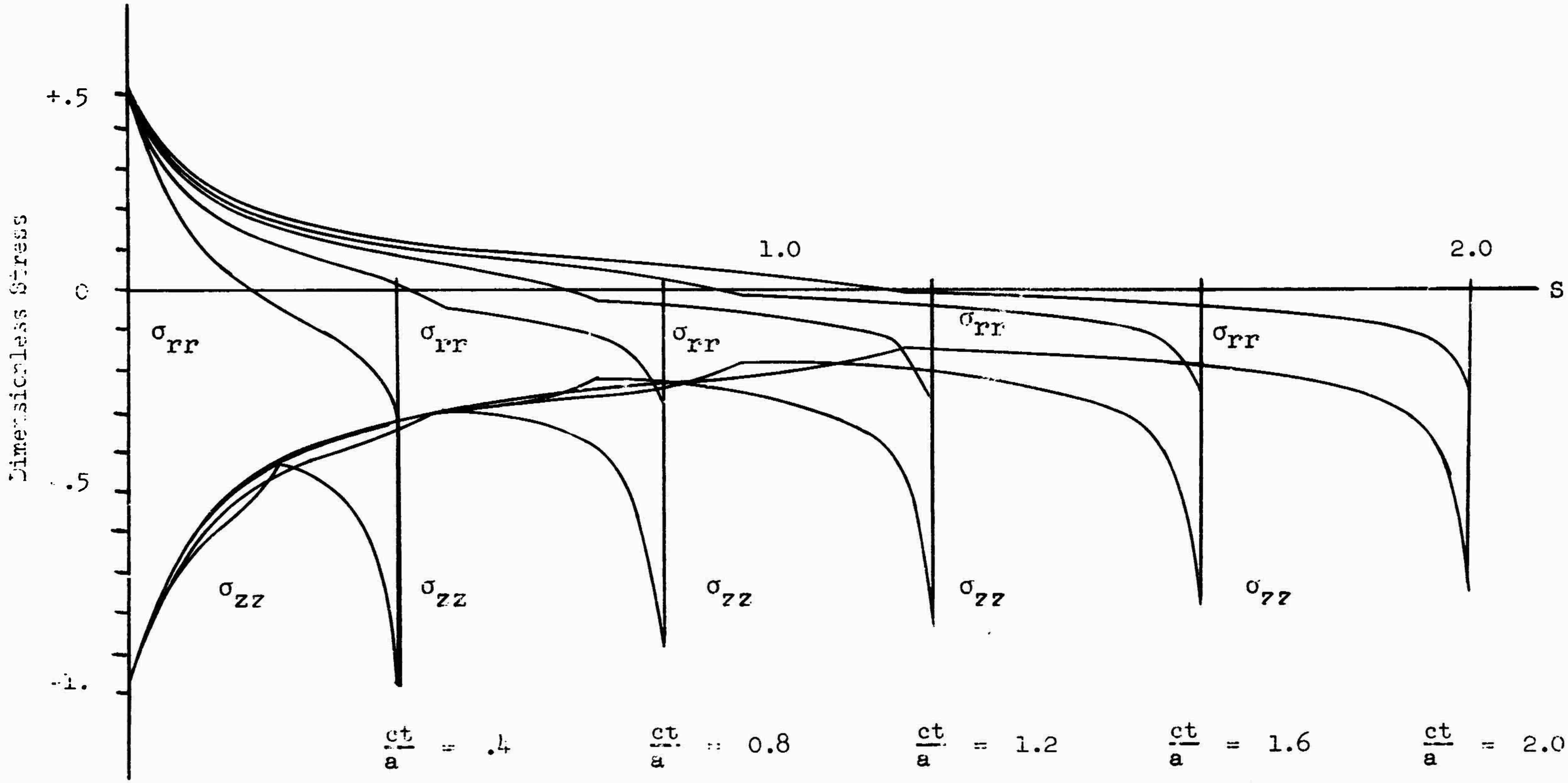

Figure B-5 RADIAL AND VERTICAL STRESS ON THE AXIS OF SYMMETRY

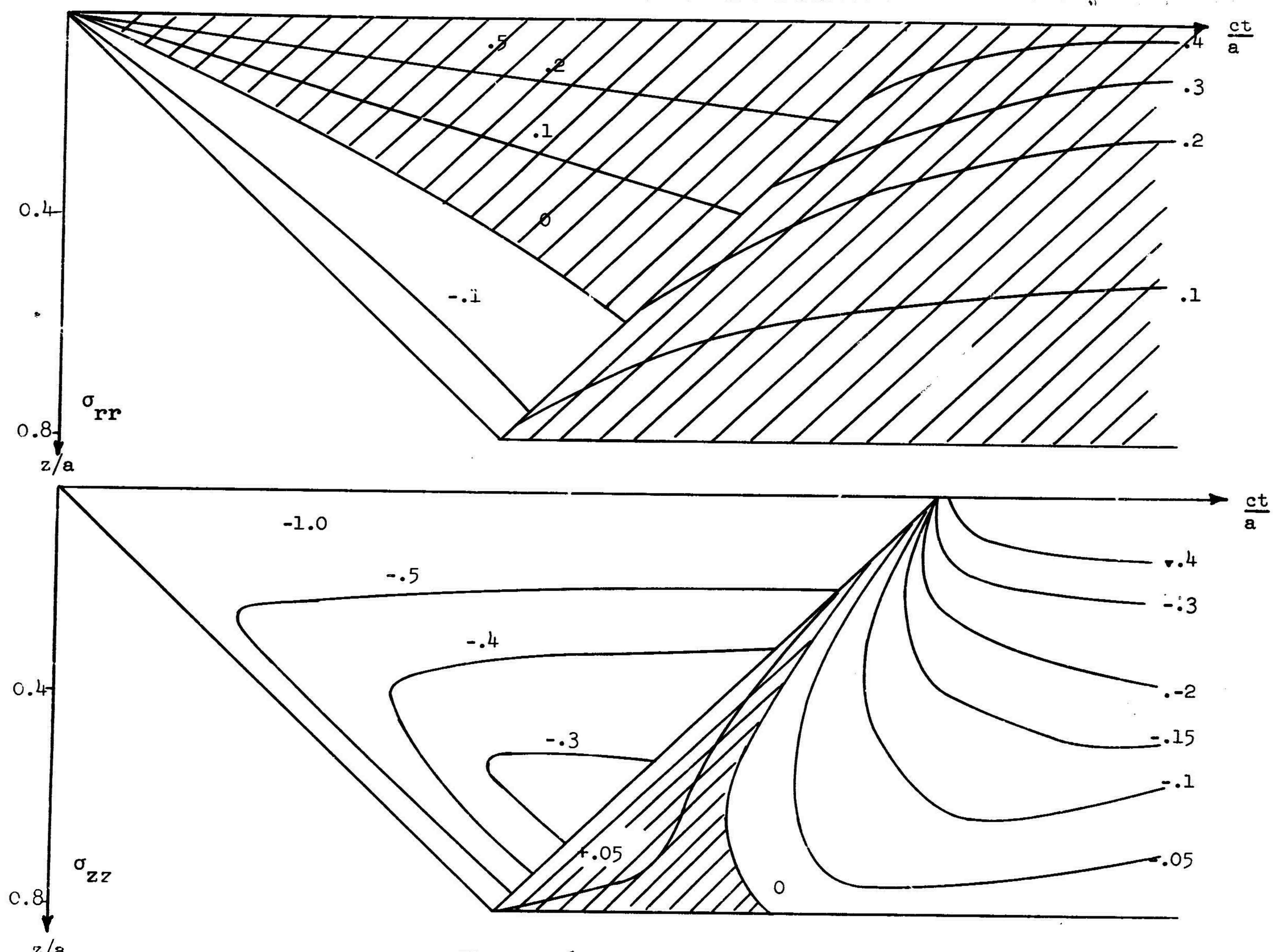

Figure B-6 STRESS DISTRIBUTION IN Fe PLATE (h/a) = 0.8

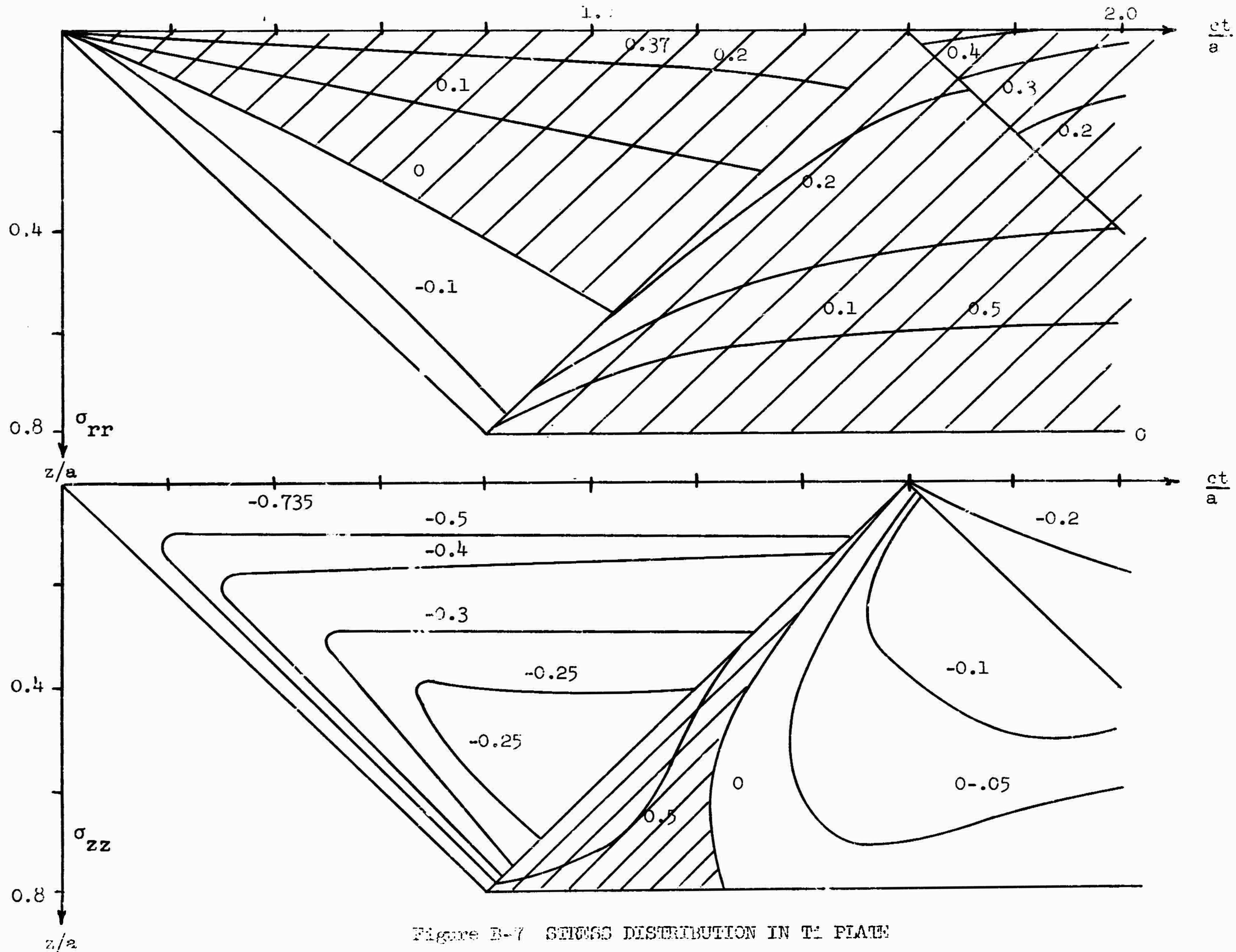

Figure B-7 STRESS DISTRIBUTION IN Ti PLATE tensile a little way from the back or free surface. It is at this point where failure by spall will occur. Failure of the plate material could also occur in the first passage of the stress wave by the fact that the compressive stresses are large.

The radial stress in the spike is compressive. After the spike has passed, the radial stress in the front wave becomes tensile. The radial stress in the reflected stress spike is tensile. The combined radial stress system adds two tensile stresses.

After the complete passage of the reflected wave has passed and, for subsequent reflections, the vertical stress in the plate is quite small.

3. Elastic Stress Waves in Laminated Plates: Using similar boundary conditions, the transient stress on the axis of symmetry was solved during the first two reflections for several interesting combinations of laminated plates.

The vertical and the radial stresses as a function of time and position on the axis of symmetry are plotted in Figures B-8 through B-13 for the following cases. The two plate materials are steel and titanium. The total thickness in each case is the same ($\frac{h}{a} = 0.8$). The ratios of the thicknesses of the materials vary from 3:1 to 2:2 to 1:3. The titanium plate is first exposed as the upper surface (toward the bullet) and then the order is reversed.

The use of a laminated plate system shows (1) an impedance match between the front plate and the projectile increases the stress generated at

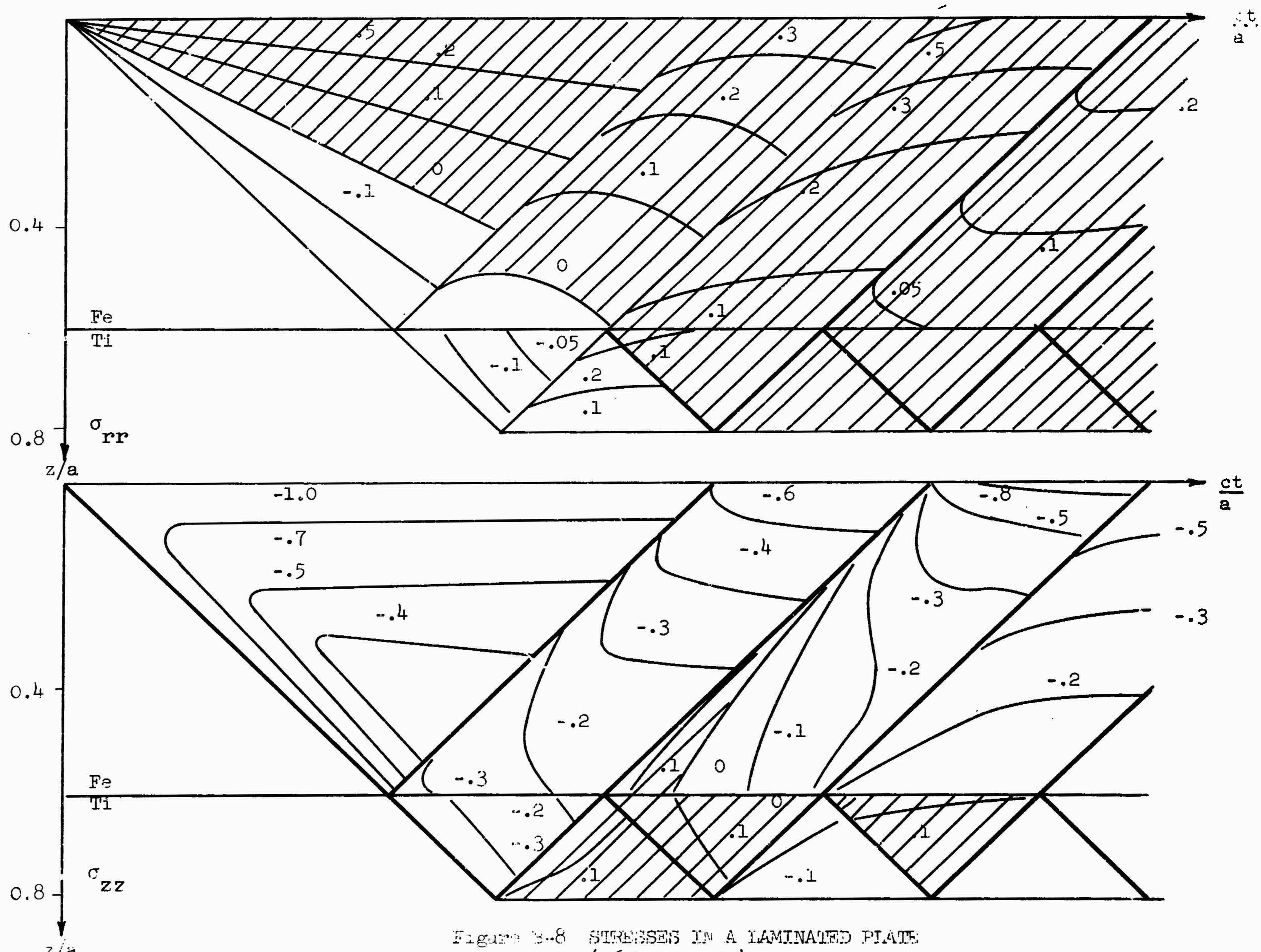

Figure 3-8 STRESSES IN A LAMINATED PLATE
(.6 Fe, .2 Ti)

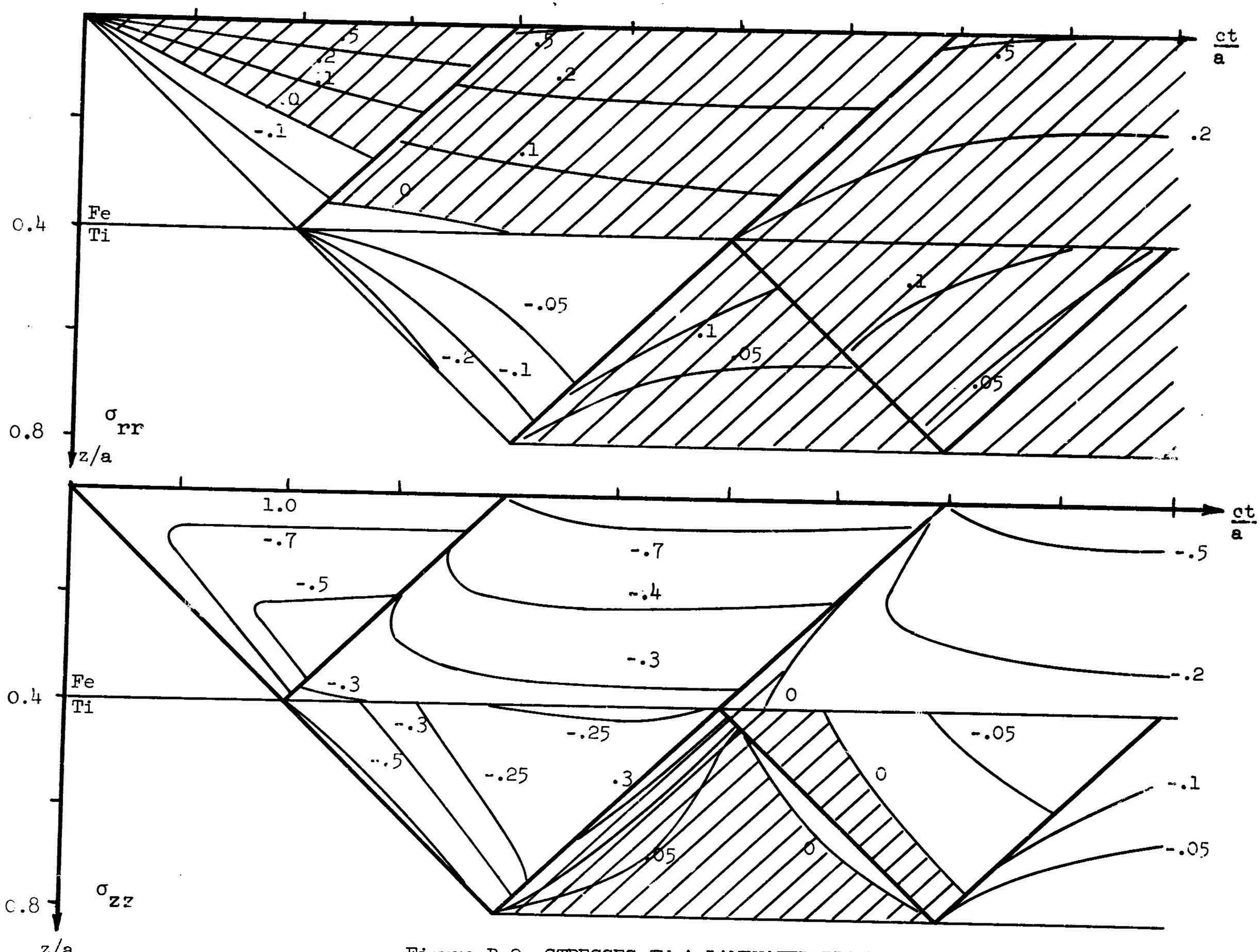

Figure B-9 STRESSES IN A LAMINATED PLATE
(0.4 Fe; 0.4 Ti)

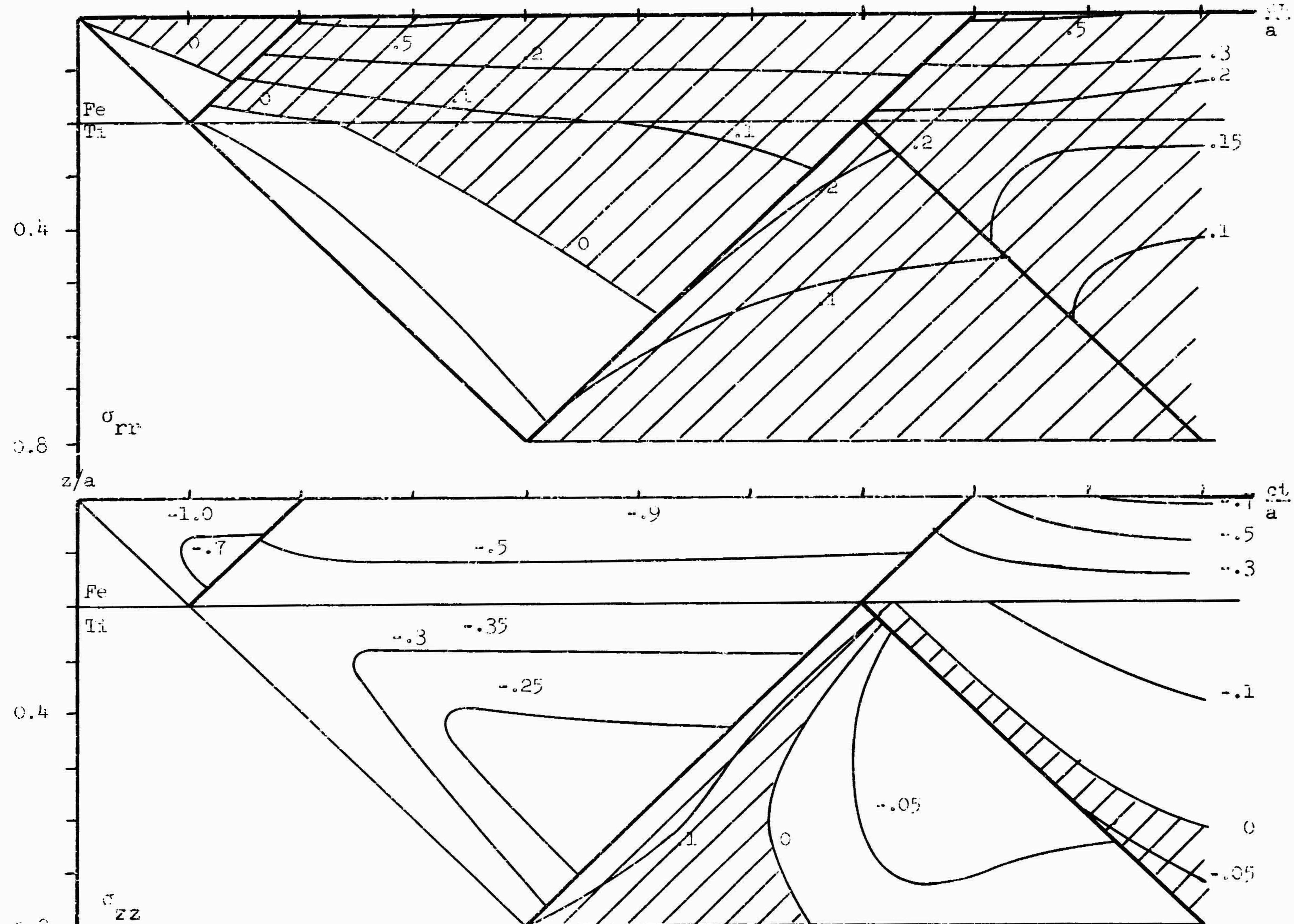

Figure B-10 STRESSES IN A LAMINATED PLATE
(.02 Fe; 0.6 Ti)

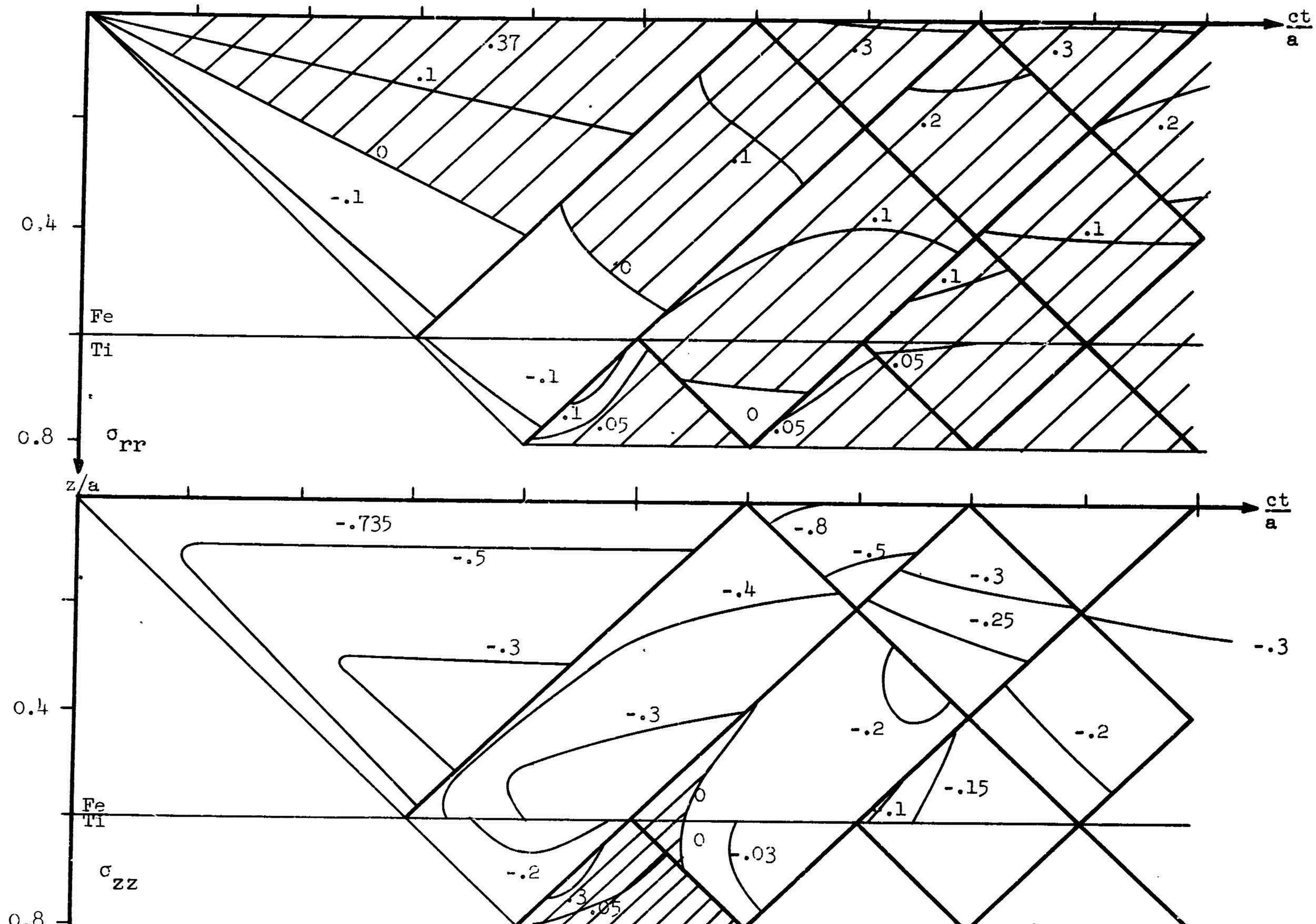

Figure B-11 STRESSES IN LAMINATED PLATE
(0.6 Ti; 0.2 Fe)

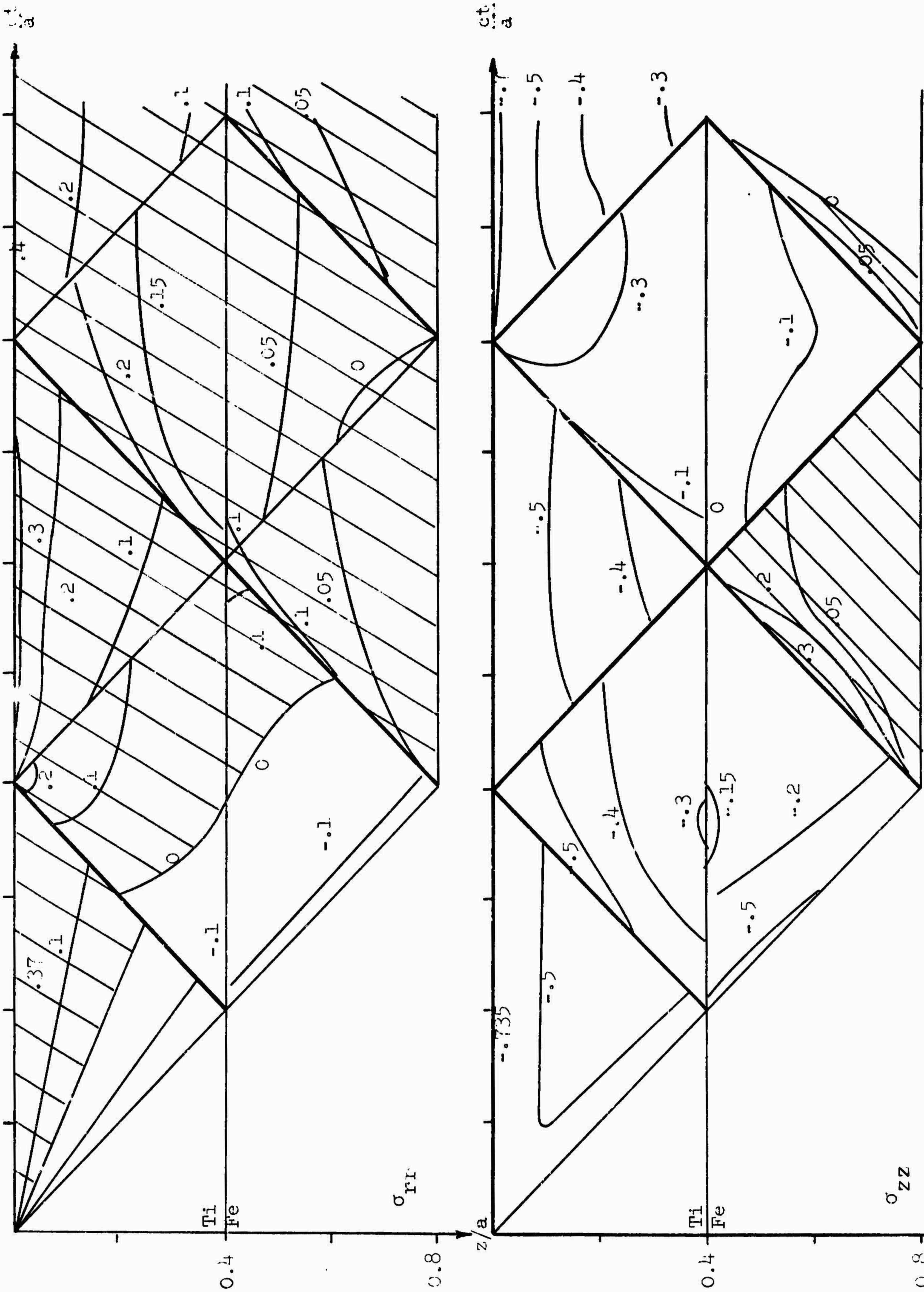

Figure B-12 STRESSES IN A LAMINATED PLATE
(0.4 Ti; 0.4 Fe)

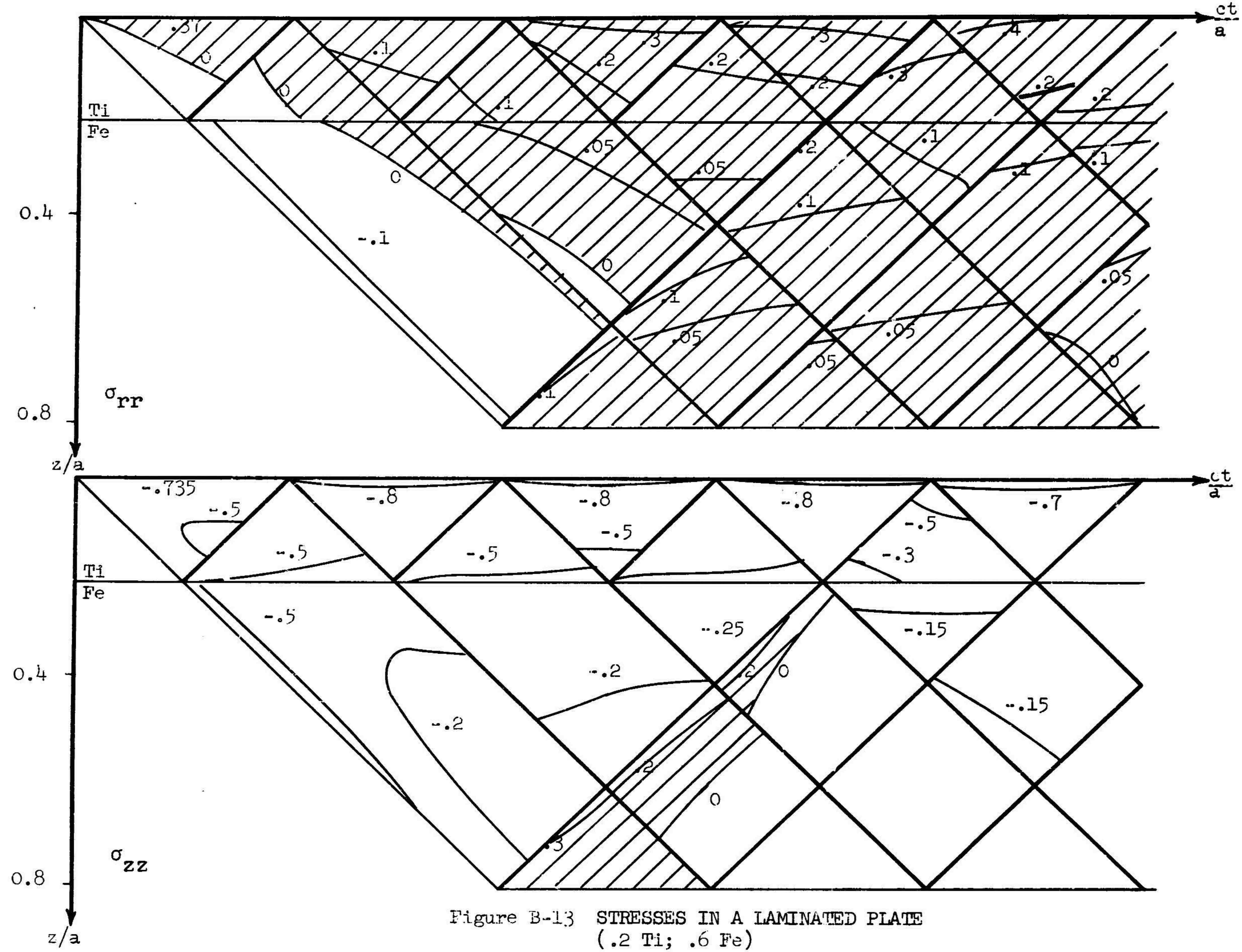

Figure B-13 STRESSES IN A LAMINATED PLATE
(.2 Ti; .6 Fe)

the impact interface, (2) the magnitudes of the stresses near the first wave front in the back plate **are** smaller than those in the single plate, and (3) higher magnitudes of tensile stresses are generated in the second and third reflected wave fronts passing through the back plate.

B.2.3 Inelastic Stress Wave Propagation

The second problem solved was the propagation of a stress wave in a plate including the effects of plastic flow. The stresses generated at impact are a monotonically increasing function of the impact velocity. For impact velocities larger than some transition velocity, the dominant stress in the plate in that impact process exceeds the static yield stress and is in the plastic range. Hopkins and Kolsky (1960) computed the transition velocity from elastic to plastic behavior for aluminum-to-aluminum impact and found it to be in the neighborhood of 40 feet per second. The striking velocities of interest for the ballistic impact studies lie above this value. Therefore, an investigation into stress wave propagation in the plate where the stresses exceed the yield stress of the material was conducted.

A study of plastic flow under dynamic and transient loading conditions has been made which far exceeded the yield point (Fugelso 1962). Using the continuum theory of microscopic imperfections of intracrystalline and inter-crystalline nature, a constitutive stress-strain-strain rate equation was developed. This constitutive equation well represented the actual material behavior for face-centered and body-centered metals. The basic strain rate equation given by this theory is

$$\frac{\partial \epsilon_{ij}}{\partial t} = \frac{\partial \sigma_{ij}}{\partial t} + \Phi_{ij} (\sigma_{kl})$$

where ϵ_{ij} is a strain

σ_{ij} is a stress

Φ_{ij} is a function of the stresses and temperature

The form of this stress-strain-strain rate equation is equivalent to that of a visco-plastic body. The actual coefficients of the body, however, are nonlinear, as indicated by the theory for dislocation movement. Temperature effects are also included in the dislocation theory.

To demonstrate that the dislocation model and its predictions indeed give reasonable stress-strain curves, the stress-strain curves generated at constant strain rate under various boundary conditions are shown. The stress system is biaxial. In both problems demonstrated, the longitudinal stress is plotted as a function of the longitudinal strain. The longitudinal strain is applied at a constant rate which is indicated (Figure B-14). In the first case, the deformation corresponds to the standard tensile test, namely, the lateral stress is zero and the body is free to deform laterally. In this case the stress starts off at zero, rises linearly until a yield stress is reached, at which point the stress-strain curve bends over and continues almost flat. For other models of microscopic behavior, a reduction in the stress reached at this point was obtained (Figure B-15).

The second case shown is the longitudinal stress vs. longitudinal strain for confined deformation. In this case, the lateral strain is zero, the lateral stress being sufficient to confine it from lateral motion. Again, the longitudinal strain is applied at a constant rate. Initially, the stress varies linearly with the strain, the modulus being equal to $\lambda + 2\mu$. When the yield

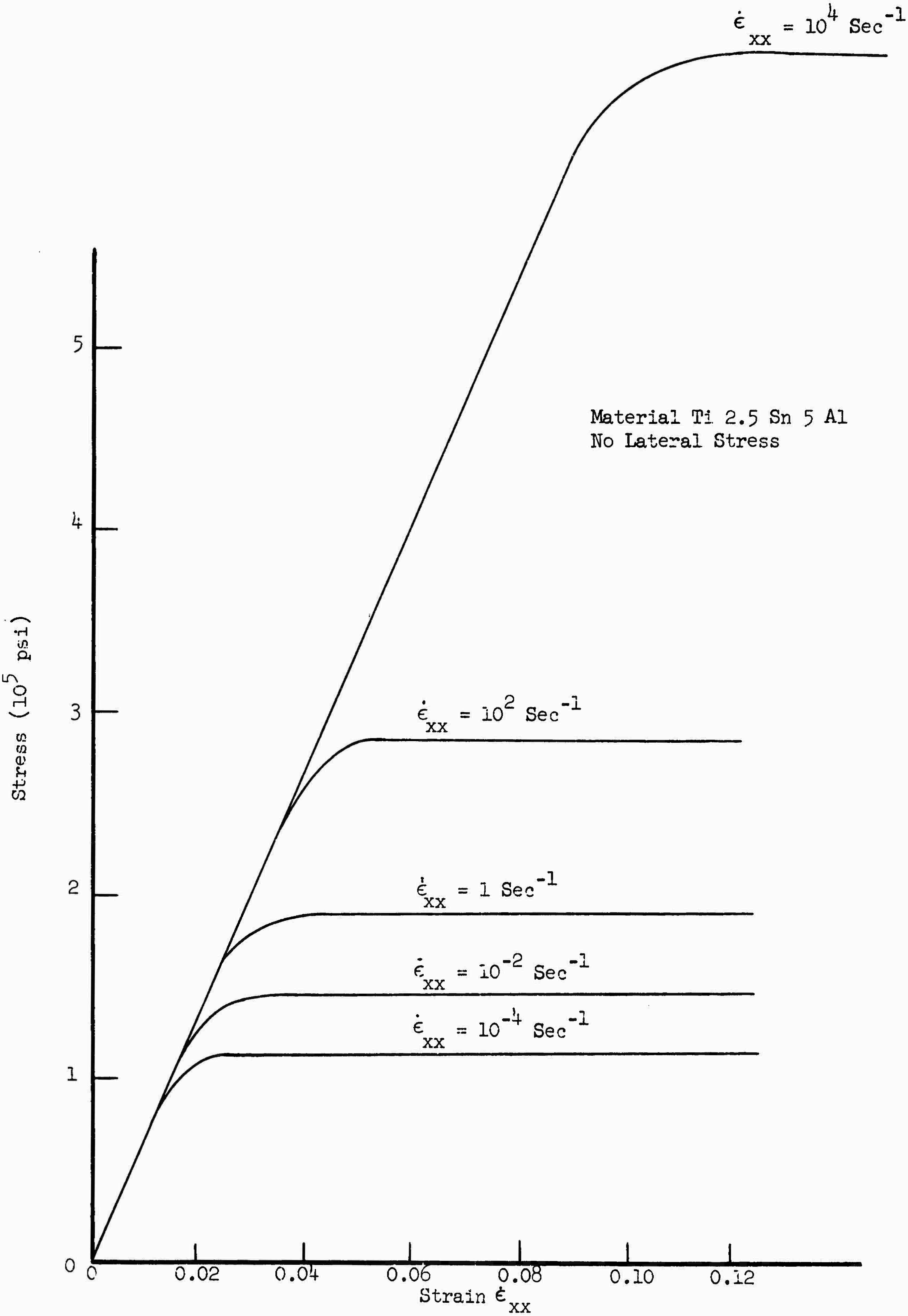

Figure B-14 STRESS VS. STRAIN AS A FUNCTION OF STRAIN RATE BY THE THEORY OF DISLOCATION MOTION - CONSTANT NUMBER OF DISLOCATIONS

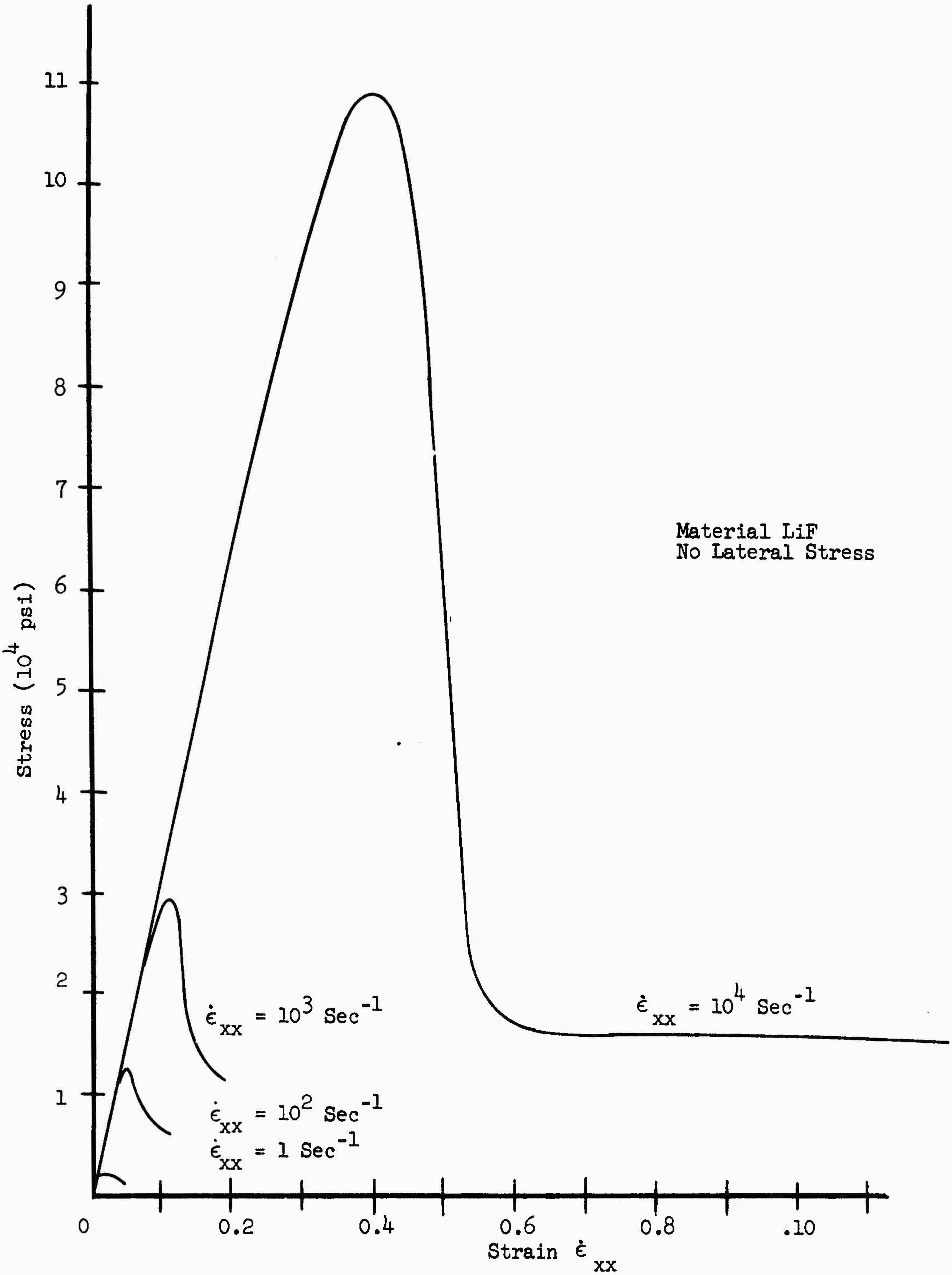

Figure B-15 STRESS VS. STRAIN AS A FUNCTION OF STRAIN RATE BY THE THEORY OF DISLOCATION MOTION - FRANK-READ REGENERATION OF DISLOCATIONS conditions are met, the longitudinal stress does not flatten out, but now proceeds as a function of the longitudinal strain, increasing at a rate equal to the bulk modulus of the material. The lateral stress increases at the same rate after yielding and has the same sign as the longitudinal stress (Figure B-16).

In these cases, the elastic portion of the deformation is linear. The various dislocation models were chosen to represent experimentally observed dislocation behavior in solids. In Figure B-17, they show the behavior of the yield stress (defined as the limiting stress) for the unconfined stress-strain deformation at constant strain rate plotted vs the strain rate. The model here is that of titanium alloy yielding by dislocation movement given by the Frank-Read source. The experimental points are the measured values of Wentz and Catlin (1955). The agreement is fairly good.

The full solution of the equations of motion for this impact problem involves the computation of both elastic and inelastic behavior in at least two dimensions and time. The linear elastic solution for the problem is already complicated and yet it is the only model which will allow us to establish an analytic solution (but not in closed form) in this particular geometry. Since the stresses are above the static yield point for most of the deformation processes involved here, an approach was desired which demonstrated the effects of the inelastic behavior on the ballistic resistance and on the properties of the perforation and penetration process in general.

Since the problem is the impact of thin plates, thin plate approximation was used and reduced the geometrical problem to one less dimension and time,

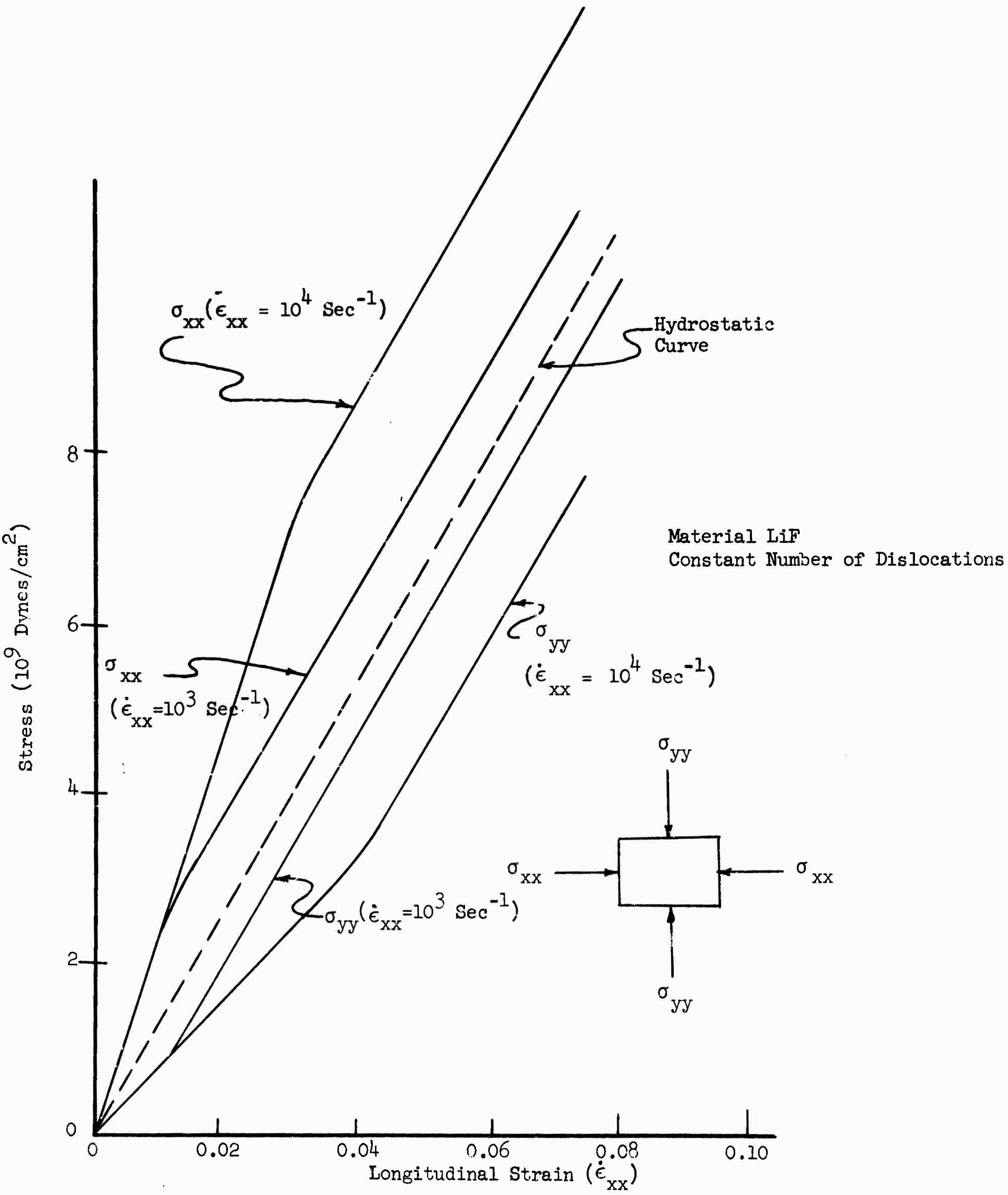

Figure B-16 STRESS VS. STRAIN-UNIAXIAL STRAIN AT CONSTANT STRAIN RATE

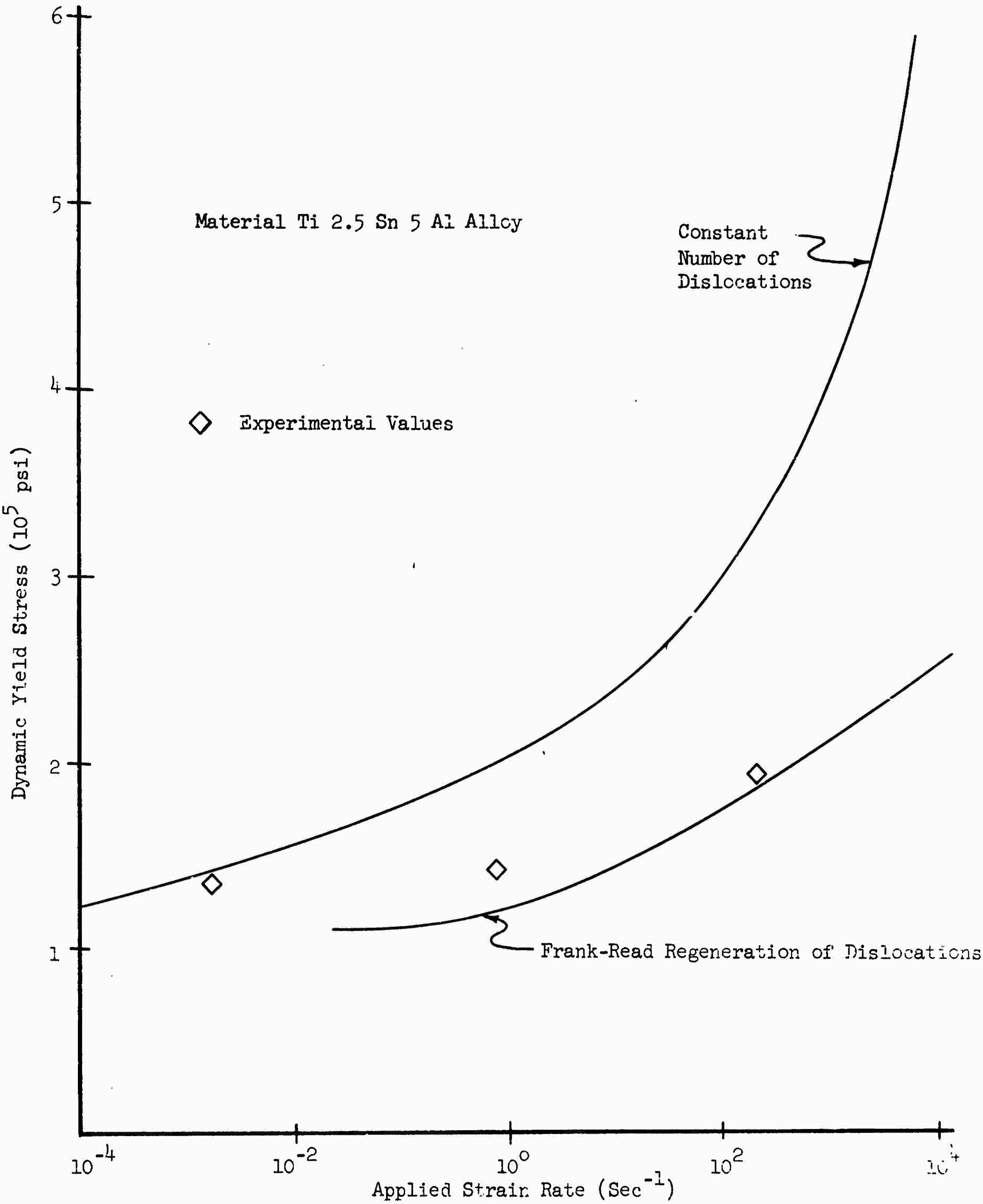

Figure B-17 DYNAMIC YIELD STRESS AS A FUNCTION OF STRAIN RATE integrating the effects over the thickness. Note, from the elastic solution, that after the stress wave has reflected at least once, the vertical variation of the stresses over the plate thickness is very small. Also, the magnitude of the vertical stress is very small.

Proceeding along this line, a mathematical model for the propagation of transverse deflections of a thin plate including plastic flow was developed. Figure B-18 shows the projectile-plate configuration. The only variation of the displacement allowed was in the vertical direction, an approximation which is a reasonable description of the impact deformation of the plate. The only spatial variation of the displacement, strains, and particle velocities allowed was in the radial direction. No variations in the vertical direction were allowed. A circular plug directly underneath the cylindrical projectile was assumed to be moving at a velocity equal to the projectile at the time t = 0. This accounted for the first stress wave traverse and the momentum transfer during this first instant of impact. The resulting equations and boundary conditions are:

Momentum equation

$$\rho \frac{\partial v}{\partial t} = \frac{\partial \tau}{\partial r} + \frac{\tau}{r}$$

Constitutive equation

$$\frac{\partial \gamma}{\partial t} = \frac{1}{\mu} \frac{\partial \tau}{\partial t} + \phi(\tau)$$

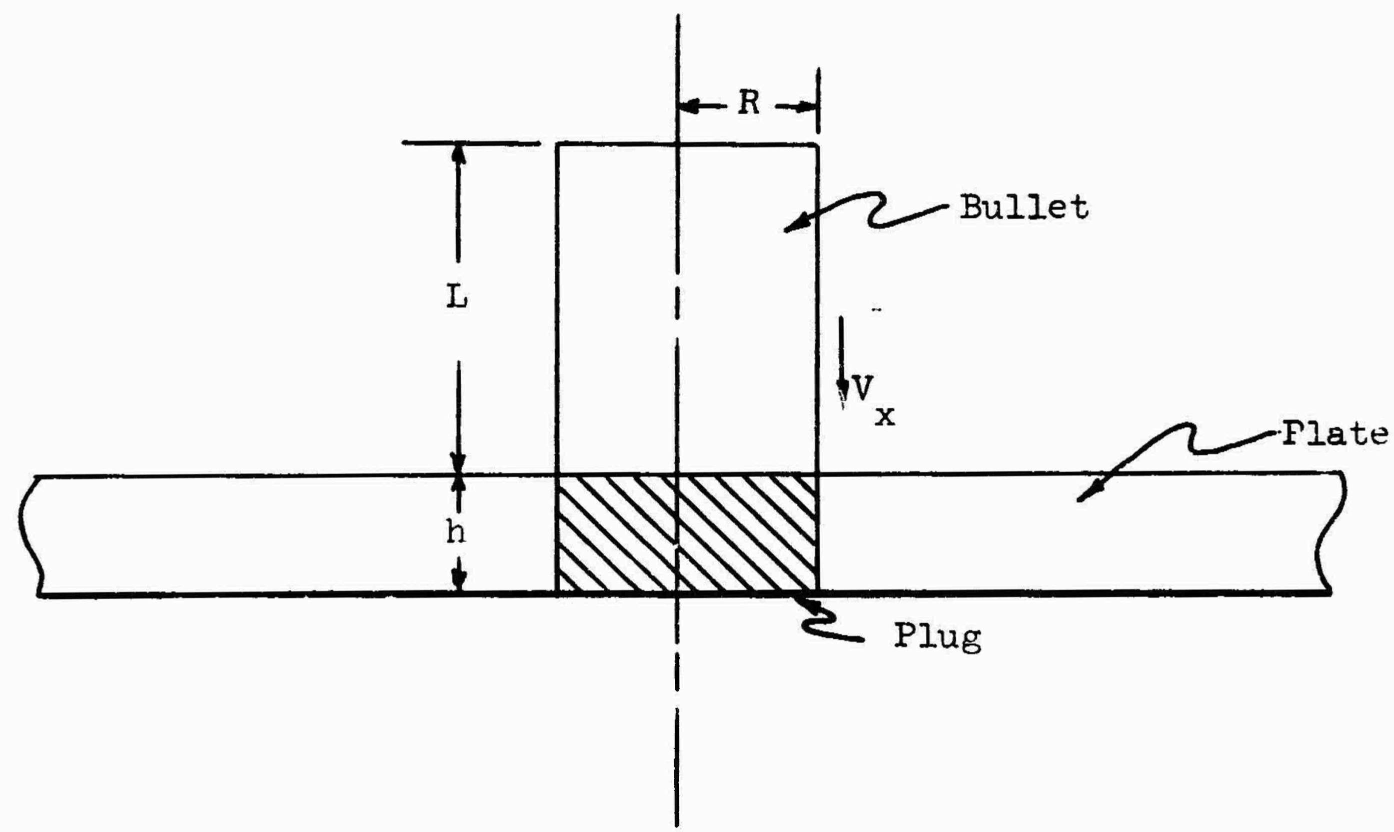

Figure B-18 CONFIGURATION OF BULLET AND PLATE FOR SHEAR MODE CALCULATION where ρ = density of plate

τ = shear stress

γ = shear strain

u = vertical displacement

v = vertical velocity

$\phi(\tau)$ = plastic strain rate component

$\phi(\tau) = A\ e^{-\beta/\tau}$ form chosen to match experimental data

The initial conditions and boundary conditions are:

$$u = v = 0; \quad t = 0; \quad r \geqq R$$

$$v = v_o; \quad t = 0; \quad r \geqq R$$

$$(M + m) \frac{\partial v}{\partial t} = \tau\ 2\pi Rh; \quad r = R;\ t \leqq 0$$

where M = mass of projectile

m = mass of plug

R = radius of projectile

h = thickness of plate

These equations of motion were solved numerically on MRD's IBM 1620 digital computer. A finite difference method for the solution of these partial differential equations was established, checked out and solved. Typical results for the velocity and the shear stress as a function of radial position and time are shown in Figures B-19 and B-20. In this particular case, an initial velocity was chosen such that the initial shear stress is 12 times that of the yield stress in shear. It is noted that the stress at the wave front decays more rapidly than the corresponding linear elastic solution to this problem.

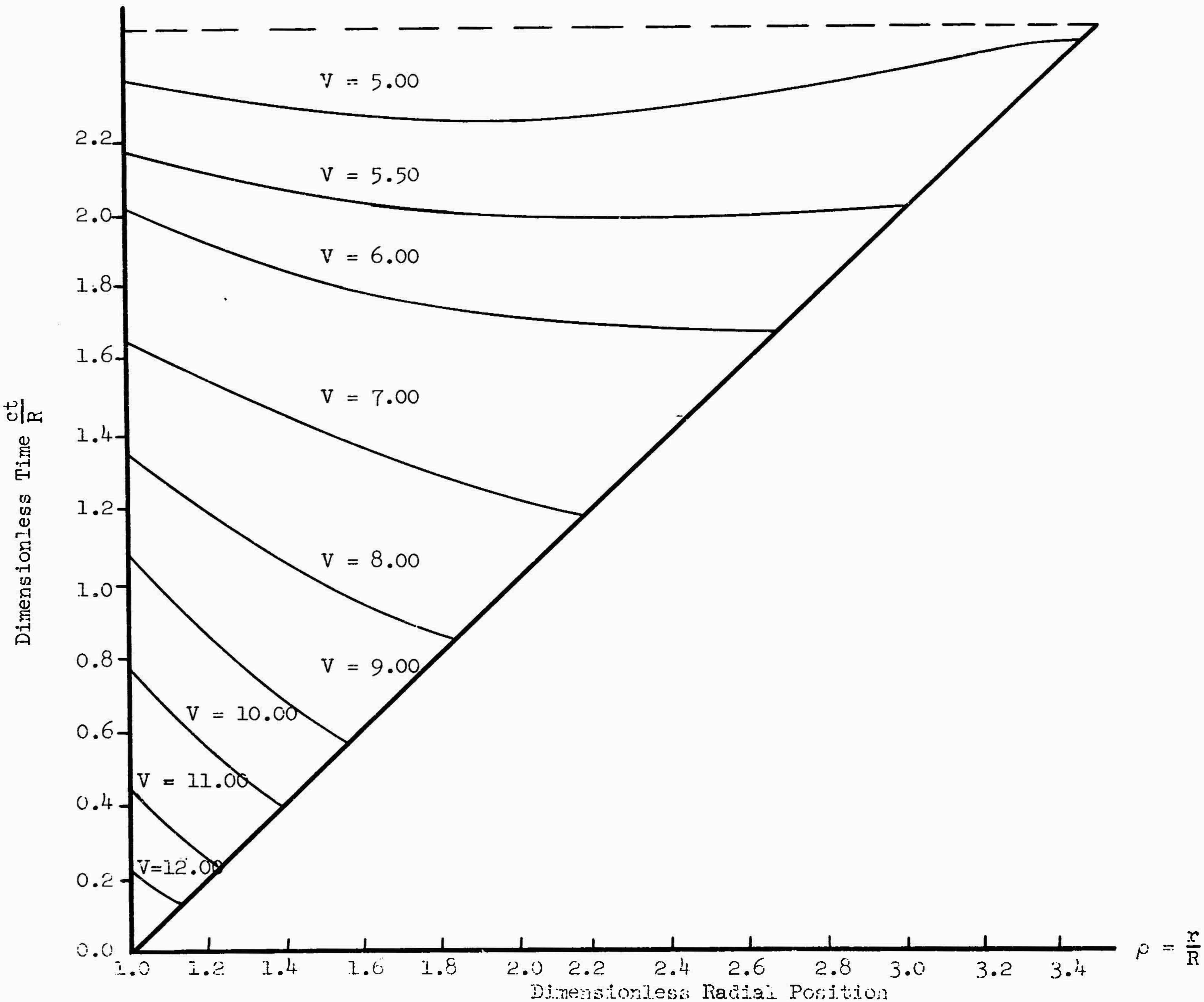

Figure B-19 CONTOURS OF DIMENSIONLESS PARTICLE VELOCITY AS A FUNCTION OF POSITION AND TIME

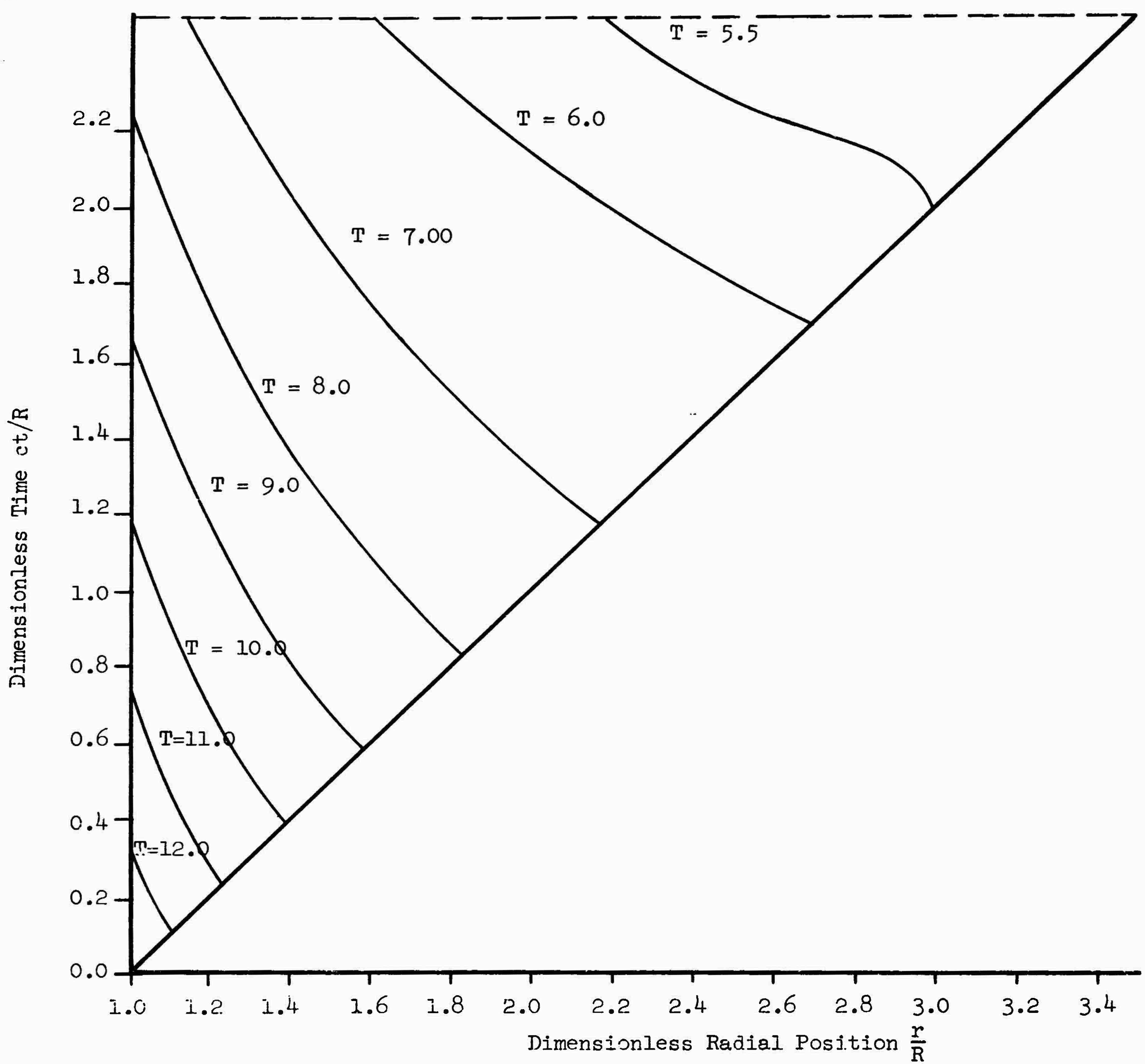

Figure B-20 CONTOURS OF DIMENSIONLESS STRESS τ_{rz}/τ_y AS A FUNCTION OF POSITION AND TIME

The solution of another specific problem contains information of interest to this particular problem. The problem solved was the propagation of a spherical wave into a plastic deforming medium (Fugelso 1962). The stress applied at the boundary of a spherical cavity was above the yield stress. It was found that the stress at the wave front which elastically decays inversely with the distance from the cavity decayed at a far greater rate. The bulk of the disturbance propagated out as a slower velocity and a large permanent deformation was found near the cavity itself.

B.3 Failure of the Plate and Calculation of the Ballistic Coefficients

B.3.1 Modes of Failure

The evaluation of the stresses in the plate as a function of position and time is an important step in the evaluation of ballistic performance. If the plate is to fail, it must fail in response to one or more of the stresses. The retardation of the projectile on its course is effected by the stresses generated at the contact surface. Therefore, two effects in determination of resistance to perforation must be established.

1. Does the plate break? If so, where and under what conditions?
2. If the plate breaks, how much is the projectile retarded?

It is conceivable that the plate could break and the bullet would not perforate the plate.

The description of the retarding and stopping of the projectile by the plate was made by integrating the stresses that act over the surface of the projectile into a resisting force acting against the projectile. The model of stress wave propagation and failure of the plate material and of the projectile material, together with the geometry of the plate and projectile, will determine the magnitude of the resisting force and the duration of the resisting force.

In response to the stresses that are generated in the plate system during the impact, the plate may fail by several mechanisms. The mechanisms are:

1. Fracture in the Direct Wave - the plate may fracture in response to high stress in the stress spike just behind the first stress wave front.

2. Spall - the plate may fracture in response to high tensile vertical stress generated by the reflection of the first stress wave from the back surface.

3. Radial Fracture - the plate may fracture in response to the tensile stress in the radial direction which is established after the decay of the initial stress peak at the wave front.

4. Petalling - after the first traverse of the first stress wave the plate may fracture in response to high radial and circumferential tensile stresses that are developed.

5. Plugging - after the first traverse of the first stress wave the plate may fracture in response to the high shear stresses developed in the plate near the projectile.

B.3.2 Calculation of the Critical Perforation Velocity and the Residual Velocity

To generate a prediction for ballistic resistance of a plate to penetration, examine the method of failure in the direct wave. Consider the following mechanism, representative of the direct stress wave failure. Assume that the plate fails in compression. The stress at the wave front directly underneath the plate in the vertical direction is compressive. The two lateral stresses, namely, the radial and the tangential stress on the axis of symmetry, are equal and are both equal to a given fraction of the vertical stress.

Since the standard material test for failure in compression has no lateral confining pressure, the following identification between the standard tensile failure test and failure is made here. The material is considered to have failed if the maximum shear stresses developed are equal to the critical shear stress. In this case the difference between the vertical stress and the radial stress, which is equal to the tangential stress, is equal then to the tensile yield strength of the material. (Figure B-21).

At the back side of the plate, the vertical stress has the lowest value of the compressive stress in the direct wave. The compressive stress there is a function of the following three parameters:

1. Impact pressure at the interface between the bullet and the projectile. The impact pressure is proportional to the acoustic impedance of the plate projectile combination and to the impact velocity.

2. The geometrical attenuation in the elastic wave propagation across the plate.

3. The attenuation by plastic flow.

An impact velocity may be computed such that the lowest stress in the back of the plate is exactly equal to the stress required for fracture.

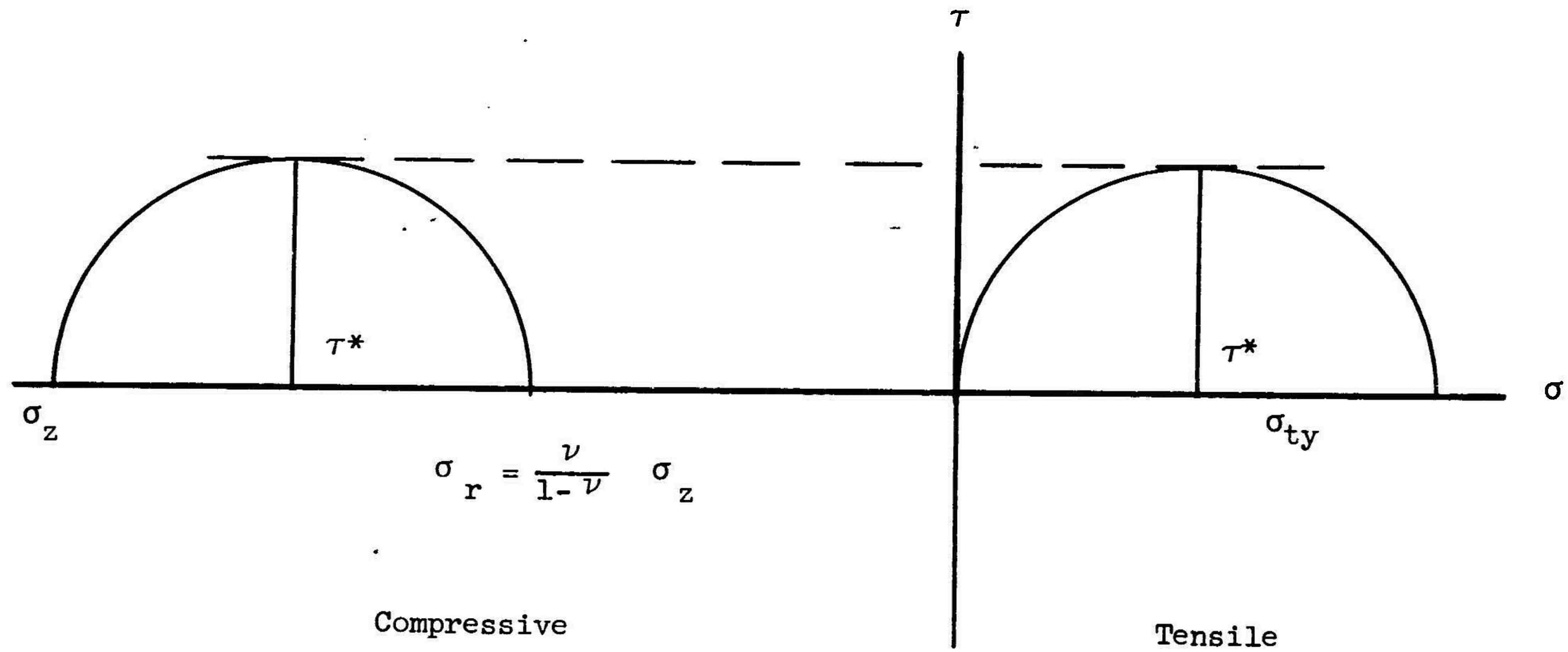

Figure B-21 FAILURE IN THE DIRECT STRESS WAVE-MOHR'S CIRCLE DIAGRAM

A critical velocity for perforation is thus generated:

$$\sigma_z(o,h,\frac{h}{c}) = \sigma_z(o,o,o)\, f(\frac{h}{a}) = \frac{1-2\nu}{1-\nu}\ \sigma_{ty}$$

$$f(\frac{h}{a}) = (1 + (\frac{h}{a})^2)^{-1/2}$$

$$\sigma_z(o,o,o) = \frac{\rho_1 C_1 \quad \rho_0 C_0}{\rho_1 C_1 + \rho_0 C_0}\, V_s$$

$$\therefore \quad V_s = (\frac{1-\nu}{1-2\nu})\ \sigma_{ty}\ (\frac{\rho_1 C_1 + \rho_0 C_0}{\rho_1 C_1 \quad \rho_0 C_0}) \times (1 + (\frac{h}{a})^2)^{1/2}$$

This critical velocity is a function of the yield strength of the plate, the plate geometry (given through the ratio of h, the thickness of the plate, to the bullet radius, a), and to the plate and projectile material properties such as the elastic constants and density. At zero plate thickness, the critical velocity is finite and at very large plate thicknesses it approaches a linear increase with h. The residual bullet velocity versus striking velocity was calculated.

$$V_r = 0 \qquad\qquad V_s \leq V_c$$

$$\frac{V_r}{V_s} = 1 - \frac{h}{L}\ \frac{\rho_0\, C_1}{\rho_1 C_1 + \rho_0 C_0} \qquad\qquad V_s \geq V_c$$

The experimental work of Zhurkov and Sanfirova (1958) has indicated that, at least in constant stress (tension), there is a relationship between the time to fracture and the level of stress. The time to fracture is essentially the inverse of the plastic component of the strain rate corresponding to that stress as determined from the dislocation theory of plastic flow. The actual magnitudes of the time to fracture that were measured by Zhurkov are very short of the order of 10^{-8} seconds for very high stresses. Figure B-22 shows an experimental time to fracture versus stress level obtained by Zhurkov in his studies on fracture.

For a first approximation, the time to fracture at a stress above the static yield stress of the material is so short that it can be ignored and the time to fracture below this yield stress is so long that the material will remain unbroken. As an approximation, this turns out to be a very good description for the fracturing and failure criteria that would follow the first wave across the plate.

For thin plates, the time to fracture is comparable to the transit time of an elastic wave. For a steel plate .01 inches thick, the time that a longitudinal stress takes to traverse across and back is

$$t \approx \frac{2 \times 0.01 \text{ in}}{200{,}000 \text{ in/sec}} = 10^{-7} \text{ seconds}$$

This time is ten times longer than the time to fracture. This time delay should be taken into account. For thinner plates correspondingly larger stresses at impact are needed to effect fracture. (This fact, by itself, does not imply that thinner plates are better, ballistically speaking). The effect of time delay to fracture, using $t_\alpha = 10^{-8}$ sec, does not significantly alter the predictions of the critical perforation velocity for plates with thickness $h = 0.01$ inches.

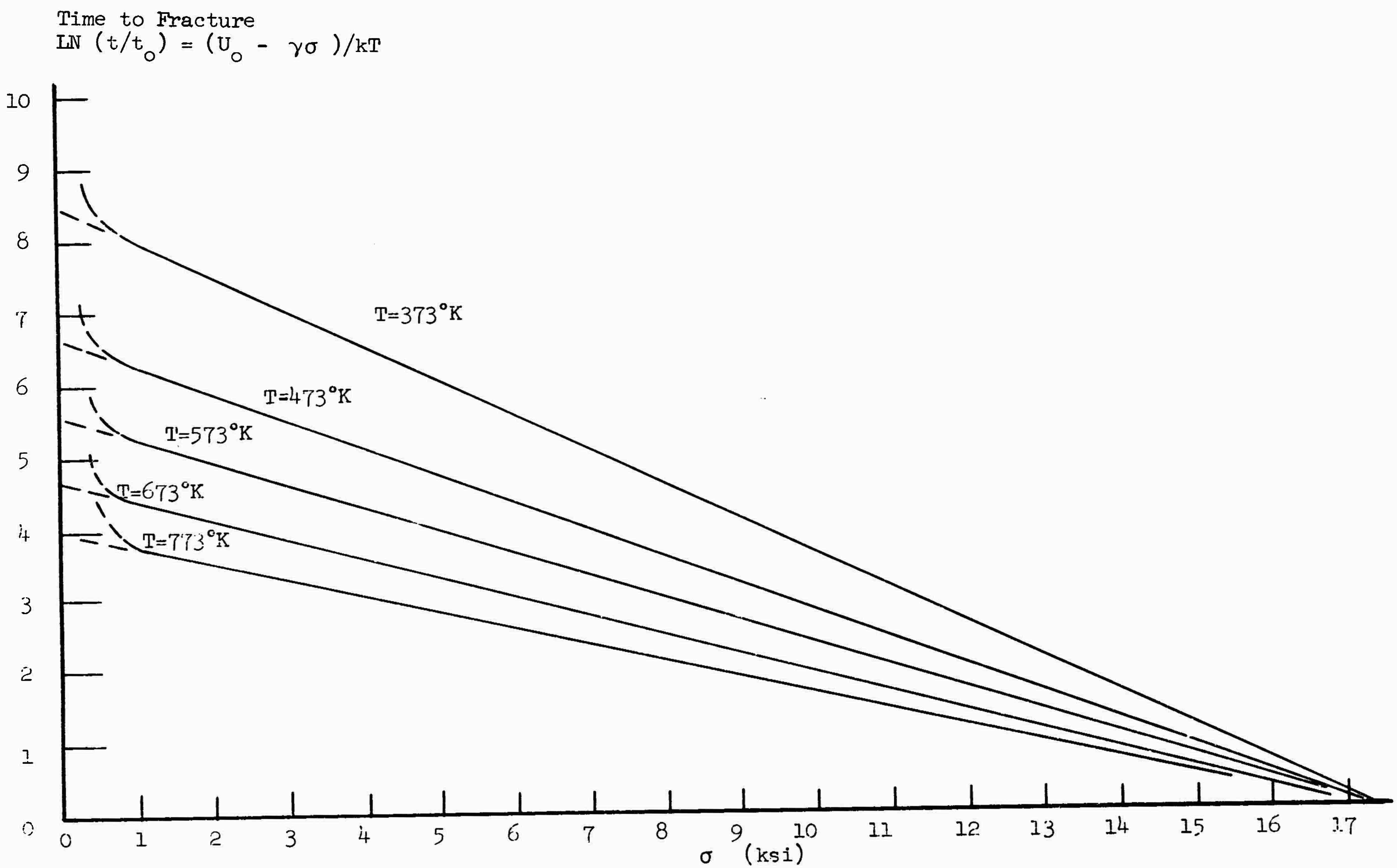

Figure B-22 TIME TO FRACTURE VS. STRESS FOR ALUMINUM (99.97% PURE) (AFTER ZHURKOV)

The stresses in the spike decay extremely rapidly by dissipation in plastic flow. Explicit expressions for the decay of a stress wave by plastic flow have been computed for the propagation of a spherical wave (Fugelso 1962) and a cylindrically expanding wave (Fugelso, Arentz and Davidson 1962). For impact stresses far above the yield stress for the distance the stress wave must propagate in the present problem, the stresses should decay by a factor of 1.5 to 2 by the time the stress wave reaches the back of the plate. Thus, the critical perforation velocity estimate should be raised by a factor of 1.5 to 2.

After the first stress wave propagates across the plate, it reflects. Since the rear surface of the plate is free, the normal or vertical stress at the reflected wave front is tensile and the radial stress in the reflected wave front is also tensile. These stresses will add to the existing stresses left after the decay of the pressure spike in the direct stress wave. The residual normal or vertical left after the passage of the spike is compressive and the residual radial stresses in the plate after the passage of the spike are tensile. These stresses add to form a composite stress system.

Since both of these stresses, the vertical and the radial, are tensile, the failure of the plate must be considered when either one of them exceeds the tensile yield stress. Consider the radial stress. Near the back surface of the plate, the radial stress due the direct wave is

$$\sigma_r = 1/2\ ZV_s f^{-1}$$

The radial stress in the reflected spike is

$$\sigma_r \approx \frac{\nu}{1-\nu} ZV_s f^{-1/2}$$

The radial stress at the back surface is

$$\frac{\sigma_r}{ZV_s} = 1/2\ f^{-1} + \frac{\nu}{1-\nu} f^{-1/2}$$

The critical perforation velocity by fracture due to radial stresses is given by the impact velocity, which makes the radial stress equal to the tensile yield stress at the rear surface of the plate. Thus,

$$V_c = \frac{\sigma_{ty}}{Z} \frac{1}{1/2f^{-1} + \frac{\nu}{1-\nu} f^{-1/2}} = \frac{\sigma_{ty}}{Z} \left[\frac{2(1-\nu)f}{(1-\nu) + 2\nu f^{1/2}}\right]$$

The vertical stress in the reflected stress wave is also tensile. At some distance sufficiently far from the rear surface so that the stress spike in the direct wave has decayed to zero, the vertical stress in the reflected stress spike is (ζ^* denotes this distance)

$$\sigma_z = ZV_s \quad 1 + \left(\frac{(h+\zeta^*)^2}{a^2}\right)^{1/2}$$

At this same point, the residual stress in the direct stress wave is

$$\sigma_z = -ZV_s \left(1 + \left(\frac{h-\zeta^*}{a}\right)^2\right)^{-1}$$

The vertical stress at $z = \zeta^*$ is

$$\sigma_z = ZV_s \left[\left[1 + \left(\frac{h+\zeta^*}{a}\right)^2 \right]^{-1/2} - \left[1 + \left(\frac{h-\zeta^*}{a}\right)^{-2} \right]^{-1} \right]$$

Making the approximation $(\frac{\zeta^*}{a}) \ll (\frac{h}{a})$

the tensile vertical stress is approximately

$$\sigma_z = ZV_s \left[f^{-1/2} - f^{-1} \right]$$

The critical perforation velocity for failure in response to large normal or vertical reflected stresses is obtained by determining the impact velocity at which the normal stress is equal to the tensile yield stress.

$$V_c = \frac{\sigma_{ty}}{Z} \frac{1}{f^{-1/2} - f^{-1}} = \frac{\sigma_{ty}}{Z} \frac{f}{(f^{1/2} - 1)}$$

This model of failure is failure by spall and is normally characterized by a plane failure near the back side of the plate. A small group of pieces between this plane and the back surface may separate and fly off the back side.

One of the features in the equations for the propagation of the stresses is the magnitude of the stress generated at the impact force. The exact determination of the magnitude of this stress is a most difficult analytic problem. For a first estimate, the uniaxial impact of two linear elastic bodies was used to estimate the stress over the contact area. For the generation of the stresses that are propagated into the plate, a linear elastic model was used to compute the stresses generated at the impact area.

In this model, the impact stress σ_I is

$$\sigma_I = \frac{\rho_1 C_1 \ \rho_0 C_0}{\rho_1 C_1 + \rho_0 C_0} V_s$$

where ρ_1, ρ_0 are the densities of the two materials

C_1, C_0 are the longitudinal sonic velocities of the two materials

V_s is the striking velocity of the impact

An additional factor in the impact process was checked. The elastic-plastic stress-strain curves in uniaxial compression were used to compute the impact stresses. The elastic-plastic curves are linear-elastic in volume compression and linear-elastic fully-plastic in shear. The maximum shear stress is one-half the tensile yield stress of the material. The stress-strain curve is shown in Figure B-23 and the impact stress vs impact velocity curve for uni-axial deformation is shown in Figure B-24. The impact stresses were lower by about 10% for steel-aluminum 2024-T6 impact at V_s = 4000 ft/sec. The increase in the critical perforation velocity in the previous mode was about 10% at that impact velocity.

If the deformation at the impact is treated as unconfined compression, the maximum stress that can be generated is σ_{cu}, the compressive ultimate stress.

Then $\sigma_I = \sigma_{cu}$

In addition to the static forces, a dynamic pressure term proportional to $\rho_1 V^2$ must also be added to account for the inertia of the plate material.

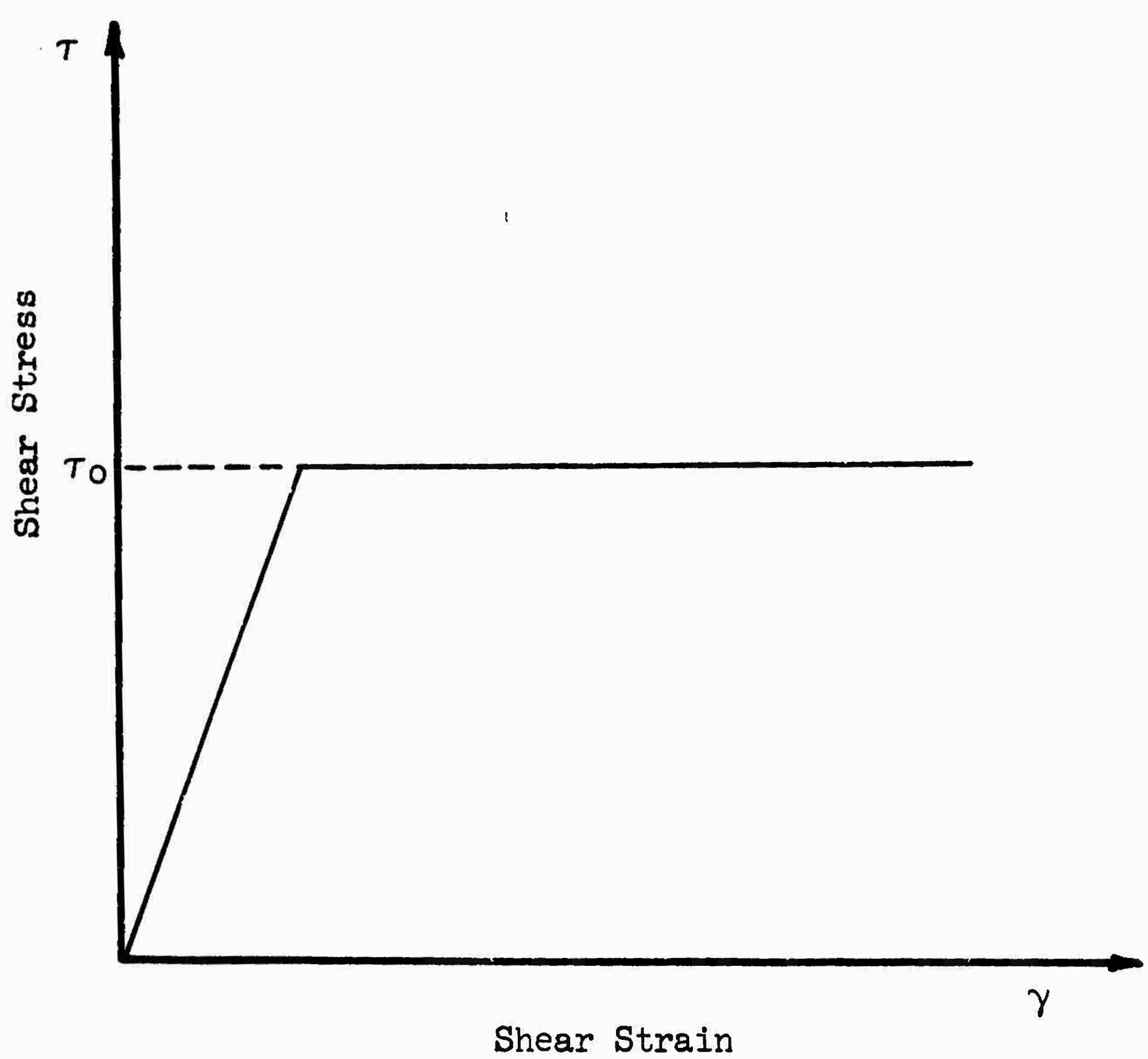

Figure B-23 ELASTIC - PERFECT PLASTIC STRESS-STRAIN RELATION IN SHEAR

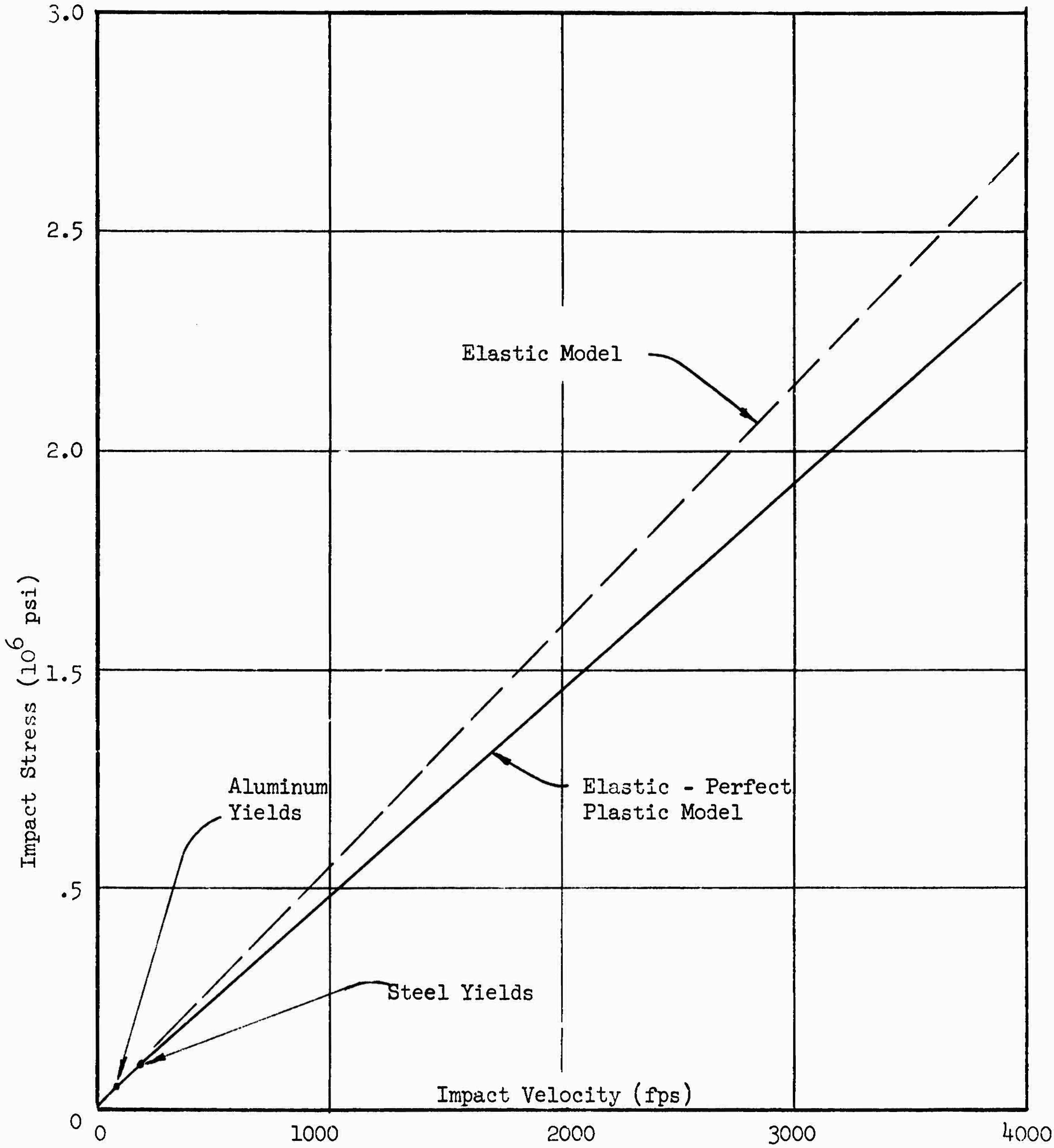

Figure B-24 IMPACT STRESS VS. IMPACT VELOCITY FOR UNAXIAL IMPACT

For the uniaxial elastic model of impact, this term is quite small compared to the stress in the ρcv term for impact velocities up to 5000 ft/sec for steel-aluminum impact. For the plastic unconfined model, however, the inertial term is quite large and cannot be neglected.

If the plate has not failed after the first traverse of the first stress wave, the projectile may still be moving with a high velocity, particularly in those impacts where the projectile length is very much larger than the plate thickness. The failure of the plate occurs as fracture in response either to the large tensile membrane stresses developed in the plate underneath the projectile or to the large shear stress developed in the plate near the edge of the projectile.

Nishiwaki (1951) derived the equations of motion for the normal impact of a cylindrical bullet with a conical cap impacting a plate. In this case, the bullet is treated as a rigid body moving in the plate with some initial velocity. The equations of motion of the projectile are the equations of motion of a rigid body acted upon by time and position dependent force and torques. The projectile is acted upon with a resisting force by the plate consisting of a static stress given by the particular mode of failure of the plate and a dynamic stress proportional to the square of the velocity. The motion of the projectile is determined until it passes through the plate without regard to the details of the deformation of the plate. In this time of passage the forces are acting upon the bullet and the bullet slows down.

The perforation parameters of ductile metallic plate for the various models of plate failure are calculated by using different forms of the static component of the resisting force. In particular, three forms of the static resisting force may be descriptive of the plate deformation. For very thin plates, the stress acting against the projectile may be a function of the plate thickness as for the shear mode computed in the previous section.

$$\sigma_I = \sigma_{ty}\left(\frac{h}{a}\right)$$

The resisting stress may also be computed as a function of plate thickness if the membrane stresses in the plate are large:

$$\sigma_I = 4\,\sigma_{ty}\left(\frac{h}{a}\right)$$

In these cases, the resisting force is proportional to the plate thickness. For moderately thick plates, the resisting forces of the plate may be estimated as the compressive ultimate stress. The compressive ultimate stress is the largest stress that can be developed in the plate since the material is assumed to be nearly unconfined and flows laterally away from the impact zone. These models were computed for the prediction of the perforation of cylindrical projectiles.

Consider an axisymmetric projectile of arbitrary cross section impacting a plate (Figure B-25). The angle of impact is such that the axis of the projectile is normal to the plate. The projectile has density ρ_0, mass M. The plate has density ρ_1, thickness h. The projectile has velocity V normal to the plate. The initial velocity is V_s. In this analysis, the lateral velocity is zero.

Just after the impact, the projectile is resisted by the stresses developed in the plate at the contact area between projectile and plate. The material in the plate next to the projectile is assumed to move laterally

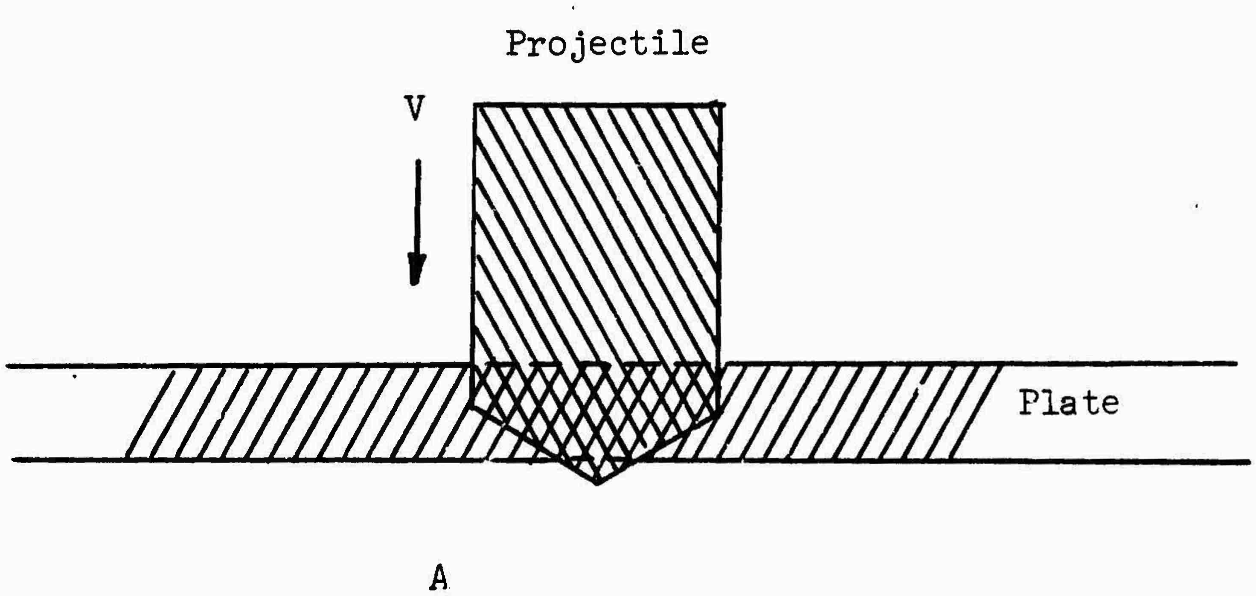

Figure B-25 CONFIGURATION OF PLATE AND PROJECTILE FOR NISHIWAKI MODEL out of the projectile's way during the penetration. Consider a differential element of the projectile surface, dA (Figure B-26). The normal to this surface makes an angle α with the horizontal. The resisting stress on this element dA is given by a static component of stress, σ_I, plus the hydrodynamic pressure.

$$\sigma = \sigma_I + \rho_2 V^2 \mathrm{Sin}^2 \alpha$$

The resisting forces act in a direction normal to the surface element. Since the projectile is axisymmetric, the force component resisting motion of the projectile can be integrated over dA. The horizontal component of the force vanishes and the vertical component is

$$dF = -(\sigma_I + \rho_2 V_n^2 \mathrm{Sin}^2 \alpha) \mathrm{Sin}\,\alpha \; dA$$

where V_n is the instantaneous velocity of the projectile at the surface.

The equation of motion of the center of mass of the projectile is

$$M\frac{dv}{dt} = -\int (\sigma_{cu} + \rho_2 V_n^2 \mathrm{Sin}^2 \alpha) \mathrm{Sin}\,\alpha \; dA$$

The expression for the deceleration of the projectile is quite general. It will be solved explicitly under the following assumptions:

1. The projectile does not deform during the impact. This implies that dA will be known from the shape of the projectile and the amount of penetration. It then also follows that $V_n = V$.

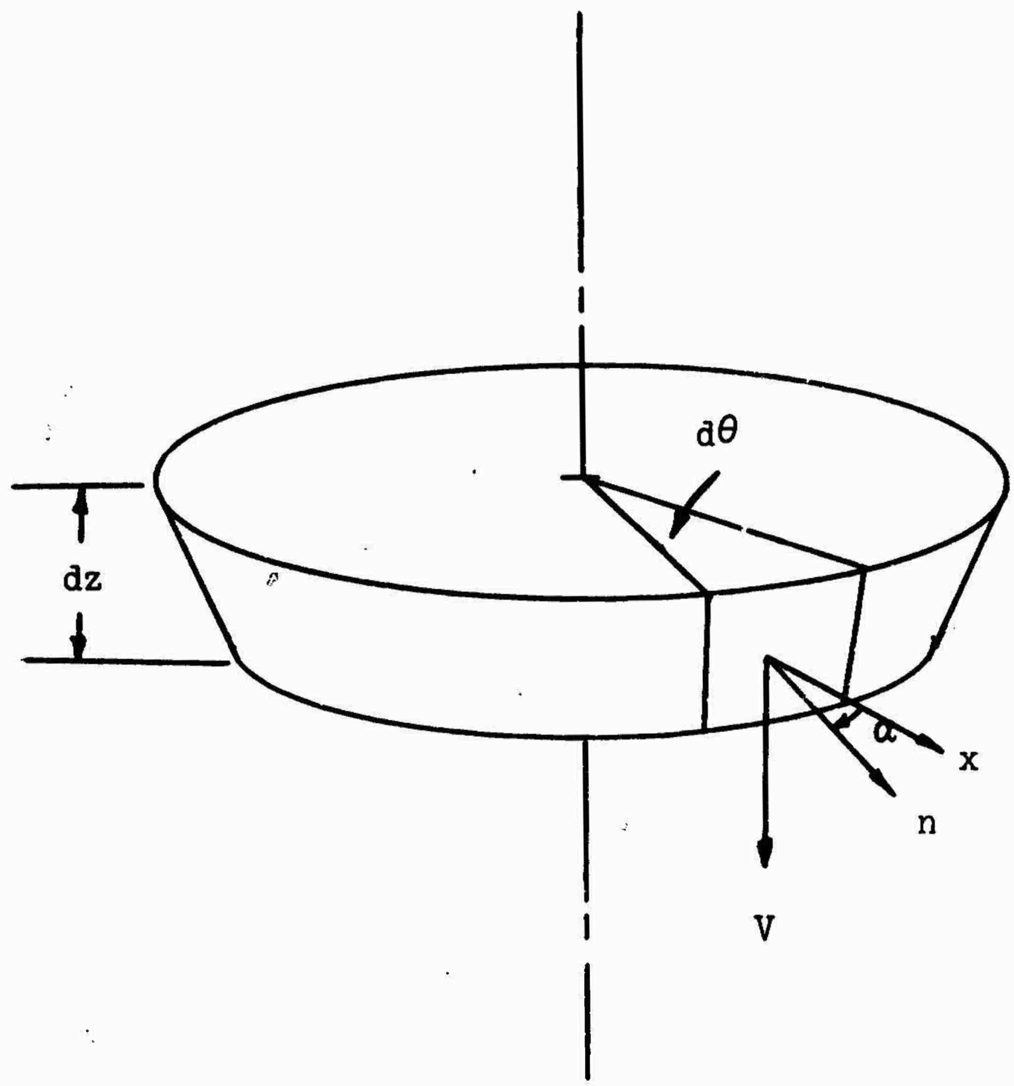

Figure B-26 ELEMENT OF SURFACE OF PROJECTILE
IN CONTACT WITH THE PLATE

2. The resistance of the plate is effective only as long as some portion of the projectile surface is attempting to move into a volume occupied by the plate. Frictional forces or shear tractions between the plate and projectile are ignored.

The residual velocity for the cylindrical projectile is made by assuming the projectile has a cylindrical body capped by a conical nose whose apex angle is α and taking the limit as $\alpha \to 90°$.

The residual velocity V_r for the cylindrical projectile is

$$V_r^2 = c^2 \left(e^{-yh} - 1\right) + V_s^2 \, e^{-yh}$$

where

$$c^2 = \frac{\sigma_{cu}}{\rho_2}$$

and

$$Y = \frac{2\rho_2}{\rho_1 L}$$

where L is the length of the cylindrical projectile

The critical velocity for perforation is the value of V_s where $V_r = 0$. Thus

$$V_s = c \left(e^{yh} - 1\right)^{1/2}$$

To extend the analysis to laminated or composite plates, the resisting force parameters are taken as a function of position corresponding to the material initially there.

The laminated plate system consists of two plates of thickness, h_1, h_2; densities, ρ_1, ρ_2; and ultimate stresses σ_1, σ_2. The index 1 refers to the front material and the index 2 refers to the back material. Let $H = h_1 + h_2$. Let ρ_o be the density of the projectile.

For the blunt nosed cylinder, which is the limit of a cone-shaped cylinder with apex angle equal to a straight angle, the equations of motion of the projectile are

$$M \frac{dV}{dt} = A\left(\sigma_i + \rho_i V^2\right) \qquad i = 1,2$$

where M is the mass of the projectile

A is the cross section area of the projectile

$V = \frac{dz}{dt}$ is the velocity of the projectile

and z is depth of penetration of the nose

The density and static stress on the right hand side of the equation of motion are given by

$$\begin{array}{llll} \sigma_i = 0 & \rho_i = 0 & z \leq 0 \\ \sigma_i = \sigma_1 & \rho_i = \rho_1 & 0 \leq z \leq h_1 \\ \sigma_i = \sigma_2 & \rho_i = \rho_2 & h_1 \leq z \leq H \\ \sigma_i = 0 & \rho_i = 0 & z > H \end{array}$$

The projectile impacts the plate with velocity V_s. The upper plate retards the projectile until the penetration depth is h_1. Just at this point, the projectile velocity is V_{r1}. The second plate then retards the projectile until the penetration distance, z, is equal to $H = h_1 + h_2$. At this time, the projectile velocity is V_r.

The projectile velocity is

$$V^2 = C_1^2 \left(e^{-Y_1^2} - 1\right) + V_s^2 e^{-Y_1^2} \qquad 0 \leq z \leq h_1$$

$$V^2 = C_2^2 \left(e^{-Y_2^2} - 1\right) + V_{ri}^2 e^{-Y_2^2} \qquad h_1 \leq z \leq H$$

with $$C_1^2 = \frac{\sigma_1}{\rho_1}$$

$$C_2^2 = \frac{\sigma_2}{\rho_2}$$

$$Y_1 = \frac{2\rho_1}{\rho_o L}$$

$$Y_2 = \frac{2\rho_2}{\rho_o L}$$

Thus, the projectile velocity in the second plate is

$$V_r^2 = C_2^2 \left(e^{-Y_2(z-h_1)} - 1\right) + C_1^2 e^{-Y_2(z-h_1)} \left(e^{-Y_1 h_1} - 1\right) + V_s^2 e^{-Y_2(z-h_1) - Y_1 h_1} \qquad h_1 \leq z \leq H$$

The critical perforation velocity for the laminated system occurs just when

$$V_r = 0 \text{ at } z = H = h_1 + h_2$$

Thus

$$V_c^2 = C_1^2 \left(e^{Y_1 h_1} - e^{Y_1 (h_1 - h_2)}\right) + C_2^2 \left(e^{Y_1 h_1} \left(e^{Y_2 h_2} - 1\right)\right)$$

The analysis of the ballistic model that best fits the data may be extended to the case of oblique impact. This has been done for oblique impact of bombs into soil (Fugelso and Jepson 1963; Fugelso, Holmstrom, Bardy and Guttenberger 1965). The solution to the oblique problem is necessarily numerical.

REFERENCES

1. Bridgman, P. W., "Large Plastic Flow and Fracture", McGraw-Hill (1952)

2. Catlin, J. P., and Wentz, W. W., "Effect of Strain Rate of the Mechanical Properties of Titanium Base Materials", WADD Technical Report 53-71 (1955)

3. Curtis, C. W., "Terminal Ballistics of Armor", Effects of Impact and Explosion, NRDC Summary Technical Report (1946)

4. Fugelso, L. E., "Analytic Study of Early Motion Caused by an Underground Detonation", Final Technical Report, Contract DA-49-046-XZ-088 (1962)

5. Fugelso, L. E., "Close-in Effects from a Surface Nuclear Burst", Final Technical Report, Contract AF 29(601)-5009 (1964)

6. Fugelso, L. E., Arentz, A. A., Jr., and Poczatek, J. J., "Mechanics of Penetration", Vol. I, Final Technical Report, Contract DA 19-129-QM-1542 (1961)

7. Fugelso, L. E., Arentz, A. A., Jr., and Davidson, D. A., "Mechanics of Penetration", Vol. II, Final Technical Report, Contract DA-19-129-QM-1542 (1962)

8. Fugelso, L. E., and Jepson, C. H., "A Theoretical Study of the Penetration of the Anti-bridge Bomb into Soil", Quarterly Technical Report, Contract AF 08(635)-3607 (1963) (C)

9. Fugelso, L. E., Holmstrom, J. S., Bardy, P., and Guttenberger, N. T., "Design of a Nose Adapter for the M-117 Bomb", Final Technical Report AF 08(635)-4334 (1965)

10. Hopkins, H. G., and Kolsky, H., "Mechanics of Hypervelocity Impact of Solids", Proc. 4th Hypervelocity Symposium (1961)

11. Nishiwaki, J., "Resistance to the Penetration of a Bullet Through an Aluminum Plate", Journal Phys. Soc. of Japan, 6, 374-378 (1951)

12. Zhurkov, S. N., and Sanfirova, T. P., Soviet Physics Technical Physics, 2, 1586-1592 (1958)

Unclassified

Security Classification

DOCUMENT CONTROL DATA - R&D

(Security classification of title, body of abstract and indexing annotation must be entered when the overall report is classified)

1. ORIGINATING ACTIVITY *(Corporate author)* MRD Division General American Transportation Corporation Niles, Illinois	2a. REPORT SECURITY CLASSIFICATION Unclassified 2b. GROUP

3. REPORT TITLE STUDIES IN THE PERFORATION OF THIN METALLIC PLATES BY PROJECTILE IMPACT: I. NORMAL IMPACT OF CIRCULAR CYLINDERS

4. DESCRIPTIVE NOTES *(Type of report and inclusive dates)*

Volume I of Final Report, February 1964 - April 1965

5. AUTHOR(S) *(Last name, first name, initial)*

Fugelso, L. E. and Bloedow, F. H.

6. REPORT DATE	7a. TOTAL NO. OF PAGES	7b. NO. OF REFS
June 1966	120	12

8a. CONTRACT OR GRANT NO. DA19-129-AMC-247(N) b. PROJECT NO. 1K024401A113 c. d.	9a. ORIGINATOR'S REPORT NUMBER(S) MR 1250 9b. OTHER REPORT NO(S) *(Any other numbers that may be assigned this report)* 66-58-CM C&OM 9

10. AVAILABILITY/LIMITATION NOTICES

Distribution of this document is unlimited.
Release to CFSTI is authorized.

11. SUPPLEMENTARY NOTES	12. SPONSORING MILITARY ACTIVITY U. S. Army Natick Laboratories Natick, Massachusetts 01760

13. ABSTRACT

The ballistic parameters were determined analytically and experimentally for the perforation of aluminum alloy and titanium alloy plates by normal impact of steel cylinders. Analytical predictions of the perforation parameters were prepared on the basis of theoretical models of the perforation process. Experimental determination of the critical perforation and residual velocities discriminated among the various models and further experimentation verified the analytical description of the perforation process.

One model of perforation was found which adequately describes the ballistic parameters for the normal impact of steel cylinders into aluminum alloy and titanium alloy plates for impact velocities up to 5000 ft/sec and plate thicknesses up to 0.25 inches.

14. KEY WORDS	LINK A		LINK B		LINK C	
	ROLE	WT	ROLE	WT	ROLE	WT
Prediction			8			
Perforating	8					
Thin	0		0			
Metal plates	9		9			
Impact	10					
Projectiles	10					
Ballistics			10			
Parameters			10			
Aluminum alloys	9		9			
Titanium alloys	9		9			
Steel	10					
Cylinders	10					
Determination			8			
Models of perforation			10			
Fracture (mechanics)			9			

INSTRUCTIONS

1. ORIGINATING ACTIVITY: Enter the name and address of the contractor, subcontractor, grantee, Department of Defense activity or other organization *(corporate author)* issuing the report.

2a. REPORT SECURITY CLASSIFICATION: Enter the overall security classification of the report. Indicate whether "Restricted Data" is included. Marking is to be in accordance with appropriate security regulations.

2b. GROUP: Automatic downgrading is specified in DoD Directive 5200.10 and Armed Forces Industrial Manual. Enter the group number. Also, when applicable, show that optional markings have been used for Group 3 and Group 4 as authorized.

3. REPORT TITLE: Enter the complete report title in all capital letters. Titles in all cases should be unclassified. If a meaningful title cannot be selected without classification, show title classification in all capitals in parenthesis immediately following the title.

4. DESCRIPTIVE NOTES: If appropriate, enter the type of report, e.g., interim, progress, summary, annual, or final. Give the inclusive dates when a specific reporting period is covered.

5. AUTHOR(S): Enter the name(s) of author(s) as shown on or in the report. Enter last name, first name, middle initial. If military, show rank and branch of service. The name of the principal author is an absolute minimum requirement.

6. REPORT DATE: Enter the date of the report as day, month, year; or month, year. If more than one date appears on the report, use date of publication.

7a. TOTAL NUMBER OF PAGES: The total page count should follow normal pagination procedures, i.e., enter the number of pages containing information.

7b. NUMBER OF REFERENCES: Enter the total number of references cited in the report.

8a. CONTRACT OR GRANT NUMBER: If appropriate, enter the applicable number of the contract or grant under which the report was written.

8b, 8c, & 8d. PROJECT NUMBER: Enter the appropriate military department identification, such as project number, subproject number, system numbers, task number, etc.

9a. ORIGINATOR'S REPORT NUMBER(S): Enter the official report number by which the document will be identified and controlled by the originating activity. This number must be unique to this report.

9b. OTHER REPORT NUMBER(S): If the report has been assigned any other report numbers *(either by the originator or by the sponsor)*, also enter this number(s).

10. AVAILABILITY/LIMITATION NOTICES: Enter any limitations on further dissemination of the report, other than those imposed by security classification, using standard statements such as:

(1) "Qualified requesters may obtain copies of this report from DDC."

(2) "Foreign announcement and dissemination of this report by DDC is not authorized."

(3) "U. S. Government agencies may obtain copies of this report directly from DDC. Other qualified DDC users shall request through ________________."

(4) "U. S. military agencies may obtain copies of this report directly from DDC. Other qualified users shall request through ________________."

(5) "All distribution of this report is controlled. Qualified DDC users shall request through ________________."

If the report has been furnished to the Office of Technical Services, Department of Commerce, for sale to the public, indicate this fact and enter the price, if known.

11. SUPPLEMENTARY NOTES: Use for additional explanatory notes.

12. SPONSORING MILITARY ACTIVITY: Enter the name of the departmental project office or laboratory sponsoring *(paying for)* the research and development. Include address.

13. ABSTRACT: Enter an abstract giving a brief and factual summary of the document indicative of the report, even though it may also appear elsewhere in the body of the technical report. If additional space is required, a continuation sheet shall be attached.

It is highly desirable that the abstract of classified reports be unclassified. Each paragraph of the abstract shall end with an indication of the military security classification of the information in the paragraph, represented as *(TS), (S), (C), or (U)*.

There is no limitation on the length of the abstract. However, the suggested length is from 150 to 225 words.

14. KEY WORDS: Key words are technically meaningful terms or short phrases that characterize a report and may be used as index entries for cataloging the report. Key words [illegible] be selected so that no security classification is re[illegible] [illegible]fiers, such as equipment model designation, trad[illegible] [illegible] military project code name, geographic location, may [illegible]ed as key words but will be followed by an indication of technical context. The assignment of links, rules, and weights is optional.